THE UNIVERSITY OF CALGARY

Low Temperature Separation of Hydrogen and Methane in SSF Membranes

by

Robin Tanis Morton

A THESIS

SUBMITTED TO THE FACULTY OF GRADUATE STUDIES

IN PARTIAL FULFILMENT OF THE REQUIREMENTS FOR THE

DEGREE OF MASTER OF SCIENCE IN CHEMICAL ENGINEERING

DEPARTMENT OF CHEMICAL AND PETROLEUM ENGINEERING

CALGARY, ALBERTA

MARCH, 1999

ABSTRACT

Experiments were conducted with hydrogen and methane in a SSF (Selective Surface Flow) membrane to determine the effect of low temperatures on separation. It was proposed that low temperatures would increase the surface flow of methane, decrease the permeation of hydrogen and improve separation. Experiments were conducted with mixtures containing 25%, 50% and 75% methane (balance hydrogen) at temperatures ranging from -25°C to 22°C. Feed pressures ranging from 50-150 psig and flow rates ranging from 4-7 L/min were investigated. At a reference of 60% hydrogen recovery, the methane rejections improved by 13%, 15% and 17% respectively for each mixture by decreasing the temperature from ambient to -25°C. There was no significant effect on flow rate with decreasing temperature and optimal feed pressures were in the range of 80-120 psig.

Experiments were also conducted with a mixture containing 49% hydrogen, 49% methane and 2% ethane to determine the effect of a more polar feed mixture. The presence of the 2% ethane was found to improve the separation of hydrogen by approximately 5% at -25°C (75% hydrogen recovery) however the permeate flow rates of this mixture were nearly 50% less than an equimolar mixture without ethane at -25°C. This suggested that more investigation is required into the effects of low temperature on polar components in the SSF membrane.

A Langmuir adsorption model was developed to predict the performance of the SSF membrane by modelling the SSF membrane layer as a Type 1 adsorbent. Isotherm data for activated carbon and experimental pure gas data were used to find Langmuir parameters and diffusivities for hydrogen and methane as a function of temperature. Experimental mixture flux data and the Langmuir parameters were then used to predict the surface diffusivities for

hydrogen and methane within mixtures. The Langmuir model predicted the surface diffusivities of methane within 4% at 22°C (for a mixture of 50% methane) however diffusivity values for hydrogen were an average of 23% above pure gas diffusivities. It was concluded that the results for hydrogen were anomalous because the model did not take into account the change in hydrogen adsorption in the presence of methane.

ACKNOWLEDGEMENTS

I wish to express my gratitude and appreciation to the following people:

My supervisor, Dr. Pruden for his help, support and guidance. Dr. Pruden was always there to answer my questions, give advice and share his wealth of knowledge.

Dr. M. Rao, Dr. M. Anand and Paul Novosat of Air Products and Chemical Inc. of Allentown, PA for their time, assistance and technical advice. Special thanks to Dr. Catherine Golden and Dr. Tim Golden for going out of their way to make my stay in Allentown worthwhile.

The present and former staff of the Industrial Hydrogen Chair Laboratory and the technicians in the Department of Chemical and Petroleum Engineering for their help in building the SSF low temperature apparatus.

Air Products and Chemicals Inc. and the Industrial Hydrogen Chair for funding this project.

Mike, for the support, helpful discussions and most importantly, for showing me how to make a no-fail Excel figure.

Dedicated to my parents Ken and Karen Morton

TABLE OF CONTENTS

LIST OF FIGURES

LIST OF TABLES

NOMENCLATURE

A	surface area of the membrane (m^2)
Å	Angstrom (1×10^{-10} m)
b	Langmuir equilibrium constant (kPa^{-1})
b_o	Langmuir constant (kPa^{-1})
C	concentration (mol/m^3)
D	gas phase diffusivity (m^2/s)
D_k	Knudsen diffusivity (cm^2/s)
D_o	diffusivity constant (m^2/s)
d_p	pore diameter (Å)
D_s	surface diffusivity (m^2/s)
E	activation energy (J/mol/K)
F(r)	shape factor
G	pressure gauge
H	pore circumference (m)
ΔH	heat of adsorption (J/mol/K)
HT	high temperature
J	flux ($mol/m^2/s$)
J_g	gas phase flux ($mol/m^2/s$)
J_s	surface phase flux ($mol/m^2/s$)
K	permeability ($mol/m^2/s/kPa$)
k_a	rate constant for adsorption (mol/min/kPa)
k_d	rate constant for adsorption (mol/min)
K_g	gas phase permeability ($mol/m^2/s/kPa$)
K_g	shape factor
K_s	surface phase permeability ($mol/m^2/s/kPa$)

L length of a pore (m)

M molecular weight

M-1 membrane used in irreversible adsorption tests

M-2 membrane used in separation experiments

MMSCF million standard cubic feet (ft^3)

N molar flow rate (mol/s)

n_s surface loading (mol)

n_s surface loading (mol/kg)

n_s^* saturation loading (mol/kg)

n_s^H surface loading on high pressure side of membrane

n_s^L surface loading on low pressure side of membrane

P permeate flow rate at STP (L/min)

Δp partial pressure difference (kPa)

P-1 membrane used in Paranjape's study (1997)

P_h feed of retentate side pressure (kPa)

P_l permeate side pressure (kPa)

PSA pressure swing adsorption

Q volumetric flow rate (L/min)

R gas constant (L-kPa/mol/K)

R rejection or recovery (%)

r radius of the pore (m)

r_a rate of adsorption (mol/min)

r_d rate of desorption (mol/min)

RT room temperature

S separation factor

S-1 membrane used in Smith's study (1998)

SSF selecitve surface flow

STP standard temperature and pressure (273 K and 101.325 kPa)

T temperature (K)

TSA temperature swing adsorption

v molecular velocity (m/s)

V valve

WTM wet test meter

x membrane layer thickness (m)

x_i mole fraction in feed

y_i mole fraction in permeate

Greek Letters

ρ bulk density (kg/m^3 adsorbent)

Θ ratio of number of moles adsorbed to moles at saturation

τ tortuosity

ε voidage

CHAPTER 1.0

INTRODUCTION

The use of hydrogen within refinery processes results in several feed streams consisting of hydrogen-hydrocarbon mixtures. For example, waste gas streams such as off-gas from fluid catalytic crackers or purge streams from pressure swing adsorption (PSA) units consist of approximately 20-40% hydrogen with a balance of mostly light hydrocarbons. These waste gas streams are normally used as fuel, as their hydrogen content is insufficient for economic recovery in any conventional separation process. While a PSA unit is a possibility, the concentration of hydrocarbons in refinery waste gases is generally too high to send directly to the unit for recovery of hydrogen due to the difficulties caused in desorbing the hydrocarbons from the adsorbent beds. Air Products and Chemicals of Allentown, PA developed a membrane that is capable of enriching low concentration, low pressure streams of hydrogen so they could be further purified in PSA units. The SSF (Selective Surface Flow) membrane developed by Air Products is capable of rejecting 90-100% of hydrocarbons such as propane and butane that would cause problems if fed to a PSA unit. Additionally, over 65% of ethane and approximately 35% of methane gases are rejected [Sircar *et al*, 1995]. This results in a stream that can be fed to a PSA unit to recover

hydrogen that would otherwise be used as fuel. Approximately 65% of the hydrogen can be recovered from a typical waste gas stream.

The objectives of this study concerning SSF membranes are outlined in Section 1.1. Section 1.2 explains the separation mechanism of the SSF membrane system and comparisons to the mechanisms employed for competing membrane systems are made in Section 1.3. Air Products has developed an SSF membrane module for pilot scale operation and results of using this module are outlined in Section 1.4. Typical operating characteristics for present technology used in hydrogen recovery are explained in Section 1.5. The advantages of membrane separation processes over competing technologies are illustrated by comparing the economics of membrane separation systems in Section 1.6.

1.1 Objectives of this Study

One of the challenges of the application of the SSF membrane to the recovery of hydrogen from waste gas streams is the poor separation of hydrogen and methane. The weak polarity of methane (it has weaker induced dipole moment) compared to components such as propane and the relatively small molecular size difference between methane and hydrogen (4.0 Å vs. 3.3 Å) results in a limited separation in the SSF membrane. It was proposed that a reduction in temperature would improve the separation of hydrogen and methane due to the stronger adsorption effects between methane and the membrane layer at lower temperatures. The purpose of this study was to determine the effect of low temperatures on the separation of hydrogen and methane. Experiments were conducted to determine the effect of temperature, feed stream concentrations and pressure on measured values of flux, permeability and separation factors. Experiments were also conducted to measure the diffusion rates of pure hydrogen and methane at high and low temperatures. From this, the development of a model to mathematically predict diffusivities was investigated. As an additional study, the composition of the feed was altered to include 2% ethane with an

equimolar composition of hydrogen and methane. It was proposed that due to the hydrogen permeation hinderance by polar molecules, the separation would improve with the presence of a more polar molecule such as ethane in the feed.

1.2 SSF Membrane Separation Mechanism

The separation mechanism employed by the SSF membrane is a adsorption-surface diffusion-desorption mechanism. Larger or more polar molecules in the gas mixture are selectively adsorbed on the surface of the membrane layer and diffuse along the pore walls through to the low pressure side. The driving force for separation is the partial pressure difference between the higher pressure feed side and the low pressure permeate side of the membrane. Figure 1.1 shows the transport mechanism of the SSF membrane. Separation is affected by the hindered permeation of smaller or less polar molecules. The larger or more polar molecules are adsorbed on the surface of the membrane layer and effectively block the passage of the smaller molecules through the pores of the membrane. Smaller molecules such as hydrogen are retained on the high pressure side of the membrane while the polar molecules travel by surface diffusion to the low pressure side of the membrane. This is in contrast with most membrane systems that involve the permeation of the smaller molecules of the gas mixture. The pore size of the SSF membrane is approximately 6-7 Å.

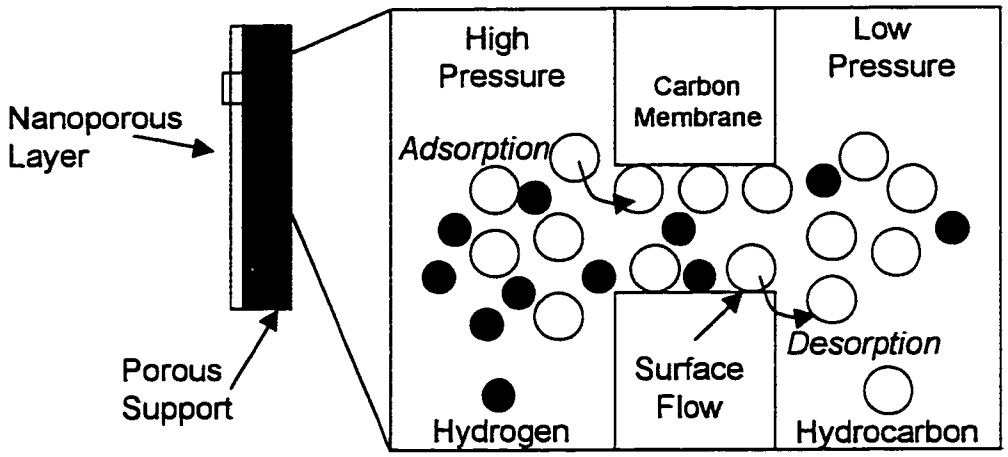

Figure 1.1: SSF Membrane Separation Mechanism [Rao and Sircar, 1993]

1.3 Porous Membrane Separation Mechanisms

The advantages of the SSF membrane separation mechanism can be illustrated by comparing the adsorption-surface diffusion-desorption mechanism with other mechanisms employed in porous membranes. There are four principal separation mechanisms that may be employed to separate gas mixtures in porous membranes [Rao and Sircar, 1993].

a) Knudsen diffusion
b) Molecular sieving
c) Partial condensation
d) Selective adsorption

Knudsen diffusion occurs in pore sizes ranging from 10 to 1000 Å when the mean free path of molecules in the gas mixture is larger than the pore diameter through which the molecules are diffusing. This mechanism is limited in separation ability according to the Knudsen equation for permeability shown below;

$$K = \frac{4\sqrt{8}\,\varepsilon f(r)}{3\sqrt{\pi}R^{1/2}M^{1/2}L\,K_g^2}\left(\frac{1}{T}\right)^{1/2} \qquad (1.1)$$

The separation factor is defined as the ratio of permeability of two components in a gas mixture. The ratio of permeabilities of two components diffusing according to the Knudsen diffusion mechanism simplifies to an equation relating the separation factor to the ratio of molecular weights of the two components to the power one half.

$$S = \left(\frac{M_2}{M_1}\right)^{1/2} \qquad (1.2)$$

This indicates that the Knudsen mechanism is limited to gas mixtures with large differences in molecular weights. For hydrogen and methane, the separation factor is limited to 2.8. Knudsen diffusion is explained in more detail in Section 5.1. The separation factor is explained in Section 4.4.

Molecular sieving is the selective passage of smaller molecules of the gas mixture based upon molecular diameter. It occurs when the pore size of the membrane layer is small enough to prevent the diffusion of the larger molecules. Molecular sieve membranes have been successfully manufactured out of carbon and zeolite. The sieving mechanism requires fine control of the pore size in the membrane layer and high temperatures to overcome the large activation energy required for diffusion to occur.

Partial condensation of some components of a gas mixture is a favourable separation mechanism due to the high flux of the condensed product that can be achieved. Ulhorn *et al* (1991) successfully used the partial condensation mechanism to separate a mixture of nitrogen and propylene at 263 K. The diffusion of non-condensing components was effectively reduced by the liquid blocking the pores of the membrane. A ceramic gamma-alumina membrane with pore sizes of 30 Å was used, and the separation factor obtained was 27. For the partial condensation mechanism, the extent of removal of the partially condensed component is limited by the component's condensation partial pressure at the system temperature (which can be determined from the Kelvin equation).

Selective adsorption of the more strongly adsorbed molecules of the gas mixture and surface diffusion of the molecules through the pores of the membrane layer occurs in the SSF membrane. Research into the addition of coatings on ceramic and alumina membrane is also being investigated as a means to employ the selective adsorption mechnism. The surface chemistry of the membrane layer can be engineered to match the adsorptive properties of the gas molecules making this mechanism very flexible. The following characteristics of the SSF membrane illustrate the specific advantages of this mechanism.

i. High partial pressures of the adsorbing components are not required to obtain significant separation. This is in contrast with non-porous membranes such as metallic and polymeric membranes that require high pressure gradients in order for separation to occur.
ii. Smaller molecules such as hydrogen are normally the desired products of membrane separation processes. The SSF membrane retains the smaller molecules on the high pressure side of the membrane. This eliminates the need for recompression of the gases to feed pressure. This is in contrast with other membrane processes.
iii. Surface flow membranes can produce high flow rates of diffusing components without high pressure gradients or ultra thin membrane layers. The surface flow of the adsorbing components contributes to the pressure gradient driving force and produces higher fluxes than other membranes.
iv. For membrane systems such as sieves and polymeric membranes, high temperatures are required to improve the separation and to increase flow rates. Low temperatures improve the separation capacity of SSF membranes allowing their operation at ambient conditions.
v. The adsorption of the more polar molecules on the surface on the membrane layer reduces the void space available for diffusion of the smaller molecules.

Membranes employing the selective adsorption mechanism require certain properties of the surface layer for effective separation. Rao and Sircar (1993) identified critical requirements for practical operation of these membranes.

a) To avoid high diffusion rates of the less strongly adsorbed molecules it is necessary to have controlled pore diameters. The diameter of the surface layer pores should not exceed three to four times the diameter of the largest molecule of the feed gas mixture to be separated.
b) The surface density (the ratio of pore area to surface area of the membrane layer) should not exceed 0.2 and the pores must be continuous across the thickness of the membrane layer.
c) The membrane layer thickness should not exceed 5 μm as permeation rate decreases with membrane thickness.
d) A porous support (meso or macroporous) is required to maintain the structural integrity of the membrane layer.

1.4 Pilot Scale Operation of an SSF Membrane System

To determine if laboratory scale tests were representative of industrial scale results a scale-up of the SSF membrane process was performed. A shell and tube module was designed and installed at the TOSCO refinery in California. The module consisted of a bundle of 106 cm membrane tubes. Membranes used in the laboratory are usually 30 cm long and a sweep gas is used to prevent concentration polarization. For the pilot scale tests no sweep gas was used. The feed stream (fed to the system at 5 atm) was a refinery waste gas consisting of approximately 14-30 % hydrogen and C_1 to C_3 impurities. A TSA (Temperature Swing Adsorption) unit with a bed of activated carbon was required upstream of the membrane system to remove any heavier hydrocarbons such as C_5^+ (pentane, pentene, hexane, etc) and ring compounds. The TSA unit also removed water with a layer of activated alumina. The feed flow rate varied from 0.57 to 0.95 mg mol/cm^2/s. The concentrations of methane, ethane, ethylene, propane, and propylene varied from 35-50%, 7-15%, 5-7%, 2-7% and 2-7%. The temperature varied from 283 to 303 K. The module was continually operated for 6 months without any degradation in the separation performance.

The SSF membrane system was able to recover an average of 60% of the hydrogen. The rejection rates for methane, ethane, ethylene, propane, and propylene at this recovery rate were approximately 50%, 87%, 90%, 93% and 95%. [Naheiri, 1997] These results were very similar to those found in the laboratory with a single 30 cm membrane. The composition of the retentate stream from the laboratory scale membrane system was approximately 51% hydrogen, 42% methane, 2% ethane, 2% ethylene, 2% propane and 1% propylene.

1.5 Hydrogen-Hydrocarbon Separations

The most common method used to separate hydrogen-hydrocarbon mixtures and recover hydrogen is PSA (Pressure Swing Adsorption). A PSA unit is capable of producing the high purity hydrogen (99.5%) required in order to reduce purge from hydroprocessing reactors that is necessary to control non-hydrogen components. The inert compounds, which consist of mainly light hydrocarbons, are easily removed from hydrogen-hydrocarbon mixtures by the preferential adsorption of the hydrocarbons on the adsorbent beds of the PSA system. Desorption of the adsorbent beds at low pressure produces a purge gas stream of approximately 40% hydrogen that is normally used as fuel gas for various reactors within the refinery. PSA units are used to purify off gas streams from hydrotreating processes that are about 70% H_2.

PSA processes are also used in hydrogen plants to purify the production stream from the shift converter, which consists of mainly hydrogen, unreacted methane, carbon monoxide and carbon dioxide. PSA units are limited in their capacity to recover hydrogen especially if the product hydrogen must be delivered at high pressure. High desorption pressures (i.e. 450 psig compared to 250 psig) reduces hydrogen recovery due to the decreased driving force for desorption of hydrogen from the adsorbent beds of the PSA unit. The recovery rates of

hydrogen from PSA units can range from 60-80% depending mainly on desorption pressure.

Competing hydrogen-hydrocarbon separation technologies are cryogenic distillation and oil scrubbing. Cryogenic distillation takes advantage of the differences in volatilities of the feed components to recover hydrogen. Hydrogen has a high volatility compared to methane and other hydrocarbons and therefore can be recovered at relatively high purity (95% with 90% recovery). The hydrocarbon impurities are condensed by Joule-Thompson refrigeration derived by throttling the condensed liquid hydrocarbons. Cryogenic distillation is most economical with high throughputs or when hydrocarbon components must be isolated. The disadvantages of cryogenic separation are the power requirements and lack of flexibility in processing varying feed compositions. The process is considered less reliable than PSA units or membrane systems [Peramanu, 1998].

Oil scrubbing or the sponge oil process is the adsorption of light hydrocarbons from a hydrogen stream into hydrocarbon solvents. The main advantage of this process is that it can operate effectively at high feed pressures and the hydrogen leaves near feed pressure, reducing makeup compression requirements. The process is capable of moderate purity (85-95%) and high recovery (85-95%). Pretreatment of the feed is usually not required, as the recirculating solvent is normally insensitive to the impurities present. Oil scrubbing is not an economical process for low pressure feed streams.

1.5 Economic Advantages of Membranes for Hydrogen Recovery

Membrane processes for the separation of hydrogen are now widespread in the ammonia and refinery industries and to a lesser extent the petrochemical industry [Noble and Stern, 1995]. Most studies demonstrate the economic advantages of membrane systems by comparing them to competing technologies

such as PSA, cryogenic distillation and oil scrubbing. The separation qualities of each system are demonstrated by using feed streams from hydroprocessing units that contain approximately 70% hydrogen. The selectivity of the SSF membrane is not suited for the purification of hydrogen streams with these concentrations, however these studies are useful in demonstrating the economic advantages of membrane systems as a whole.

Hydrogen is produced by naptha and steam-methane reforming and consumed in a variety of processes within refineries. Precise assessment of the economics of membrane processes for hydrogen recovery isn't possible due to operating conditions being highly site specific. However, several studies have been carried out comparing competing technologies with membrane systems and the general economic advantages of membrane processes can be illustrated.

Dupont developed a pilot size scale membrane system to recover hydrogen from hydrodesulfurization streams with 60-75% hydrogen, reformer off gas process streams with 80% hydrogen and FCC tail gas streams with 20% hydrogen. All studies were conducted at Cononco's refinery in Ponca City. The membranes used were hollow fiber, polymeric membranes [Heyd, 1986].

The use of the hollow fiber permeators resulted in a 90% recovery of the hydrogen with 98% purity at a permeate pressure of 315 psig and a feed of 75% hydrogen. Results showed that increasing the permeate pressure decreased product purity and product recovery. It was also shown that a reduction in permeate pressure increased separation due to the increase in driving force for permeation of the hydrogen. Increasing the driving force then decreased the cost of the membranes due to the reduced need for membrane surface area. The economic study compared the membrane process with a PSA system, cryogenic distillation system and a steam-methane reforming plant for the direct production of hydrogen for reference. The basis for the comparison was the recovery of 75% of the hydrogen in a 15 MMSCF/day stream at 98% purity and product pressure of 315 psig. Taking into account any compression and pretreatment costs the results showed that the membrane capital investment costs were 65 to

75% below PSA and cryogenic distillation. Recovery costs were 25-30% below PSA and cryogenics and 15% below incremental steam-methane reforming costs assuming a price of $3.25/MMBTU for natural gas. A graph summarizing the results is available in Figure 1.2.

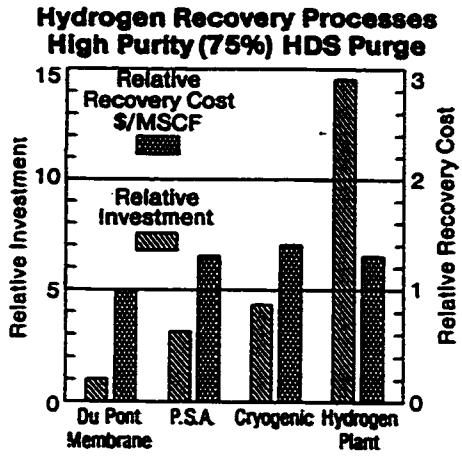

Figure 1.2: Costs and investments of high-purity hydrogen recovery from a hydro-desulfurization off-gas [Heyd, 1986].

The Fluor Corporation [Noble and Stern, 1995] compared two PSA processes with a polymeric membrane process for the recovery of hydrogen from a hydrotreater off gas stream. The stream was 72% hydrogen at 815 psig with a flow rate of 7 MMSCF/day. The membrane system was capable of producing 93% purity hydrogen at 265 psig, recovering 81%. The PSA processes delivered 99.5% hydrogen at pressures of 465 and 265 psig and recoveries of 60 and 80%. The cost analysis showed that the capital cost of the membrane system was 51 and 62% lower than the costs of the PSA systems. Conclusions were that if high purity hydrogen is not required (having low purity hydrogen may result in higher reactor purge rates and thus higher use rates) then the membrane system offers the best combination of installed cost, operational cost and ease of operation.

Ube industries investigated the use of a polyamide membrane system to recover hydrogen from refinery off gas. They compared the membrane system

with an adsorption and a cryogenic distillation system. The operation of the membrane system at two temperatures, 80 and 120°C, resulted in 97 and 96% hydrogen purity and 87 and 91% hydrogen recovery. The adsorption system and the cryogenic system produced streams with 98 and 96% hydrogen purity and 73 and 90% hydrogen recovery. The power consumption and the space requirements for the membrane systems were found to be significantly less than for the competing technologies resulting in 50 and 70% reductions in the cost requirements for the membrane system [Noble and Stern, 1995].

A study published in 1990 by Liquid Air Engineering investigated a membrane process to recover hydrogen from a gas oil hydrotreater stream. The membrane process produced 95% pure hydrogen and recovered 75% of the total hydrogen from a feed stream of 71% hydrogen. The product stream was then used in a hydroprocessing unit. Benefits of the membrane system were improved product quality, improved catalyst life, reduced power consumption, more feedstock flexibility, and a payback time of only 1.7 years for the membrane system [Noble and Stern, 1995].

CHAPTER 2.0

LITERATURE REVIEW

2.1 Membrane Technology

A membrane process uses a permselective barrier to separate a feed stream into two streams, a retentate stream and a permeate stream. The retentate stream consists of the components that remain on the feed side of the membrane layer. The permeate stream is made up of the components that cross the permselective barrier.

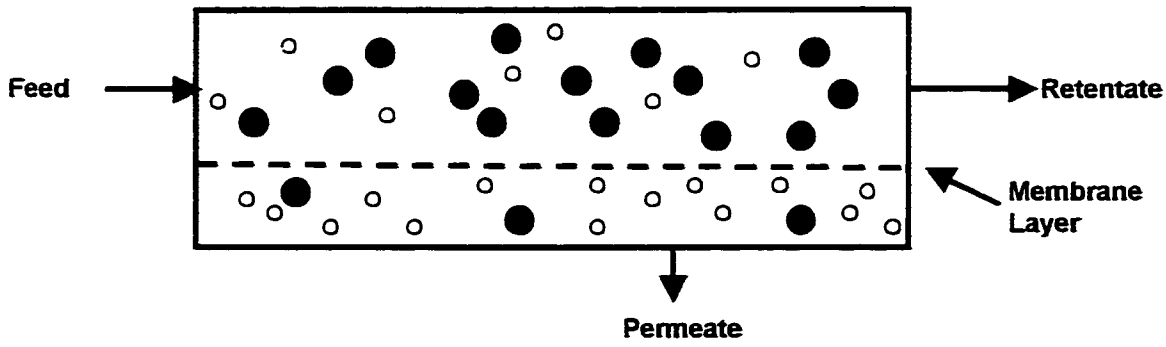

Figure 2.1: Schematic representation of a membrane process.

The driving force for permeation in a membrane may be a difference in pressure, concentration or electric potential. The objectives of a membrane separation process may be a combination of the following:

- Concentration: enrichment of a desired component that is present in low concentrations
- Purification: removal of undesirable impurities
- Fractionation: separation of a mixture into two desired components
- Reaction mediation: continuous removal of reactants as a means to drive the reaction

2.2 Classification of Membrane Processes

Membrane separation processes can be divided into two groups: processes with liquid feeds and processes with gas phase feeds. The charts in Figure 2.2 a and b illustrate the most common membrane processes, their driving forces for separation and their principles of separation.

2.2.1 Membranes with Liquid Feeds

The first membranes developed used liquid phase feeds to investigate the separation properties of different membrane materials. Organic materials such as nitrocellulose were tested as a means to purify drinking water. This began the commercial use of microfiltration technology in approximately 1927 [Noble and Stern, 1995]. Reverse osmosis and ultrafiltration followed. Table 1.1 gives examples types of liquid feed separation process.

Table 2.1: Example membrane separation processes for liquid feeds.

Process	Example
Ultrafiltration	Automotive industry: removal of paint from wash water
Microfiltration	Beverage industry: clarification of fruit juices, wine and beer
Dialysis	Hemodialysis: removal of metabolic wastes from blood
Reverse Osmosis	Desalination of brackish and seawater
Electrodialysis	Desalination of water

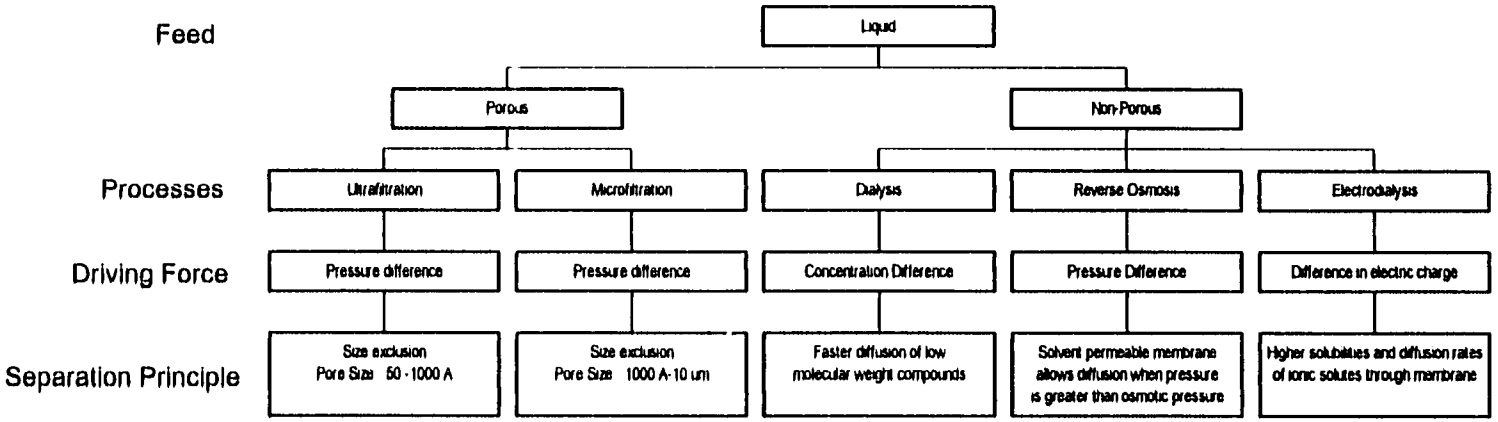

Figure 2.2 a): Membrane separation processes for liquid feeds

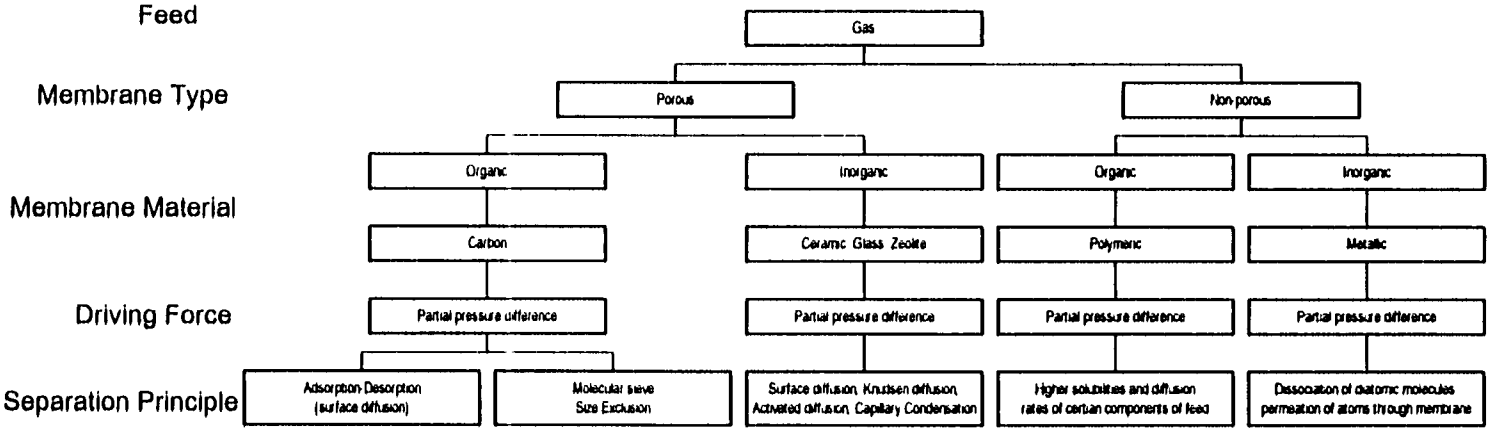

Figure 2.2 b): Membrane separation processes for gas feeds

2.2.2 Membranes with Gas Phase Feeds

The technology for the separation of gaseous mixtures in membranes is less developed than the separation of liquid feeds. Generally there is a trade off between purity and permeation rate in membranes used for gas separation. There is also the concern of membrane layer stability.

Membranes with gas phase feeds can be divided into two distinct groups: porous and non-porous membranes. These groups and the different types of membranes that exist in each group are shown in Figure 2.2 b. Each type of membrane and examples of their applications are explained below.

Polymeric Membranes

The most developed technology for gas separation is the use of polymeric membranes. The membrane layer consists of a polymer coating that solubilizes the smaller, lower molecular weight molecules in the gas mixture. These molecules then diffuse to the low pressure side of the membrane leaving the larger molecules of lower solubilities and lower diffusion rates on the high pressure side of the membrane. This separation mechanism has been termed the "solution-diffusion" mechanism. Polymers are classified as glassy or rubbery. The permeability of rubbery polymers allows for faster diffusion rates however separation factors tend to be lower. The mobility of the polymeric chains within the structure of the rubbery polymer layer allows the diffusing molecules to move faster through the layer. The structure of glassy polymers is rigid and therefore more selective and less permeable [Mulder, 1996]. Examples of some polymers used are polytrimethylsilylpropyne (PTMSP) and polyethersulfanone. Research into improving the performance of these membranes has resulted in two main surface treatments to improve selectivity and stability while keeping high permeation rates. These surface treatments are classified as reactive and physical (antiplasticization). Air Products and Chemicals Inc. have studied reactive fluorination of PTMSP and have found that with a slight decrease in the

permeation rate the membrane layer is less sensitive to high molecular weight organic compounds in the feed and selectivity improves [Mulder, 1996]. Antiplasticization of polymers has been found to be less attractive than reactive treatments because the antiplasticization agents are removed from the layer by the high passage rates of the permeating gases [Mulder, 1996].

There are two types of polymeric membranes commercially available for hydrogen recovery: asymmetric and composite. Two layers of a single polymer make up an asymmetric membrane. There is a dense layer, which performs the separation, and a microporous substrate layer that mechanically supports the membrane. Composite membranes consist of two different polymers; a separation polymer coated on a substrate polymer. Composite membranes allow the selection of a polymer based upon its separation abilities for a given feed stream without regard for mechanical abilities [Miller and Stoecker, 1989].

The use of the polymer ethylcelluose has been commercially developed for air separation by several membrane manufacturing companies. Membrane systems are attractive for processes that require 95% nitrogen however PSA is the dominant technology for 98% nitrogen.

Metallic Membranes

The use of metallic membranes such as palladium or silver alloys have received attention of late due to their complete selective permeation for hydrogen or oxygen. The process occurs by first adsorption of the molecules on the surface of the metal. The palladium or silver then acts as a catalyst, which dissociates the diatomic molecules. Hydrogen or oxygen diffuses through the metal as atoms, reassociates and desorbs on the low pressure side of the membrane. Palladium membranes are alloyed with Ag, or Ni to prevent embrittlement of the palladium. The temperature requirement to drive the dissociation reaction and prevent failure of the metallic layer is above 250°C. The use of metallic membranes has been investigated for the development of catalytic membrane reactors. These reactors

involve simultaneous reaction to form hydrogen from steam methane reforming (SMR) and separation of the hydrogen product to drive the reaction forward. Concerns with this process are catalyst poisoning (with silver alloy membranes), durability and cost [Noble and Stern, 1995]. Recent research conducted by Roy (1998) has shown that the use of high flux palladium membranes in a pilot scale fluidized bed-SMR reactor produced a 15% improvement over the performance of a conventional equilibrium SMR reactor. Additionally, the flux of hydrogen was 10-15 times greater than the flux through metallic membranes reported by other researchers.

Ceramic, Glass and Zeolite Membranes

Research into the use of inorganic porous membranes for gas separation has increased due to the greater stability of these membranes and their superior performance at high temperatures compared to polymeric membranes. Typical pore sizes of glass membranes are less than 40 Å. The glass membranes are prepared by etching out pores with acid solutions. Ceramic membranes have been prepared with pore sizes of 25 Å [Noble and Stern, 1995]. The primary separation mechanism for glass and ceramic membranes is Knudsen diffusion which separates gas molecules based upon difference in molecular weights. Separation factors that can be achieved with Knudsen diffusion are limited and therefore there is presently research being conducted into improving the properties of ceramic and glass membranes. To improve separation while taking advantage of their stability and their ability to operate at high temperatures, research has been conducted into the development of membranes with top layers to improve separation. Research conducted thus far has shown that there is a trade off between permeation rate and selectivity of membranes with top layers. The addition of a top layer results in a decrease in pore size and therefore an increase in selectivity. However, decreased pore size also decreases the permeation rate of gases through the membrane. A decreased permeation

requires that the size of the membrane surface area be increased which then increases the membrane cost.

Zeolite membranes have been prepared with pore sizes small enough to act as molecular sieves (4Å) [Noble and Stern, 1995]. The use of zeolite in membranes is attractive due to the uniform structure that can be achieved in the membrane layer and the high separation factors that can be achieved through molecular sieving.

The technique used to deposit porous top layers on ceramic, glass or alumina membranes is named the sol-gel process. The addition of a polymeric macroporous top layer on ceramic membrane was investigted as a means to increase ceramic selectivity without compromising permeation rate. Separation occurred due to the combination of the solution-diffusion mechanism and activated diffusion of the smaller, lower molecular weight molecules through the membrane layer. Separation factors improved with temperature because of the increased energy supplied for activated diffusion to occur. [deLange, 1995]. The sol-gel process was also used to deposit a layer of SiO_2 on top of a 40Å (pore size) alumina tubular membrane. The separation factor for H_2/N_2 separation was reported as 190 at 450°C [Goldsmith *et al*, 1992]. The permeation of hydrogen was one order of magnitude less than for the polymeric top layer. The best separation factor achieved for H_2/CH_4 separation (H_2/N_2 not reported) with the polymeric layer was 28 at 200°C.

Carbon Membranes

Carbon molecular sieve membranes formed by the pyrolysis of polymer layers on the surface of a porous support have been shown to give selectivities of hydrogen 1000 times over methane. [Noble and Stern, 1995] The primary problem that exists with these membranes is the possibility of condensation of molecules in the feed gas, such as water, and high temperature requirements.

The SSF membrane developed by Air Products can be classified as a porous carbon membrane. The separation mechanism of the SSF membrane is unique and has been classified as an adsorption-surface diffusion mechanism. The adsorption of larger more polar molecules on the surface of the membrane helps to block the permeation of smaller molecules and improve separation. This mechanism was explained in Section 1.2.

2.3 Membrane Modules

Membrane modules are required in order to apply membranes on a technical scale. There are two main classes of membrane modules: tubular and flat. Tubular membrane modules consist of the shell-and-tube, capillary and hollow fiber configurations. These are shown in Figure 2.3 and 2.4. Due to the ease of cleaning, shell-and-tube configurations are used when frequent membrane fouling occurs. Hollow fiber configurations are most popular for polymeric membranes. The feed enters on the outside of the fibers and the permeate exits through the hollow side of the fibers. Hollow fibers give the highest packing density of all the tubular modules. Capillaries have dimensions between those of the shell-and-tube and hollow fiber membranes. Ultrafiltration and microfiltration processes employ the capillary module with the pore size ranging along the length of the capillaries.

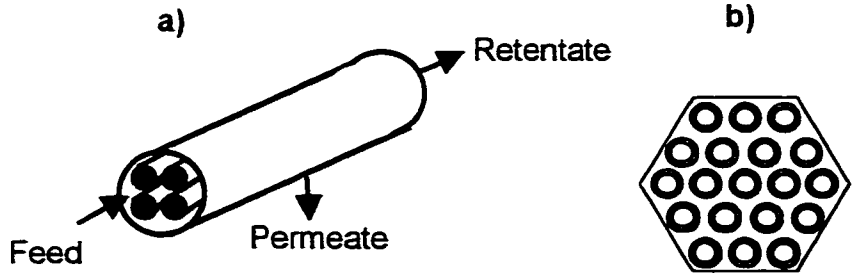

Figure 2.3: Shell and tube membrane module. **a)** Tubular membranes within a shell casing. **b)** Example support face plate.

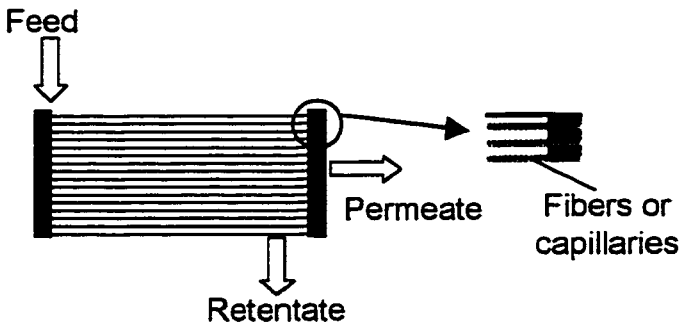

Figure 2.4: Hollow fiber and capillary membrane modules.

The flat modules consist of plate and frame and spiral wound configurations (Figures 2.5 and 2.6). In the plate and frame configuration the feed stream is fed between two plates of membranes facing each other with a spacer situated between the membrane layers. The spacer helps to improve mass transfer and prevent concentration polarization. The plate and frame module is used in electrodialysis and is popular for inorganic membranes. The spiral wound module consists of a sandwich of flat sheet membrane spacers and porous material wrapped around a central permeate collecting tube. Spiral wound modules are also used for polymeric membranes.

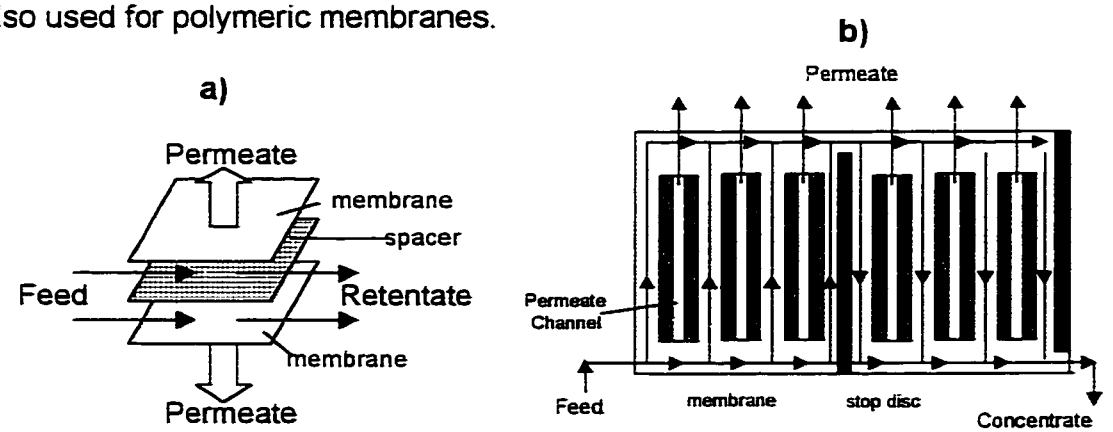

Figure 2.5: Plate and frame membrane module. **a)** Two-plate schematic. **b)** Flow pattern in a plate and frame membrane module.

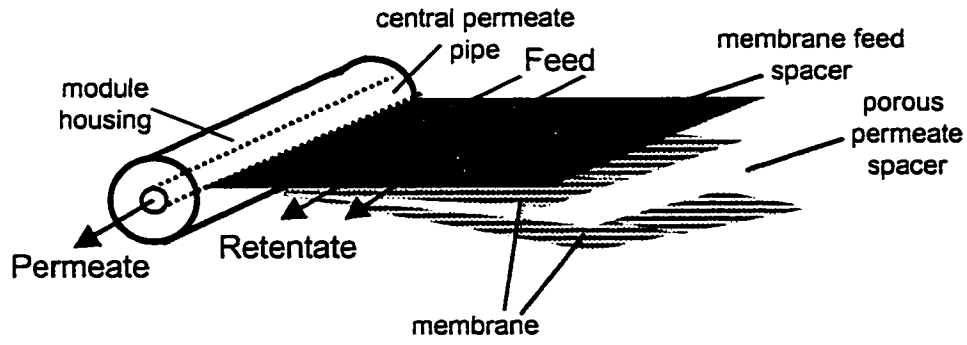

Figure 2.6: Spiral wound membrane module

2.4 Preparation of SSF Membranes

The SSF membrane which consists of essentially an active layer coated on the inside of a porous alumina tube is formed by carbonizing a layer of polymer on to the surface of a porous support. Parrillo *et al*, 1997 and Rao *et al*, 1993 describe the preparation process for the SSF membranes. A tube of macroporous alumina (pore size ~0.7 μm) is coated with a layer of latex polymer and spun to remove any excess. The polymer used is poly (vinylidene chloride)-acrylate terpolymer latex. The polymer solution is prepared by mixing the polymer beads (0.1-0.4 μm) in a solution with water (55% solids). After drying at room temperature the coated support is further dried under nitrogen at 150 °C for a few minutes followed by heating under a nitrogen purge at 1000 °C. The temperature is ramped at a rate of approximately 1 °C/min during the heating period. After holding at 1000 °C for three hours, the temperature is then reduced to ambient at a rate of approximately 10 °C/min while still under nitrogen. The result is a carbon layer of approximately 2-3μm thickness. The layer is formed by crosslinking and carbonization of the polymer coating. Only one coat of the polymer and a single heating step are used. The one coat membranes have pore sizes that range from 6-7 Å.

2.4.1 Electrochemistry of Activated Carbon

The carbon layer formed by crosslinking and carbonization of the polymer coating during preparation of SSF membranes results in a layer of microcrystalline carbon similar in properties to activated carbon. The following paragraphs describe characteristics of activated carbon that account for its adsorptive capabilities.

Microcrystalline carbon has pores spaces interspersed between ordered, stacked layers of carbon. The layers of carbon, characteristic of graphite, are arranged as stacked hexagonal sheets. The layers, also referred to as basal planes, are held together by van der Waals forces. The groupings of graphite-like layers in microcrystalline carbon are called crystallines. These form short-range layers of hexagonal carbons that differ in orientation and arrange to form pore spaces. The structure of microcrystalline carbon is depicted in Figure 2.7. The edges of the basal planes may contain various defects, dislocations and discontinuities that create several kinds of unsaturated sites within the microcrystalline carbon.

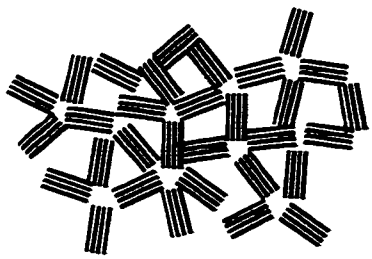

Figure 2.7: Structure of microcrystalline carbon.

The termination of the regular array of atoms comprises most of the material and the unsaturated sites present on the pore edges are capable of reacting with other elements. Research conducted to determine the chemical nature of the unsaturated sites suggest that functional groups such as carboxyl, phenol, quinone, lactone and anhydride are present at the edges of the sites [Golden *et al*, 1983]. These functional groups are depicted in Figure 2.8.

Physical adsorption of certain species occurs at these unsaturated sites. It is associated with heats of adsorption generally less than 10 kcal/mol, reversible adsorption and small activation energies for desorption. Chemical adsorption or chemisorption, occurs when there is a change in the chemical make-up of the edge sites such as electron sharing or electron exchange. This results in higher heats of adsorption and high activation energies for desorption. Chemisorption is also referred to as irreversible adsorption. The commercial use of activated carbon is based upon its ability to either chemically or physically adsorb certain species. For example, chemical adsorption may occur with the functional groups in Figure 2.8 through chemical reactions with the sorbate molecules or physical adorption may occur through van der Waals forces.

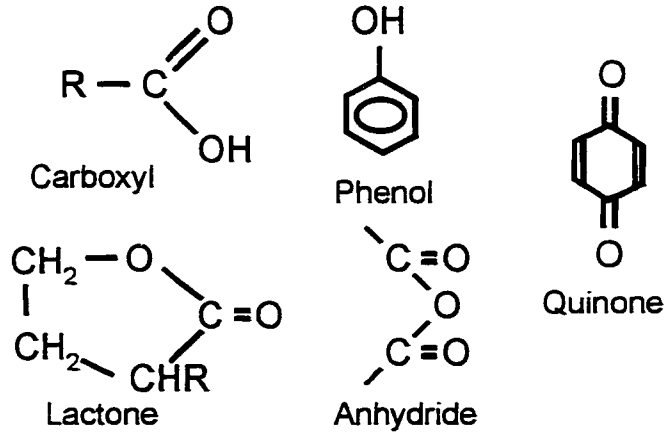

Figure 2.8: Examples of functional groups found on activated carbon edge sites.

Deactivation of crystalline carbon adsorbents commonly occurs due to a loss in crystallinity. This can then result in a decrease in mass transfer through the adsorbent. Irreversible breakdown of the crystal structure may occur due to the chemical adsorption of reactive hydrocarbons such as olefins. Thermal regeneration may remove the chemically adsorbed species, however a decline in the useful capacity of the adsorbent may occur [Ruthven, 1984].

2.5 Previous Studies with SSF Membranes

Rao and Sicar of Air Products and Chemicals Inc. introduced the SSF membrane in a publication in 1993. The paper included a detailed description of the patented preparation procedure, explained the SSF separation mechanism and introduced applications for the membrane. A plate and frame module was built to test the recovery of hydrogen from a waste gas stream. Each membrane plate was prepared by coating and carbonizing five layers of polymer. The results indicated that at –11.0 °C, the membrane was capable of rejecting 100% butane, 92% propane, 67.5% ethane and 36% methane. The hydrogen recovery was 63% at a feed pressure of 4.3 atm. The suggested application of this system is illustrated in Figure 2.9. It was reported that the use of the SSF membrane system for the recovery of hydrogen from a waste gas stream and purification of hydrogen in a PSA unit would result in an overall recovery of 43% of the hydrogen in the waste gas stream. Without this system the hydrogen would simply be used as fuel. The economics of this process were not reported.

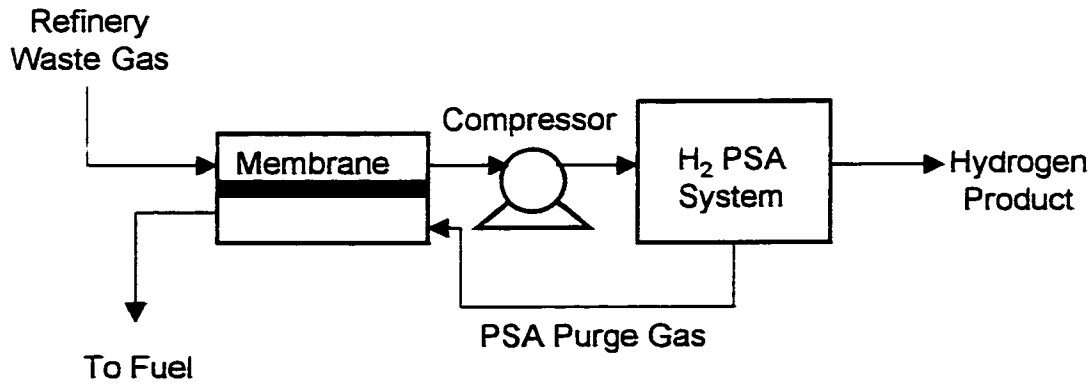

Figure 2.9: Flow schematic for hydrogen production from a refinery waste gas in a SSF membrane-PSA system.

To determine the pore size of the SSF membrane layer, atomic force microscopy (AFM) and scanning tunnelling microscopy (STM) scans were conducted [Rao and Sircar, 1996]. Neither scannning technique could quantitatively measure the pore size of the SSF membrane because the pore

diameter was comparable to the surface roughness. However from AFM it was indicated that the size of a depression, assuming it to be a pore was approximately 5.3Å. STM indicated a typical pore size to be 4.5Å. To obtain a quantitative measure of pore size in the SSF membrane, estimations based upon comparision of values in the literature were made. Using values for methane diffusivity as a function of pore size and comparing to diffusivities of methane in the SSF membranes the pore size distribution was determined. Data was collected from the literature for sizes 10 to 20 000Å. Results indicated that the pore sizes of SSF membranes with multi-layer coatings were 5-6Å. Results also indicated that a very small change in pore size such as a few angstroms could result in a change in diffusivity by an order of magnitude. The membranes used in the above study were flat disc membranes.

Studies were also conducted to determine the type of diffusion occurring in SSF membranes. Knudsen diffusion was used to predict the pore size of the membrane based upon pure gas fluxes for helium. Helium was assumed to be non-adsorbing and therefore would have followed the equation for Knudsen diffusion through the SSF membrane. The equation predicted that the pore size of the membrane was 0.018Å at 273 K. This value was clearly erroneous and therefore it was concluded that Knudsen diffusion was not occurring in the membrane. The diffusion type was assumed to be activated diffusion which dominates in pore sizes less that 10 Å. It was also suggested that with activated diffusion being the only type of diffusion occurring, the only separation mechanism would be selective adsorption. In this case the selective passage of smaller and less strongly adsorbed molecules through the void space between adsorbed molecules would not exist [Rao and Sircar, 1996].

Anand *et al* (1995) published the results of the operation of a tubular SSF membrane and compared separation efficiencies with Poly-Trimethylsilylpropyne (PTMSP) membranes. The SSF membrane was shown to produce higher rejection values than the glassy polymeric membrane at the same conditions.

The feeds studied were an FCC off-gas at 3 atm and a PSA purge gas at 4 atm. Their concentrations were 20% H_2, 20% CH_4, 8% C_2H_4, 8% C_2H_6, 29% C_3H_6, 15% C_3H_8 and 35% H_2, 55% CO_2, and 10% CH_4 respectively. At a recovery rate of 60% hydrogen, the rejection rates for all hydrocarbons except for CO_2 and CH_4 were higher than 94% for the SSF membrane. The rejection rates for the polymeric membrane ranged from 72% to 86%.

Paranjape (1997) studied the separation of mixtures of hydrogen and hydrogen sulfide for the recovery of hydrogen at the University of Calgary. Initial experiments were conducted with hydrogen and carbon dioxide mixtures to test the laboratory scale shell and tube apparatus and to act as a comparison study for the hydrogen-hydrogen sulfide experiments. It was found that the separation factors for hydrogen sulfide separation experiments were much higher than for carbon dioxide. The separation factors for the hydrogen sulfide experiments in SSF membranes (7-15) were higher than for ceramic membranes (1-2) and Vycor glass (1-3). The study determined that the SSF membrane could be used to separate high concentration mixtures of H_2S and the surface layer properties were not severely affected by the H_2S.

Air Products and Chemicals Inc. conducted additional hydrogen-hydrogen sulfide separation experiments. They determined that a two-stage operation could effectively separate an equimolar mixture at room temperature and feed pressures of 0.24 to 1.5 MPa. A recovery of 80% of the hydrogen and 98% rejection of H_2S was attained. The two stage process consisted of the permeate stream from the first stage being fed to the second stage. The high pressure retentate was then mixed with the feed to the first stage. Two product streams, enriched hydrogen and H_2S waste, were produced.

To determine the performance of the SSF membrane at high temperatures, a study was conducted to separate hydrogen and carbon dioxide at temperatures ranging from ambient to 150°C. The apparatus used was the laboratory scale shell and tube apparatus in the Industrial Hydrogen Chair Laboratory at the

University of Calgary. Results showed that there was a significant decrease in the separation potential of the membrane at high temperatures [Smith, 1998]. This was due the decreased physical adsorption of the carbon dioxide at high temperatures.

CHAPTER 3.0

MATERIALS AND METHODS

3.1 Apparatus

The experimental SSF membrane apparatus was designed and assembled in the Industrial Hydrogen Chair Laboratory at the University of Calgary in 1996. The initial studies conducted with the membrane apparatus were separations of hydrogen and carbon dioxide and hydrogen and hydrogen sulfide, carried out by Paranjape (1997). It was required that the experiments with hydrogen sulfide be carried out in a hydrogen-safe laboratory and therefore it was essential that the apparatus be easily transported. It also required the use of materials that would not corrode with the use of high concentrations of hydrogen sulfide. Stainless steel tubing (SS 316, 0.25 in) and standard Swagelock unions (SS 400-6) and elbows (SS 400-9) were used in the construction of the apparatus. Modifications of the apparatus were required for the high temperature experiments and the low temperature experiments in this study. The two experimental set-ups are shown in Figures 3.1 and 3.2.

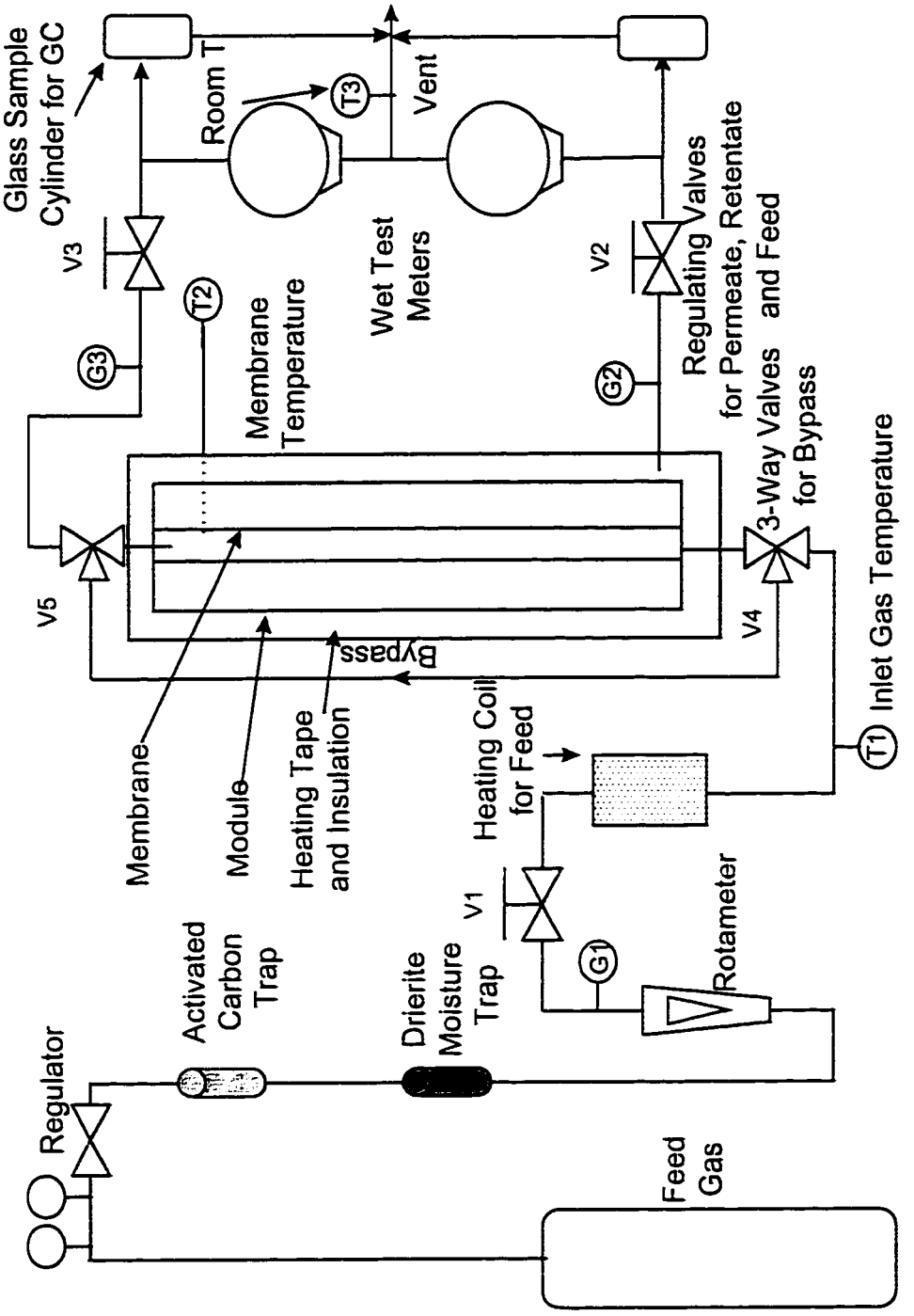

Figure 3.1: High temperature apparatus

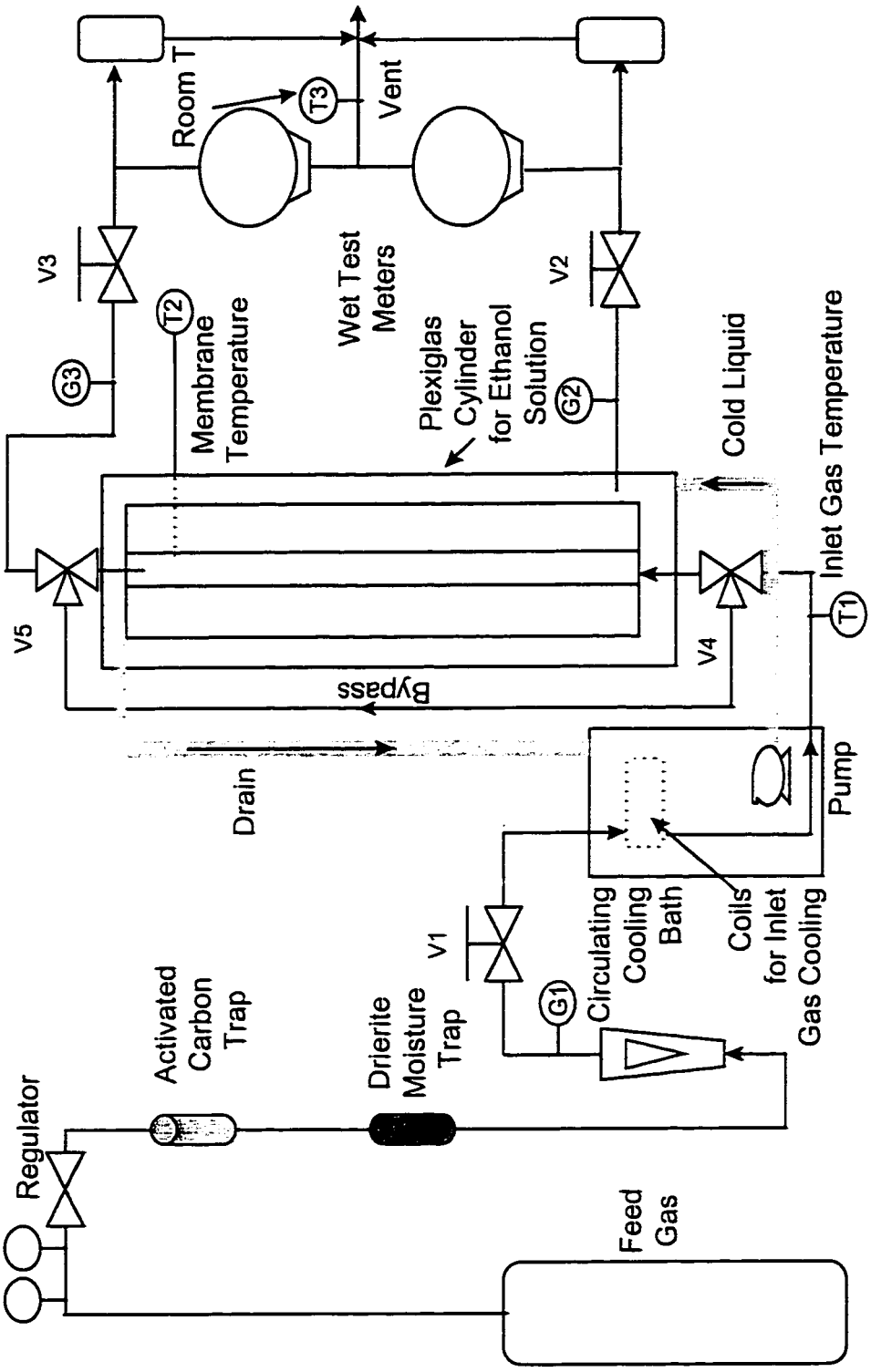

Figure 3.2: Low temperature apparatus

3.1.1 Membranes

The membrane used in Paranjape's study was not used in this study due to the decrease in permeability of the membrane. The membrane had been stored under inert nitrogen pressure but over a year had passed since the membrane had been used. Regeneration of this membrane had been attempted by Smith (1998) yet was not successful. Smith used a new membrane (S-1) in November 1998 to investigate high temperature separations. Preliminary permeability tests conducted with (S-1) gave very high flow rates and hence the membrane was assumed damaged. This membrane was not used for the hydrogen and methane separation tests. A third membrane was used in the investigation irreversible adsorption (M-1). Subsequent tests with Smith's membrane showed that the membrane was not damaged and the leak occurred due to the failure of an o-ring during high temperature experiments. S-1 was also used in irreversible adsorption tests. A fourth membrane was used for the hydrogen and methane separation tests (M-2).

3.1.2 Membrane module

The membrane module was a shell and tube design with a single SSF membrane. The orientation of the module was vertical, as this is the orientation used for commercial scale tube bundles. Horizontal orientation is not recommended due to the risk of tube buckling. The module shell provided by Air Products had a diameter of 2.3 cm (1 in) and a length of 40 cm (16 in). The membranes consisted of a porous tube with the membrane layer coating the bore side of the tube. The dimensions of the membrane tubes used for this study were:

Outer diameter	0.96 cm
Inner diameter	0.5 cm
Length	30.0 cm
Thickness of support	2.2 mm
Membrane surface area	47.1 cm^2

Air Products prepared the membranes using the patented procedure outlined in Section 2.4. Three different membranes were used in this study (S-1, M-1 and M-2). The first two membranes were used to investigate irreversible adsorption on the surface of the carbon layer (described in section 3.3). The third membrane was used in all hydrogen-methane separation tests.

Total leak-proof sealing was required for the module, as a very small leak could produce bulk flow of the feed gas to the permeate side of the membrane. Sealing the membrane within the module shell was especially a problem in carrying out the high temperature experiments. Ultra-torr fittings by CAJON with Viton o-rings were initially used to seal the membrane to the module shell, however it was found that leaks would occur after approximately 10 hours of use at high temperatures, and feed pressures ranging from 20 to 150 psig. It was also found that the Viton would degrade over time as its temperature limit was only 200°C. For the membrane to reach as high as 165°C the heating surface would exceed 200°C causing the Viton to melt and partially vapourize. The use of stainless steel Swagelock fittings with Teflon ferrules was suggested by Air Products to eliminate leaks. Swagelock fittings (SS-400-6) were used to seal the bottom of the membrane tube (where the feed first enters the membrane) to the module. Once the Swagelock fittings were sealed to the membrane, the membrane could only be removed by cutting the Teflon ferrules. The CAJON fittings were used at the top of the membrane module where the heating tape was no longer in contact. It was necessary to use the CAJON fittings at one end of the membrane as they allowed the membrane to be removed by simply pulling the tube out. Figure 3.3 shows how the membrane was sealed to the module shell. Part b) of Figure 3.3 shows how the CAJON fitting sealed the membrane, a), to the module through the use of Viton o-rings. The o-rings were compressed against the tube of the membrane by the stainless steel ferrule as the round nut was tightened. The second end of the fitting sealed

the 3/8 in tubing (part i, figure d) of the module in the same manner. Figure c) shows the Swagelock fitting. Teflon ferrules were used to seal one end of the membrane to a piece of 3/8 in tubing. Two Teflon ferrules were used on the membrane side to prevent the fitting from cracking the porous support. The module was then sealed from the atmosphere by tightening the large stainless steel nuts against 1 1/4 in Viton o-rings placed on either end of the module shell (figure d). Part ii of figure d) is repeated on the upstream side of the membrane. The 3/8 in tubing protruding from the module shell was attached to the remaining parts of the membrane apparatus through standard Swagelock unions. Countercurrent operation of the system was used without a sweep gas on the permeate side of the membrane. Figure 3.3 d) shows how the position of the permeate outlet position creates countercurrent flow.

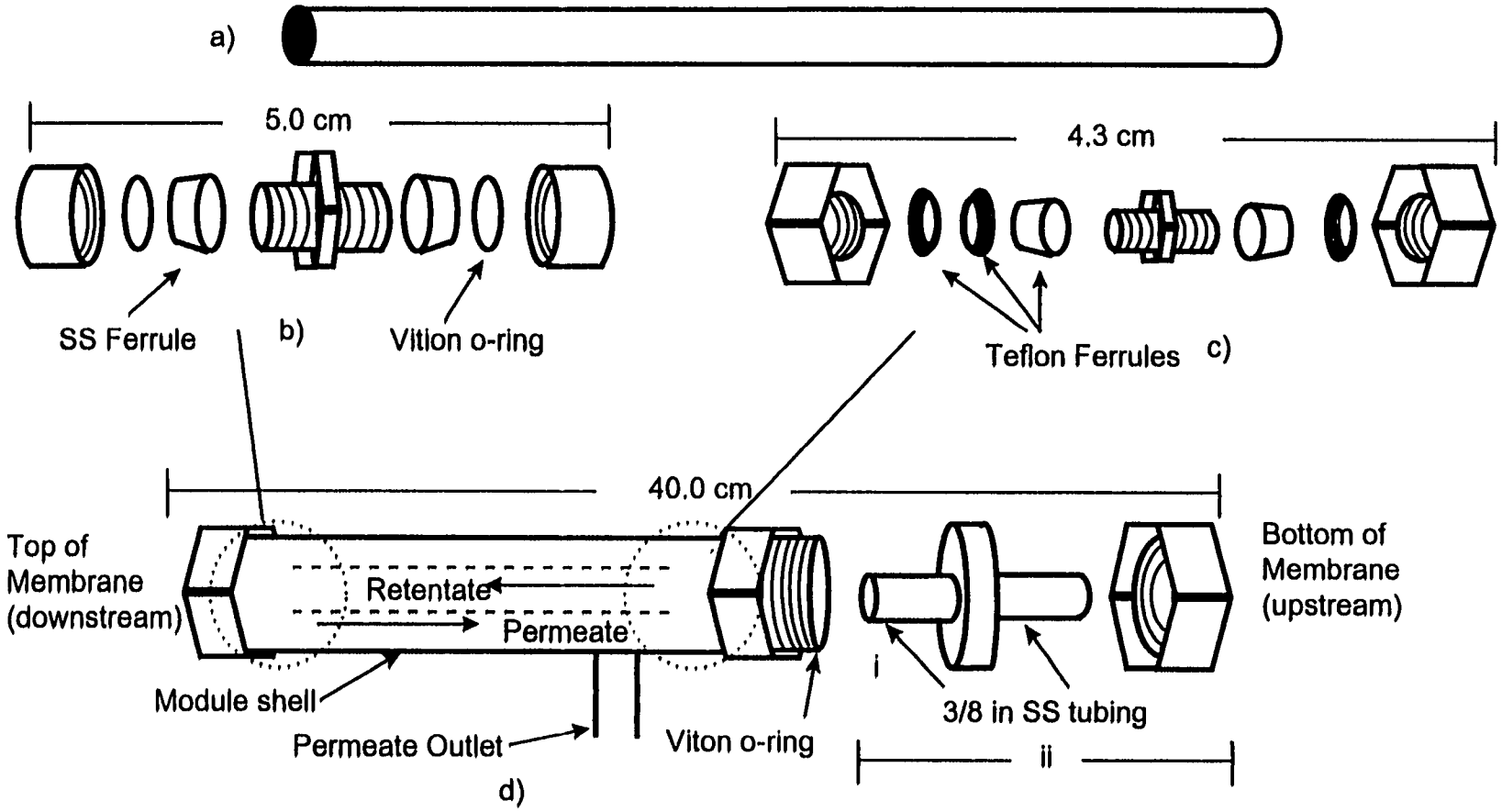

Figure 3.3: Assembly of the SSF membrane module

3.1.3 Traps

A Drierite dessicant (anhydrous $CaSO_4$, 8 mesh, colour indicator) and an activated carbon trap (12 to 20 mesh) were used upstream of the membrane to adsorb moisture and heavy hydrocarbons (C_5^{+}, ring compounds) that could irreversibly adsorb on to the membrane surface and cause a decrease in permeability or separation potential. Sintered metal fittings were used at the inlets and outlets of the traps to act as filters. An in-line filter was also used immediately upstream of the membrane to trap any dust particles (not shown on Figures 3.1 and 3.2.

3.1.4 Instrumentation and Control

Pressure Control

To measure the driving force for permeation it was necessary to have pressure controls on the feed, permeate and retentate sides of the membrane. As the pressure drop across the membrane was very small, the feed stream and the retentate streams were essentially at the same pressure. The pressure gauges were manufactured by Wika and ordered from Zimco Gauge in Calgary. The permeate side pressure, G2 (Figures 3.1 and 3.2) was maintained at 1 psig for all experiments and therefore required a gauge with a small range (0 to 5 psig). The feed pressure (G1) and retentate (G3) gauges had ranges of 0 to 250 psig. The accuracy of the pressure measurements was ±0.5%. Pressure was regulated by valves controlling the feed flow rate (V1), permeate flow rate (V2) and retentate flow rate (V3). The pressure of the feed gas from the regulator was set at 160 psig. The moisture trap and the rotameter had pressure limits of 200 psig. The activated carbon was contained in a stainless steel sample cylinder with a pressure limit of 1800 psig.

Flow Measurement

Feed, retentate and permeate flow rates were measured by wet test meters (WTM). For low flow rates (< 1L/min), a Midget WTM manufactured by Alexander-Wright, London with a volume displacement of 0.25 L was used. For higher flow rates a larger DM3C WTM (Alexander-Wright, London, volume 1 L) was used. Feed flow rates were measured with an accuracy of ±0.25%. The WTM's were placed in a fume hood to vent the flammable gases. A rotameter (Omega model E166101-E406) located upstream of the membrane was used to give an indication of the feed flow rate. The accuracy of this rotameter was only ±5% and hence the feed flow rate had to be determined from the wet test meters. In order to obtain this reading the two 3-way valves (V4 and V5) were turned to bypass. The feed stream then bypassed the membrane and was measured by the wet test meter attached to the high pressure outlet.

Temperature Control

High temperature experiments were conducted with pure hydrogen, pure methane and hydrogen-methane mixtures. To heat the feed stream and membrane, heating tape (Omegaflux® rope heater) was wrapped around an inlet gas coil (3 m) and the membrane module. The temperature was controlled by an Omega CN76000 controller that was also connected to two display panels (Omega 115K units). The thermocouples were placed upstream of the feed gas heating coil and on the membrane approximately 5 cm from the top of the membrane. Grafoil™ ferrules were used to seal the thermocouples within the stainless steel tubing. A third thermocouple and display unit was used to monitor room temperature.

The low temperature experiments were conducted at temperatures ranging from –25°C to room temperature (22°C). To attain steady state operation of the membrane system at these temperatures a circulating cooling bath (VWR Model 1190A) was used. The bath had a capacity of 13L in which

two copper coils were placed as a means to cool the inlet gas. The coils were approximately 6.1m (23 coiled segments each) in length and made from 0.25 in copper tubing. A 50/50 mixture of ethanol (denatured, 15% wood alcohol) and distilled water was used as the cooling liquid. The inlet gas was fed from the feed gas cylinder through the traps, rotameter and the feed gas regulating valve into the bath through a 0.25 in hole drilled in the top of the bath. The inlet gas was fed through the coils and exited a second 0.25 in hole at the top of the bath. The inlet was then fed to the membrane through a 8 in length of Teflon bore stainless steel flexible tubing (SS-TH4-TA4-TA4–8). A thermocouple was placed at the exit of the bath to ensure the gas had been sufficiently cooled before entering the membrane module. To cool the membrane, the module was placed inside a Plexiglas cylinder (total volume of 25L) filled with recirculating liquid. A Swagelock bulkhead union (SS-400-61) sealed the inlet gas tubing to the cylinder. The inlet gas was connected to the membrane module through the bulk head fitting at the bottom of the cylinder.

The cylinder was insolated with 1 in thick Kawool fiberglass insulation wrapped around and under the cylinder. Styrofoam chips were left floating on top of the liquid just above the membrane module to prevent heat gain through the top of cylinder. The centrifugal pump within the cooling bath continually circulated the liquid at a rate of 15 L/min. Tygon tubing (R3603, -40°C, 1.3 cm ID, 0.4 cm-wall thickness) connected the bath to the inlet and drain on the Plexiglas cylinder. The liquid was pumped up through the bottom of the cylinder and was drained back to the bath through a 1.3cm ID drilled hole in the Plexiglas just above the membrane module. Cooling to the desired temperature required less than 4-5 hours and steady state was effectively maintained in the system. A thermocouple was sealed to the module and placed in contact with the top of the membrane as shown in the diagram. The temperature of the liquid in the bath and the Plexiglas cylinder were controlled by the digital set point control on the cooling bath. The temperature in the bath was approximately 1-1.5 degrees

higher than the temperature reading on the membrane. It was assumed the liquid was heated slightly when draining back to the bath and this caused the temperature difference. For example, to obtain an accurate membrane temperature of -25°C it was necessary to set the temperature control on the bath approximately -23.5°C. Maximum temperature fluctuations of the membrane were ±1°C.

3.1.5 Concentration Measurements by Gas Chromatography

For the hydrogen and methane separation experiments it was necessary to obtain concentration measurements of the feed, permeate and retentate streams in order to determine the separation factors and rejection and recovery rates. These streams were sampled by routing them through a glass sample bulbs. A syringe was then used to collect a sample of the gas. A Shimadzu gas chromatograph (GC)-8A IT was used to determine molar concentrations of hydrogen and methane. The GC had a thermal conductivity detector (TCD) with isothermal mode of operation. Ultra high purity argon was used as the carrier gas and 60μL gas samples were injected through a syringe into the injection port. The carrier gas flow rate was 25cc/min

Column

The column used was a 10 ft stainless steel, 0.085 in ID column with Hayesep D packing of 100/120 mesh. The column was connected to the SS sample port by 1/8in stainless steel fittings. The column temperature was kept at 200°C. The injection port temperature was kept at 230°C.

Thermal Conductivity Detector (TCD)

The detector had a tungsten filament with a current supply unit that was used to determine thermal conductivity levels relative to a reference gas. The current was set to 60 mA.

3.2 GC Calibration

A Shimadzu CR501 chromatopac integrator was used to obtain the results of the GC analysis. Output data for concentration was initially in terms of area, however to reduce the number of hand calculations required the integrator was programmed to supply output in terms of molar concentrations. A calibration was carried out to determine the relationships between area and molar concentration for hydrogen and methane. Known volumes of hydrogen and methane were injected into the GC and the areas for each volume were collected from the integrator. The integrator settings were as follows:

Attenuation: 2

Slope: 70

Minimum Rejection Area: 1000

Chart Speed: 10 mm/min

The ideal gas law was assumed for hydrogen and methane and therefore molar concentrations were determined directly from the area recorded for each volume. Two volumes of 20, 40 and 60 μL of both hydrogen and methane were injected and averaged. With 60 μL designated as 100% hydrogen or methane (the amount injected of a mixture sample was always 60 μL) a curve was constructed for each gas plotting area versus flow rate. Setting the intercepts to zero the slopes of the calibration curves in Figure 3.4 were found. The inverses of the slopes were given as input calculation factors to the integrator and the number of moles of each component were calculated accordingly. From the sum of the number of moles for each component the integrator was able to calculate output as molar concentration. Each component was also given an ID based upon its retention time so that the component would be identified by name. The retention times of hydrogen, methane and ethane were approximately 4.5, 6.8 and 9.1 minutes respectively.

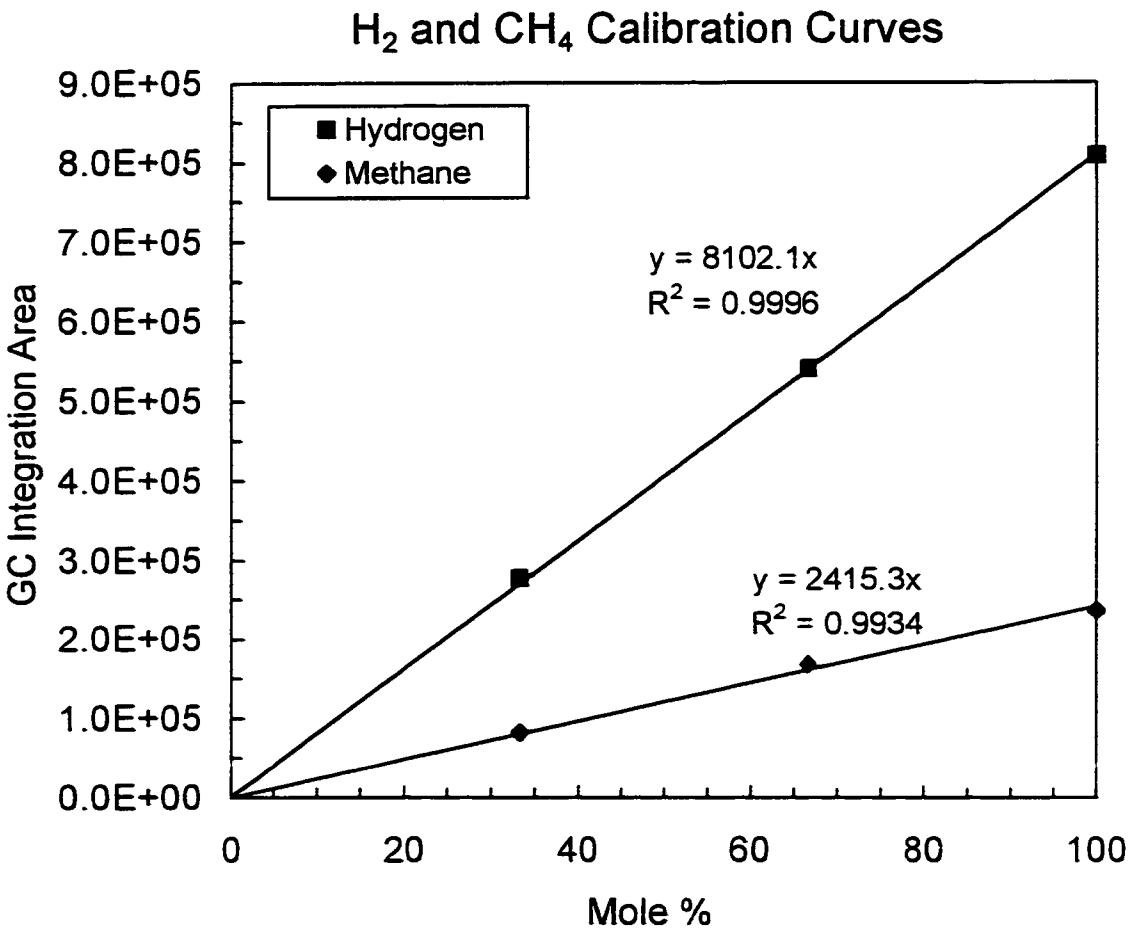

Figure 3.4: GC calibration curves for hydrogen and methane. The equations of the least squares best fit line are shown.

A calibration curve for ethane was not calculated, however the concentration of the ethane in the feed gas (1.98%) was given by the gas supplier (Praxair). Based upon three area readings for 1.98% ethane, a linear approximation was made for the calculation of the molar concentration of methane. Concentrations given by the gas supplier were used as a means to calibrate the GC in Paranjape's (1997) work.

3.3 Experimental Procedures

3.3.1 Pure Gas Permeability Tests

Pure gas permeability tests were conducted to compare permeation rates of certain gases between different membranes and to ensure constant properties of the membrane surface layer over time. A change in the membrane surface properties could result in a decrease or increase in permeation rate over time. Permeability tests involved feeding pure gas to a dead-ended membrane. This meant that there was no retentate flow from the membrane and all the gas fed was transported through the membrane layer. These tests were conducted with nitrogen, carbon dioxide, methane and hydrogen for the three membranes used in this study.

Procedure

Referring to Figure 3.1, the membrane was dead-ended by closing valve V3. This forced all feed through the permeate side of the membrane. The feed flow rate was manipulated by V1 and indicated by G1. Flow rates were measured by the wet test meter attached to the permeate stream for feed pressures of 20, 50, 80, 100, 120 and 150 psig. The GC was not required for these tests as pure gases were used. The permeate side pressure was kept at 1 psig. When the feed gas was changed, it was necessary to purge the system for approximately one hour to ensure all residual gas was flushed out. For each pressure the system was allowed to come to steady state. When there was no

visual fluctuations in the pressures, the system was assumed to be at steady state. This took approximately 10-15 min. The results of the pure gas permeability tests for hydrogen and methane at temperatures ranging from -25 to 165 °C are included in Chapter 5. Permeability tests were also conducted to investigate irreversible adsorption on the membrane. The results of these tests are included in section 3.4.

3.3.2 Procedure for Hydrogen-Methane Separation Experiments

1. For cold temperature experiments, the temperatures were set and allowed to reach steady state. This took from 1 to 5 hours. No gas was purged through the system at this time, as costly volumes of gas would have been used.
2. The volumes of water in the wet test meters were checked.
3. The dessicant trap was checked to ensure the Drierite was okay. The trap was refilled with fresh dessicant if ¾ of the trap had been saturated.
4. The activated carbon trap was changed after approximately 20 hours of use. A different trap was used for different gases (different traps for pure hydrogen, pure methane, pure nitrogen, mixtures and mixtures containing ethane).
5. Ice was collected for the activated carbon trap to improve its adsorption capabilities. The trap was placed inside the ice bath.
6. For high temperature experiments, the membrane was allowed to heat up under a nitrogen purge until steady state had been reached. The temperature of the membrane was greatly affected by the feed gas entering the membrane and if the purge was not used the membrane would have been too hot when the gas was finally fed to the membrane. This was because the heating system was trying to attain high temperatures of a stationary volume of gas in the feed line. Once the gas was no longer stationary (when the flow was initiated) the hot tubing conducted the heat to the larger volume of gas and this increased the temperature of the membrane. Nitrogen was used as a

purge gas during heating, as it was much less expensive than the mixtures. The feed gas was switched to the mixture and allowed to purge for 1 hour after the temperature set point had been reached.

7. If the activated carbon was replaced, the system was purged until the adsorption sites of the carbon were saturated with the polar compounds in the feed such as methane and ethane. Saturation was tested by bypassing the membrane and measuring the feed concentration to ensure it matched the concentration of the feed without the carbon trap. This process took approximately 30 minutes. The feed concentration was noted so that a material balance could be calculated.
8. The barometric pressure and exit temperature for the gas streams were noted. These values were required in order to calculate the flow rates at standard temperature and pressure (STP). Standard conditions were taken as 101.325 kPa and 273.15 K.
9. All gas mixture tests were conducted at constant feed flow rates. Each mixture was tested at a high flow rate and a low flow rate. To set the feed flow rate, V1 was opened and V2 and V3 were adjusted to ensure that there would be sufficient flow at the highest feed pressure. Once it was ensured that the feed flow rate was high enough, the rotameter reading was noted. For high flow rates, the flow rate was set based upon a retentate flow rate greater than 1 L/min. A low rate was considered to be a flow rate that produced a retentate flow less than 1 L/min.
10. V2 was adjusted to give the appropriate feed pressure reading on G1. V3 was adjusted so that G3 read 1 psig.
11. The system was allowed to reach steady state for approximately 15 minutes for each feed pressure.
12. The flow rates of the retentate and the permeate streams were measured with the appropriate wet test meters. The flow rates were measured three times each with a stop-watch to reduce error.

13. The retentate and the permeate flow paths were switched from the wet test meters to flow through the glass sample bulbs. The syringe was purged with the retentate or the permeate gas and a 60μL sample was withdrawn and injected into the GC.
14. From the known feed gas composition, and the compositions and flows of the retentate and permeate gas streams, a material balance was calculated. If the material balance was not within ±3%, the GC analysis and the flow rate measurements were repeated.
15. The three-way valves V4 and V5 were switched to bypass to allow the total feed flow rate to be measured by the wet test meters.
16. V2 was adjusted in order that the desired feed pressure was maintained while measuring the total flow rate.
17. The concentration of the feed flow rate was measured by the large wet test meter (same procedure as step 11).
18. The bypass flow pattern was switched back to flow through the membrane.
19. Steps 8-16 were repeated, checking that the rotameter remained at the feed flow rate initially set. The feed concentration was measured according to step 16 at least three times (i.e. the feed concentration was measured for only three of the 5 pressures)

3.4 Irreversible Adsorption

One of the major differences between the membrane apparatus used for this study and the membrane apparatus used for Paranjape's work (1997) was the use of an activated carbon trap to adsorb heavy hydrocarbons. Commercial operation of an SSF membrane system requires a TSA unit with a bed of activated carbon to adsorb compounds such as ring hydrocarbons and C_5^+ hydrocarbons. An activated carbon trap was not used for Paranjape's work or for the initial permeability tests of this study. This section shows the effects of heavy

hydrocarbons adsorbed on the surface of the membrane in the absence of an activated carbon trap.

The membrane to be used for the hydrogen and methane separation tests was first placed in the membrane module in May 1998 (M-1). Permeability experiments were conducted to compare the fluxes of nitrogen and carbon dioxide to the pure gas fluxes recorded by Paranjape. When measuring the pure gas flow rates of nitrogen through the new membrane, feed pressures up to 70 psig were tested, as the gas cylinder did not have sufficient pressure to go beyond 70 psig (test date May 21, 1998). The feed gas was switched to CO_2 until a new nitrogen cylinder was acquired. The CO_2 was left to purge for approximately two hours. The permeability test was then conducted with CO_2 and the results are shown in Figure 3.5. The flow rate of CO_2 through the membrane was very similar to Paranjape's (shown on graph) with a slight deviation at high pressures. The next permeability test conducted (on May 22, 1998) was the continuation of the nitrogen permeability test of May 21, 1998, beginning at a pressure of 80 psig. The results of this test are shown in Figure 3.5. The flow rate deviated from Paranjape's data beginning at 80 psig. From this it was concluded that the properties of the membrane layer had changed with the exposure of the membrane to CO_2.

Assuming that CO_2 had adsorbed on the surface of the membrane and had not been purged by the nitrogen, the membrane was heated and purged with nitrogen at 125°C in an attempt to reverse the adsorption. A second N_2 permeability test was conducted and the results are shown as the nitrogen curve for June 3, 1998. The nitrogen flow rate through the membrane was slightly higher than the data collected by Paranjape. The membrane was heated, purged and a second permeability test was also conducted with CO_2. The flow rate of CO_2 through the membrane was also higher than the first CO_2 test and Paranjape's work. The results are shown as the CO_2 curve of June 3, 1998.

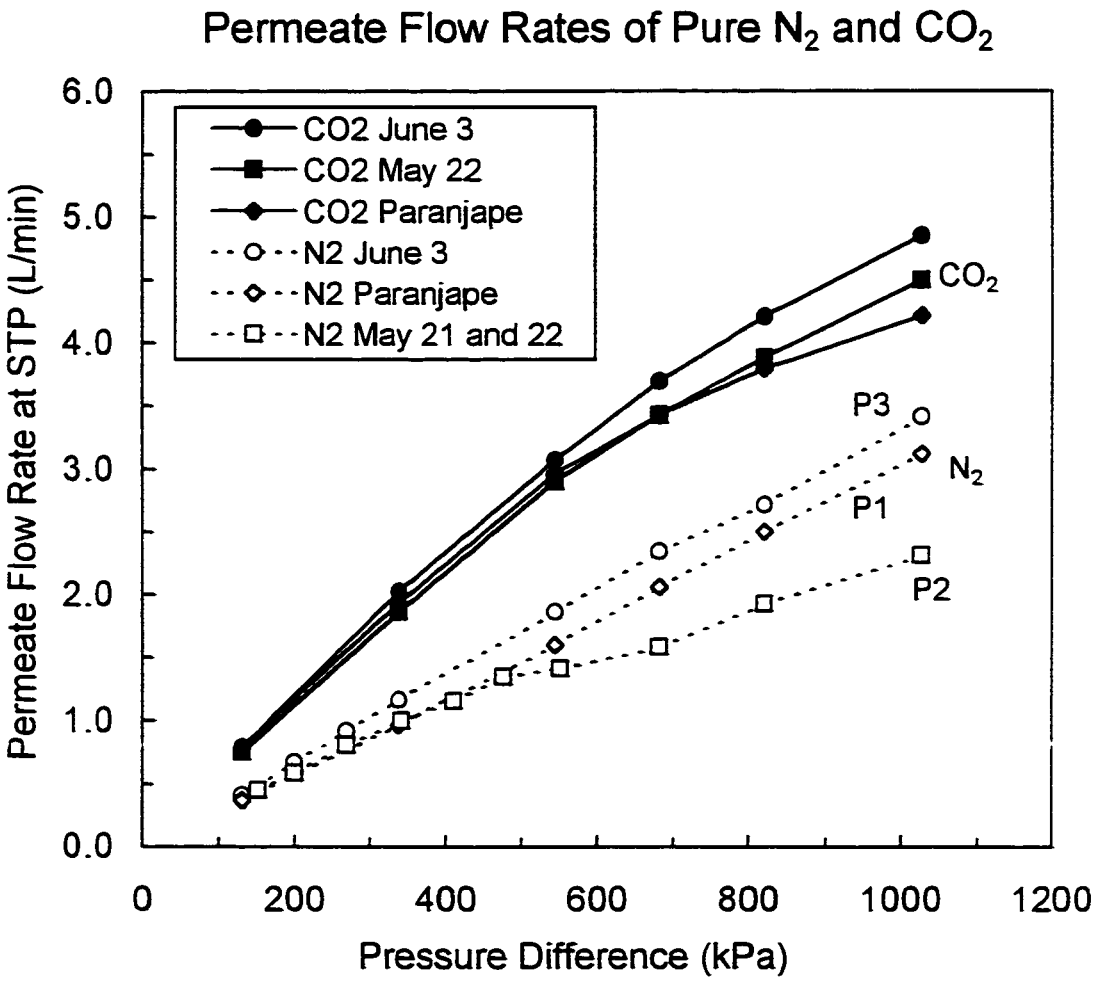

Figure 3.5: Results of N_2 and CO_2 permeability tests conducted with M-1 at 22°C.

With these experiments the barometric pressure and the temperature were carefully measured and the flow rates were reported at STP. The sequence was as follows:

- Measure N_2 permeability (P1)
- Measure CO_2 permeability
- Measure N_2 permeability (P2) – it had decreased, P1>P2
- Heat and purge with N_2
- Measure N_2 permeability (P3), P3>P1>P2

With these initial experiments it was shown that it was possible to regenerate the membrane by heating it to high temperatures with a nitrogen purge. It was assumed that a high temperature purge was required after the use of CO_2 in the membrane in order to purge any residual physically adsorbed CO_2. With this assumption further pure gas tests were conducted with methane. The sequence was as follows (Figure 3.6):

- Measure N_2 permeability (P1)
- Measure CH_4 permeability
- Measure N_2 permeability (P2) – it had decreased, P1>P2
- Heat and purge with N_2
- Measure N_2 permeability (P3), P1>P3>P2

A reduction in permeability (P2) was also seen, however the reduction was much larger with the use of methane (compared to carbon dioxide). For these tests two membranes were used, S-1and M-1. Figures 3.6 and 3.7 show the reduction in the N_2 permeability (P2) of the membranes after the use of methane and room temperature purges of nitrogen. Since methane does not have as strong of an induced dipole moment as carbon dioxide, its irreversible adsorption as the cause of the reduction in permeability was questioned. Also included on Figure 3.6 is the nitrogen flow rate before methane was ever used on the membrane. The results showed that adsorption could not be completely reversed after methane was used in the membrane (probably as a result of high

molecular weight impurities in CH_4). The second permeability test with nitrogen (P3) was lower than before methane was used in the membrane showing that a high temperature purge could not bring the membrane back to its original state. After discussion with researchers at Air Products it was concluded that there were impurities in the feed gas (below dectection limits) that were causing the irreversible adsorption. Their solution was to add an activated carbon trap to the apparatus. Activated carbon was used successfully by Air Products in removing heavy hydrocarbons from refinery waste gases and allowed their membrane system to be operated for 6 months without any degradation the performance of the membrane [Naheri *et al*, 1997]. To ensure that the adsorption of the heavy hydrocarbons was successful for the hydrogen and methane separation studies the activated carbon trap was placed in an ice bath. Some adsorption of components of the feed gas such as methane and ethane occurred, however once the carbon was saturated with these compounds the feed gas exiting the carbon trap was shown to have the same composition as the feed gas without a carbon trap. The strength of adsorption of heavier hydrocarbons on the surface of the activated carbon was clearly stronger than that of methane or ethane and it was assumed that the carbon would preferentially adsorb the heavier compounds even when saturated with methane and ethane.

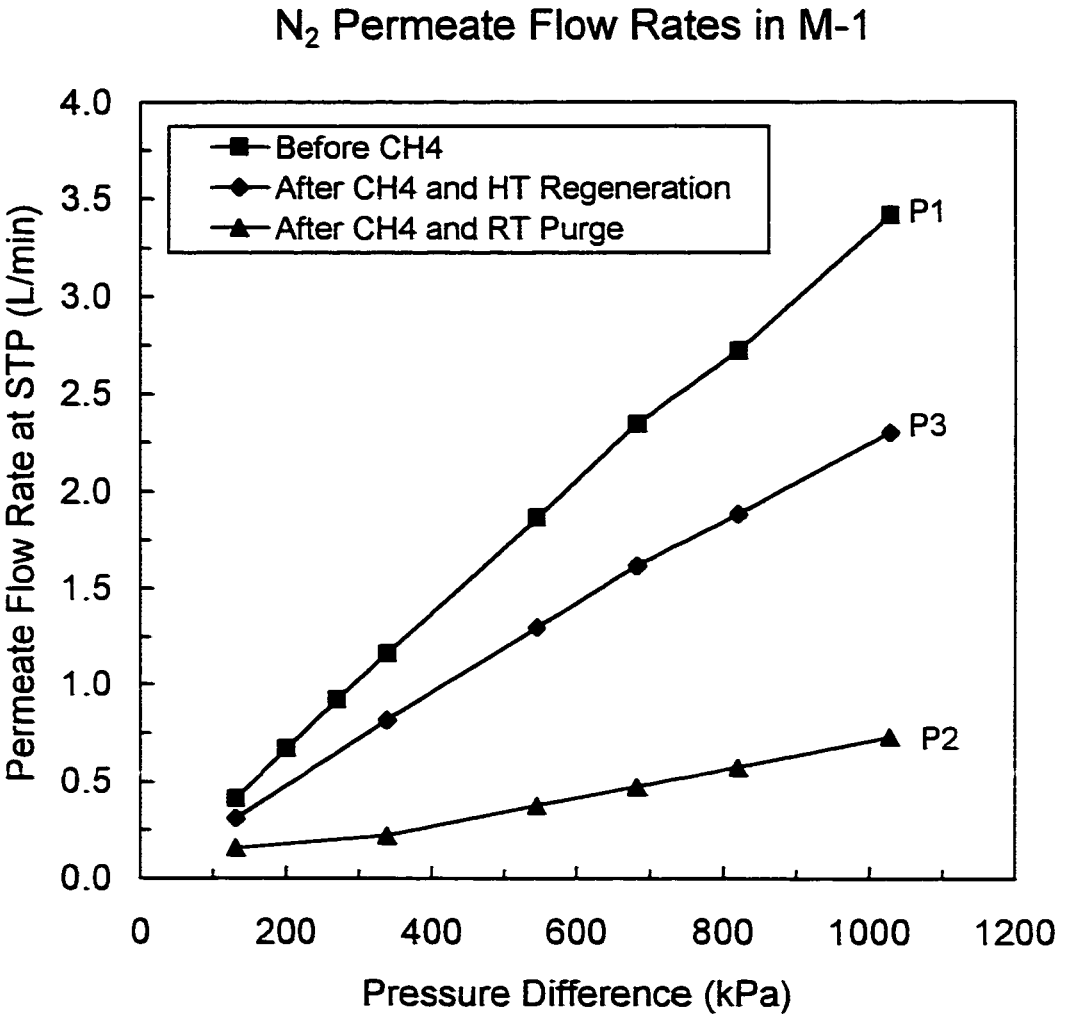

Figure 3.6: Results of the permeability tests conducted with nitrogen before and after CH_4 permeability tests (M-1, 22°C)

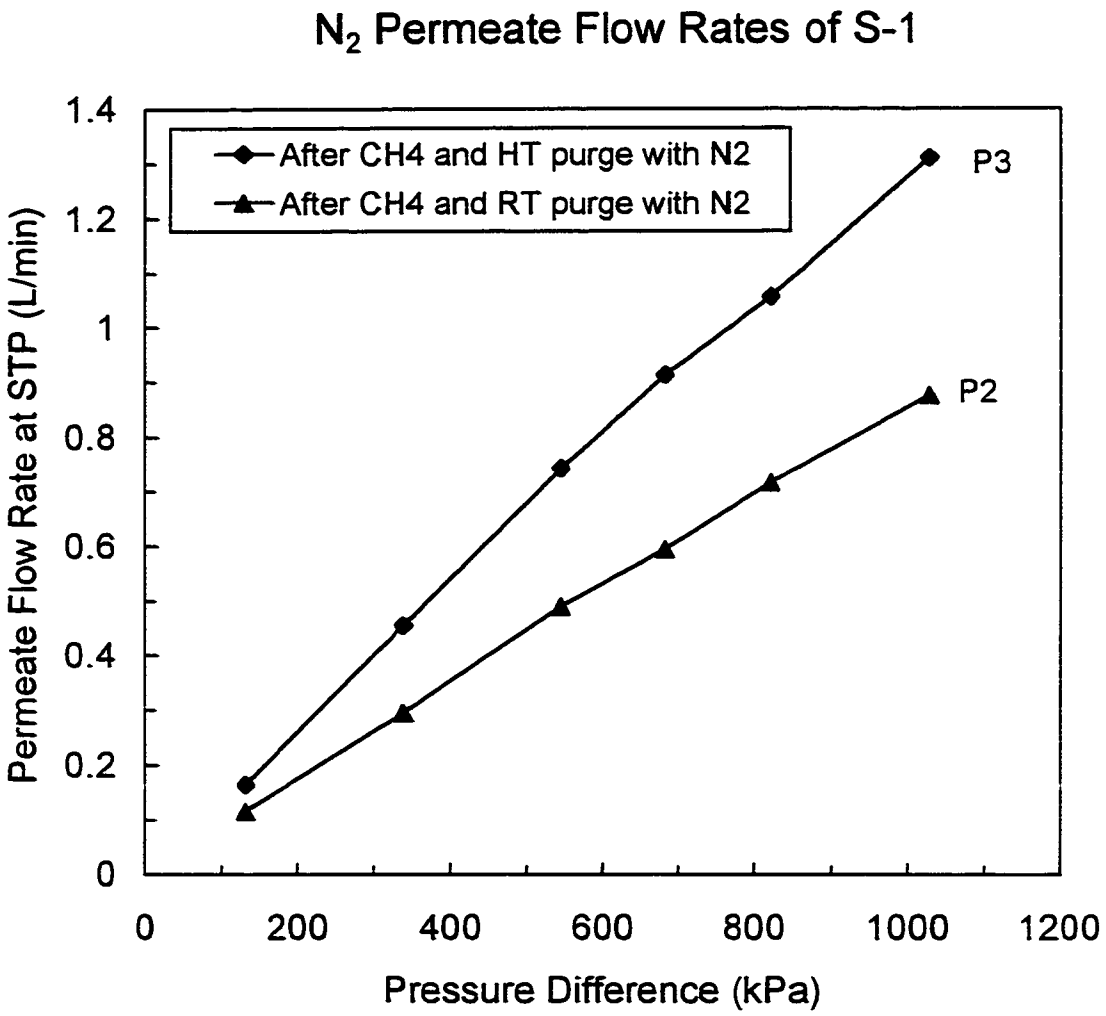

Figure 3.7: Permeability of nitrogen before and after methane permeability tests (S-1, 22°C)

The concentration of the hydrocarbon impurities within a typical commercial grade methane gas cylinder was 1600 ppm (as per telephone conversation with Roger Bailey, Praxair, October 27, 1998). Praxair had no information on the specific impurities that were present therefore a mass spectrophotometer (MS) analysis was initiated to obtain a qualitative measurement. The MS analysis conducted in the University of Calgary's Department of Chemical and Petroleum Engineering Analytical Laboratory detected no hydrocarbon impurities, perhaps due to the concentration of any hydrocarbon being lower than the detection limit of the MS (10 ppm). The methane cylinders supposedly contained less than 10 ppm of water however the colour indicating Drierite trap showed significant adsorption of water over time. A simple calculation demonstrates the effect of small quantities of impurities on the surface layer of carbon.

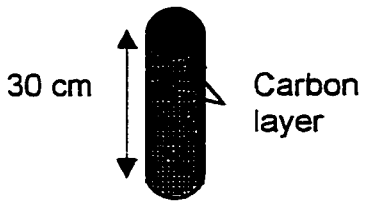

Figure 3.8: Illustration of the membrane carbon layer on the porous support.

If the surface layer of the membrane is 2 μm thick and 30 cm in length, the volume of the carbon layer on the porous support is 0.0095cm^3. For a bulk density of 600 kg/m^3 the mass of activated carbon is 0.0057g. The surface loading of pentane reaches saturation (0.4 mmol/g at 30°C) at less than 10 kPa and for the SSF membrane (lowest feed pressure is 300 kPa) this corresponds to 0.00228 mmol. For a feed flow rate of 5 L/min (0.22 mol/min) and an impurity concentration of 10 ppm (10×10^{-3} mmol/mol) the impurity flow rate is 2.2×10^{-3} mmol/min. It takes approximately 1 minute of flow for the pentane to saturate the membrane layer. Pentane's adsorptivity is 15 times greater than methane (saturation loadings of 0.4 and 6.1 mmol/g) and saturation of methane on

activated carbon does not occur until pressures greater than 10000 kPa. This shows the importance of the activated carbon trap for hydrocarbons. The trap is required to adsorb components like pentane that will saturate and irreversibly adsorb on the surface of the membrane layer. Saturation of the membrane layer with large hydrocarbons has shown to decrease the permeability of the membrane and due to higher adsorptivities could adversely affect the separation of hydrogen and methane (there would be no surface flow of methane to block hydrogen permeation if the adsorption sites are taken by pentane). Conducting calculations to determine saturation time for the activated carbon trap (assuming 10 ppm of pentane) it would take 63 days for saturation to occur.

CHAPTER 4.0

EXPERIMENTAL DATA ANALYSIS

Several equations were used to calculate the experimental values describing flow through the SSF membrane. These values included flow rates, flux and permeability. Separation factors, rejection rates and recovery rates were also calculated as a means of measuring the performance of the SSF membrane. In this chapter, these equations are explained and/or developed for pure gases and mixtures.

4.1 Flow Rate

Feed, permeate and retentate flow rates were calculated by measuring the time it took for the streams to displace 1 or 0.25 L of water, depending on the volume of wet test meter used. The average of three readings was taken and converted to give results L/min. Flow rates for this study are reported in L/min at STP (273 K and 101.325 kPa).

4.2 Flux

Flux through a membrane is defined as the permeate flow rate divided by the area for permeation per unit time. The area A, of the SSF membranes used

in this study was 47.1 cm^2. The equation for pure gas flux is as follows, where Q is the permeate molar flow rate.

$$J = \frac{Q}{A} \tag{4.1}$$

The flux for a permeating mixture with y_i as the mole fraction of component *i* in the mixture is defined as:

$$J = Jy_i = \frac{Q}{A} y_i \tag{4.2}$$

Flux is reported in units of $mol/m^2/s$. Since the flow rates were converted to STP, molar flow rates were easily found by dividing by 22.4L/mol.

4.3 Permeability

Permeability is defined as the ratio of flux to the driving force for permeation. In the case of the SSF membrane, the principle driving force is the pressure gradient for pure gases or partial pressure gradient for gas mixtures. The equation for pure gas permeability is:

$$K = \frac{J}{(P_h - P_l)} \tag{4.3}$$

where the term (P_h-P_l) is the pressure difference in the membrane. The driving force for permation of pure gases is the pressure gradient. No concentration gradient exists since the component fraction is 1 on both the permeate and retentate sides of the membrane.

The permeability of a gas mixture is defined as:

$$K_i = \frac{J_i}{(\Delta p_i)} \tag{4.4}$$

where Δp_i is the partial pressure driving force. To calculate the partial pressure driving force, an equation (4.5) for the log mean pressure difference was used. It is dependent upon the flow regime in the membrane which is shown in Figure 4.1.

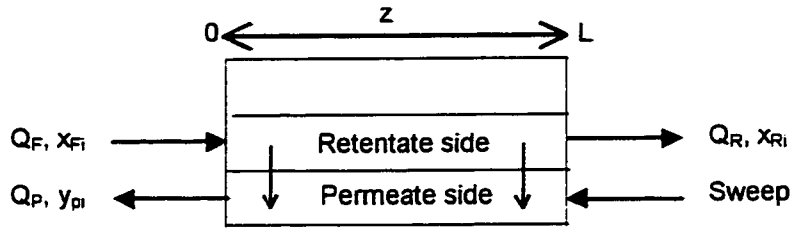

Figure 4.1: Flow direction inside the membrane apparatus.

$$\Delta p_i = \frac{(\Delta p_i)_{z=0} - (\Delta p_i)_{z=L}}{\ln \frac{(\Delta p_i)_{z=0}}{(\Delta p_i)_{z=L}}} \tag{4.5}$$

$$(\Delta p_i)_{z=0} = P_H x_F - P_L y_{Pi} \tag{4.6}$$

$$(\Delta p_i)_{z=L} = P_H x_{Ri} \tag{4.7}$$

Equation 4.6 is the difference in partial pressures for component *i* (hydrogen or methane) at the feed side of the tube where z=0. Equation 4.7 is the difference in partial pressures at the retentate exit. There is no sweep gas at this point and therefore the partial pressure on the permeate side at z=L is assumed to be zero for both components.

The logarithmic partial pressure difference assumes the following:

- permeability is not a function of pressure
- partial pressures vary linearly with flux and the difference in the inlet and outlet concentrations on the permeate and retentate sides of the membrane is very small.

The flow regimes on the permeate and retentate sides of the membrane are unknown. The concentrations may change along z or they may be well mixed (which would make the unchanging concentration assumption reasonable). Since the regime is unknown, the log-mean partial pressure differences are considered acceptable approximations for the permeability calculations.

4.4 Separation Factor

The separation factor is a measure of the performance of the membrane. It is calculated based upon the amount of gas permeated versus the amount of gas retained in the feed. A high permeation of gas 2 ($y_{P2}>>y_{P1}$) and a low amount of gas 2 in the feed ($x_{F2}<<x_{F1}$) results in a high separation factor. The true definition of the separation factor is:

$$S = \frac{\left(\frac{y_{P2}}{y_{P1}}\right)}{\left(\frac{x_{F2}}{x_{F1}}\right)} \tag{4.8}$$

Equation 4.8 can also be shown to give an ideal definition of the separation factor. Under ideal conditions, when the permeate pressure is very low and the feed pressure is very high, the real separation factor (4.8) is equal to the ideal separation factor (equation 4.9).

$$S = \frac{(K_2)}{(K_1)} \tag{4.9}$$

The ideal separation factor is a ratio of the permeabilities of the two components to be separated. In terms of the SSF membrane, K_2 refers to the permeability of the preferentially adsorbed gas. Separation factors calculated based upon the equation 4.9 are discussed in Appendix A. Permeabilities were calculated using equations 4.4 and 4.5 and were termed log-mean permeabilities. Separation factors developed based upon the ratio of these permeabilities were termed log-mean separation factors. Comparision of real and log-mean separation factors is discussed in Appendix A.

4.5 Recovery and Rejection Calculations

Calculating recovery rates for hydrogen and rejection rates for hydrocarbons was a convenient way to illustrate the performance of the

membrane. Perfect separation was defined by a rejection rate of 100% and recovery rate of 100%. For a plot of rejection versus recovery, separation improved as the data moved towards the upper-right side of the chart.

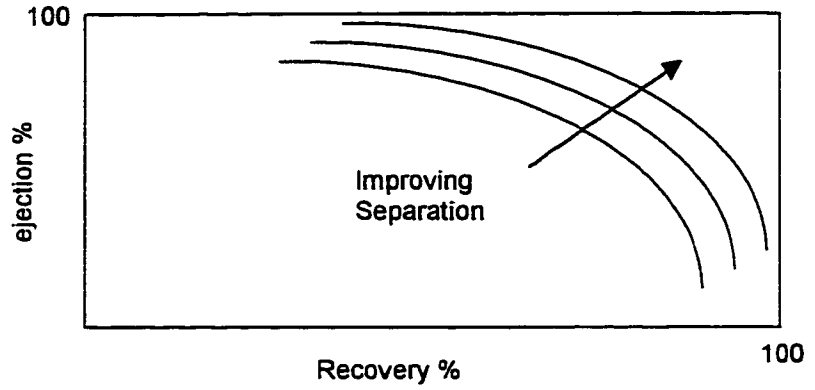

Figure 4.2: Example rejection-recovery plot

Hydrogen rejection was defined as the amount of hydrogen in the retentate stream divided by the amount of hydrogen in the feed stream.

$$\%\ H_2\ \text{Recovery} = \frac{Q_R X_{RH_2}}{Q_F X_{FH_2}} \times 100 \qquad (4.10)$$

Methane rejection was calculated by dividing the amount of methane in the permeate stream by the amount of methane in the feed stream.

$$\%\ CH_4\ \text{Rejection} = \frac{Q_p X_{pCH_4}}{Q_F X_{FCH_4}} \times 100 \qquad (4.11)$$

Rejection and recovery rates were calculated for all of the hydrogen and methane separation experiments. Separation effciency was determined by comparing the rejection-recovery plots for experiments conducted at different temperatures and feed flow rates.

4.6 Error Analysis

Two types of experimental errors were calculated, repeatability error and experimental apparatus error. Repeat experiments were conducted for every mixture at -25°C. Required data was collected at temperatures of -25°C, -10, 0,

10 and 22°C and the repeat experiments were the last to be recorded. These experiments were useful in obtaining a measure of error for each mixture but did not predict any random errors that may have been occurring with the use of different mixtures. The membrane layer was very sensitive and a measure of error with changing mixture concentrations was required in order to measure the overall repeatability of the experiments. Additional repeatability tests were conducted on one set of data to obtain a measure of combined random and systematic errors within the experimental system (including errors that may have occurred due to a change in mixture). A Taylor series expansion was used to obtain a measure of the systematic errors present in the apparatus (experimental apparatus error).

Repeatability tests were conducted by measuring the same experimental point four times at different stages in the experimental procedure. The standard deviation within these points represented the percent error in repeatability of all hydrogen-methane separation experiments. The mixture chosen for these experiments was 75% CH_4, 25% H_2. The points were collected at -25°C with a feed pressure of 100 psig a feed flow rate of 5.7 L/min. The times at which the data were collected and the rejection-recovery results are given in Table 4.1.

Table 4.1: Experimental repeatability test results.

Point	Conditions under which data was collected	H_2 Recovery	CH_4 Rejection
1	Regular data point (3/11/1998)	75.7	60.8
2	Pressure switched to 120 psig data recorded, pressure switched back to 100 psig, point 2 collected (3/11/1998)	74.7	60.3
3	Temperature changed to –10, 0, 10°C, data collected for 5 pressures at each temperature, switched back to –25 °C, point 3 taken (17/11)	74.6	58.6
4	Feed gas cylinder switched from 75% CH_4 to 25% CH_4, purged, 75% CH_4 cylinder put on-line, point 4 taken (20/11/1998)	74.6	59.8

The standard deviations for recovery and rejection were computed as 0.535 and 0.943. The maximum differences between values were 1.1% and 2.2%.

Repeat experiments that were conducted for each mixture resulted in average absolute differences of 1.7% and 1.6% for the rejection and recovery results respectively. The maximum difference was approximately 3.5% for a single rejection or recovery point.

Accurate results of the hydrogen and methane separation experiments were based upon the accurate measurements of compositions, flow rates, temperatures and pressures. The errors inherent in the GC analysis, wet test meters, thermocouples and pressure gauges were ±2.02%, ±0.25%, ±0.4% and ±0.5%. Using a Taylor series (equation 4.12) to compute the error for all data points, the result is an average of ±3.0% error. R_i represents recovery or rejection results.

$$\nabla R_i = \left|\frac{\partial R_i}{\partial x}\right| \nabla x + \left|\frac{\partial R_i}{\partial Q}\right| \nabla Q + \left|\frac{\partial R_i}{\partial T}\right| \nabla T + \left|\frac{\partial R_i}{\partial P}\right| \nabla P \qquad (4.12)$$

CHAPTER 5.0

PURE GAS PERMEABILITY TESTS

Permeability tests were conducted using M-2 with pure hydrogen and methane according to the procedure outlined in Section 3.3.1. The purpose of these experiments was to obtain flow rates and permeabilities for pure hydrogen and methane as a function of temperature. Temperatures ranging from –25°C to 155°C were investigated. The relationship between temperature and flow rate helped to identify the type of diffusion occurring in the membrane. The permeabilities were also calculated in order to compare with permeabilities of hydrogen and methane mixtures discussed in Chapter 6. Three types of diffusion have been identified as possibly occurring in the membrane and are explained in Section 5.1.

5.1 Types of Diffusion

5.1.1 Knudsen Diffusion

Knudsen diffusion occurs when the mean free path of the diffusing molecule is larger than the size of the pore. In this case, collisions between diffusing molecules occur less frequently than collisions between the molecules and the pore walls [Ruthven, 1984]. The pore size in the SSF membrane is estimated at 5-7 Å. The mean free paths of H_2 and CH_4 calculated using the

Lennard-Jones collision diameters are 565 Å, and 1197 Å respectively. Knudsen diffusion is known to occur within a pore range of 20 to 1000 Å.

Knudsen developed the following equation for molar flow rate through capillaries [Matson and Quinn, 1977]:

$$N = \frac{4}{3} \frac{v}{\int_0^L \frac{H}{A} dL} \frac{P_2 - P_1}{RT} \tag{5.1}$$

Where v is the mean molecular velocity, H is the circumference of the pore, A is the cross-sectional area of the pore and L is the thickness of the porous layer. The above equation was modified by Miller *et al* (1994) to give the Knudsen permeability of a gas through a porous membrane with porosity ε. Permeability, K, can be defined as the ratio of molar flux to the concentration gradient along the pore [Matson and Quinn, 1977].

$$K = \frac{4 \varepsilon v f(r)}{3 R T L K_g^2} \tag{5.2}$$

The term $f(r)$ is a function that describes the characteristic dimension of the pore for transport. For example, if the pore is cylindrical, $f(r)$ is equal to r/2. K_g is the tortuosity of the medium. For porous media with significant surface roughness the tortuosity will be greater than one [Barrer, 1967]. The definition for molecular velocity is as follows:

$$v = \left(\frac{8RT}{\pi M} \right)^{1/2} \tag{5.3}$$

By substituting the equation for molecular velocity into the Knudsen permeability equation, the permeability can be shown to be proportional to the inverse square root of temperature.

$$K = \frac{4 \sqrt{8} \varepsilon f(r)}{3 \sqrt{\pi} R^{1/2} M^{1/2} L K_g^2} \left(\frac{1}{T} \right)^{1/2} \tag{5.4}$$

Knudsen diffusion is considered a type of "gas phase" flow as it occurs in the absence of any adsorption effects.

5.1.2 Surface Diffusion

Surface diffusion occurs when there is a direct flux contribution by the gas that is physically adsorbed on the surface of the porous media. The presence of a mobile adsorbed film on porous media may greatly augment the flow that would otherwise occur due to gas phase flow [Aylmore and Barrer, 1965]. The mobility of the adsorbed phase is much lower than the mobility of the gas phase; however the concentration of diffusing molecules in the adsorbed phase is normally high enough for surface flow to make a significant contribution to overall flux at certain conditions [Ruthven, 1984]. Surface diffusion is known to occur in porous media with pore sizes ranging from 10-1000 Å.

Surface flow is a function of the amount of surface area of the medium, the condensibility of the gas and the interaction potential between the gas and the solid [Miller *et al*, 1994]. Mathematically, surface flux can be explained by the use of Fick's First Law of Diffusion:

$$J_s = D_s \frac{dC_s}{dx} \tag{5.5}$$

It states that the surface flux, J_S, is proportional to the concentration gradient and the surface diffusivity D_S. The concentration gradient is often defined by the partial pressures on either side of the diffusion media, however the situation may exist where partial pressures are equal but a driving force such as adsorption may contribute to the overall flux. For porous media, the concentration gradient is defined as the difference in surface loading, n_s, over the thickness, x, of the porous medium.

$$J_s = \rho(1-\varepsilon)D_s \frac{dn_s}{dx} \tag{5.6}$$

The term ρ is the bulk density of the porous media. If the surface flow is assumed to be uniform throughout the thickness of the adsorbent the flux can be expressed as:

$$J_s = \rho D_s \frac{\Delta n_s}{\Delta x} \tag{5.7}$$

5.1.3 Activated Diffusion

The activated diffusion process occurs in porous media when a gas molecule surmounts an energy barrier and is able to jump from position to position within the solid. It occurs in pore sizes of less than 10Å and is often associated with diffusion within catalysts. Fick's Law also defines activated diffusion and the diffusivity term has the following Arrhenius type relationship with temperature:

$$J = D \frac{dC}{dx} \tag{5.8}$$

$$D = D_o \exp\left(-E/RT\right) \tag{5.9}$$

The difference between activated and surface diffusion is that the diffusivity term rather than the concentration gradient is thought to contribute the majority of activated diffusion. It is analogous with catalysis processes which require increasing temperature to increase the activity of the catalyst. Activated diffusivity increases with temperature due to the increased activation energy (E) supplied at higher temperatures. The concentration gradient is normally not the primary contributor to diffusion, unlike with surface diffusion.

5.2 Knudsen Diffusion in SSF Membranes

Barrer (1967) investigated diffusion through activated carbon plugs (pore diameter ~20-85Å) and found it could be attributed to two type types, surface and gas phase flow. The surface flow occurred due to the mobility of the physically adsorbed gas on the surface of the activated carbon. The gas phase

flow was due to the diffusion of non-adsorbed gas. Measurement of the flow rates of non-adsorbing gases such as hydrogen and helium through the activated carbon plugs showed that the gas phase flow occurred by the Knudsen diffusion mechanism. Measurements of polar gases such as CO_2 showed that the diffusion rates were much higher than those calculated by the Knudsen equation. The flow above the Knudsen flow rate was attributed to surface flow. The mobility of the physically adsorbed gas within the internal surfaces of the adsorbent was found to contribute significant amounts of surface flow.

Experiments were carried out by Air Products to determine whether Knudsen diffusion occurred in the SSF membrane. Experimental diffusivities were found for hydrogen and helium and the results were used in an equation for Knudsen diffusivity. They postulated that if Knudsen diffusion occurs in the SSF membrane, the pore size of the membrane would be correctly predicted from the Knudsen equation.

Experimental gas phase diffusivites of hydrogen and helium were calculated by Rao and Sircar (1996) using the following equation:

$$D = \left(\frac{\tau}{\varepsilon}\right)\left[\frac{Jl}{A\Delta C_g}\right] \tag{5.10}$$

The term τ, was the tortuosity of the membrane and was assumed to be 1.0. The term ε was the porosity of the membrane layer and was found to be 0.4 through calculated bulk and chemical densities of the nanoporous carbon film. The experimental flux *J* was measured and *l* was the thickness of the membrane layer. The concentration gradient in the SSF membrane was calculated using the following equation developed from the ideal gas law:

$$\Delta C_g = \left(\frac{P_H - P_L}{RT}\right) \tag{5.11}$$

Using the experimental values of diffusivity, the pore size of the SSF membrane was calculated according to the following Knudsen equation adopted from Satterfield (1970):

$$D_k = 4.85 \times 10^{-5} d_p \left(\sqrt{T/M}\right) \qquad (5.12)$$

This equation for diffusivity was developed from the Knudsen equation for diffusion through a straight, cylindrical capillary (5.1). The pore diameter in Angstroms was d_p. The use of this equation with values of diffusivity for helium resulted in a predicted pore size of the membrane of 0.018 Å. Rao and Sircar concluded from this that Knudsen diffusion was not a major contributor to flow in the SSF membrane. Table 5.1 shows the diffusivities found using equation 5.10.

Table 5.1: Experimental Diffusivities calculated according to equation (5.10) [Rao and Sircar, 1996]

Temperature (K)	Diffusivity He ($cm^2/s \times 10^5$)	Diffusivity H_2 ($cm^2/s \times 10^5$)
256.1	0.55	3.00
273.1	0.72	3.59
298.1	1.01	4.26

5.3 High Temperature Experiments

Research conducted by Smith (1998) demonstrated that permeation rates within the SSF membrane decreased with increasing temperature (for both CO_2 and H_2). This is the effect of temperature according to Knudsen diffusion (K or J $\propto T^{-1/2}$, see equation 5.4). Air Products however, determined that Knudsen diffusion did not contribute significantly to flux through the SSF membrane. Conflicting experimental results created motivation to conduct additional tests to determine the type of diffusion within the SSF membrane.

For the procedures used by Air Products to determine the type of diffusion, the tortuosity and pore shape of the membrane was not accounted for in calculating the pore size of the SSF membrane using the Knudsen equation (5.10). Moreover, AFM and STM scans of the membrane showed that the surface roughness was the same order of magnitude as the pore sizes of the

membrane layer demonstrating that perhaps tortuosity could account for the erroneous result of the pore size calculation using the Knudsen equation. High temperature experiments were conducted as part of this study to determine whether Knudsen diffusion occurred in the SSF membrane.

In several literature sources (Ruthven; 1984, Barrer; 1967, Aylmore and Barrer; 1965, Ulhorn *et al*; 1995) a method to independently measure gas phase diffusion (Knudsen diffusion) and surface phase diffusion is documented. The method is based on surface and gas phase flux or permeabilities being additive.

$$K = K_g + K_s \tag{5.13}$$

$$J = J_g + J_s \tag{5.14}$$

Using a non-adsorbing gas such as helium, the permeability is measured. The experimental permeability is then compared to the permeability predicted by the Knudsen equation. If there is agreement, it can be concluded that surface diffusion is not present and the gas phase flow is pure Knudsen flow. The Knudsen equation is then used to predict the gas phase flow for an adsorbing component such as CO_2. The flow not accounted for is equal to the surface flow. This method was used by Barrer (1967) to determine the surface diffusivity for several gases and several types of porous media.

Ruthven (1984) explained how high temperature experiments were used to isolate gas phase flow and the data was extrapolated to measure the amount of gas phase flow and surface flow at lower temperatures. It was hypothesized that from a combination of Ruthven's and Barrer's procedures, the gas phase and surface phase flows within the SSF membrane could be measured.

At sufficiently high temperatures only gas phase or Knudsen diffusion occurs. The Knudsen equation was used in two ways to determine if gas phase flow could be measured.

Method 1

The original Knudsen equation (equation 5.1) was used to develop an equation relating flux to temperature for a pure gas. At two temperatures (125 and 155°C) the flow rates were calculated to have the following ratio:

$$J_1 = J_2\left(T_2/T_1\right)^{1/2} \qquad (5.15)$$

Using this equation it was possible to determine if Knudsen diffusion was occurring without knowing tortuosity. The flux or flow rate at 125°C was designated J_1. The flow rates of hydrogen and methane were measured at 155°C and equation 5.15 was then used to predict the flow rate J_1. (It was assumed that no surface flow of hydrogen and methane occurred at these temperatures). The results are shown in Figure 5.1. The flow rates of hydrogen and methane were predicted within an average of 6 and 11%.

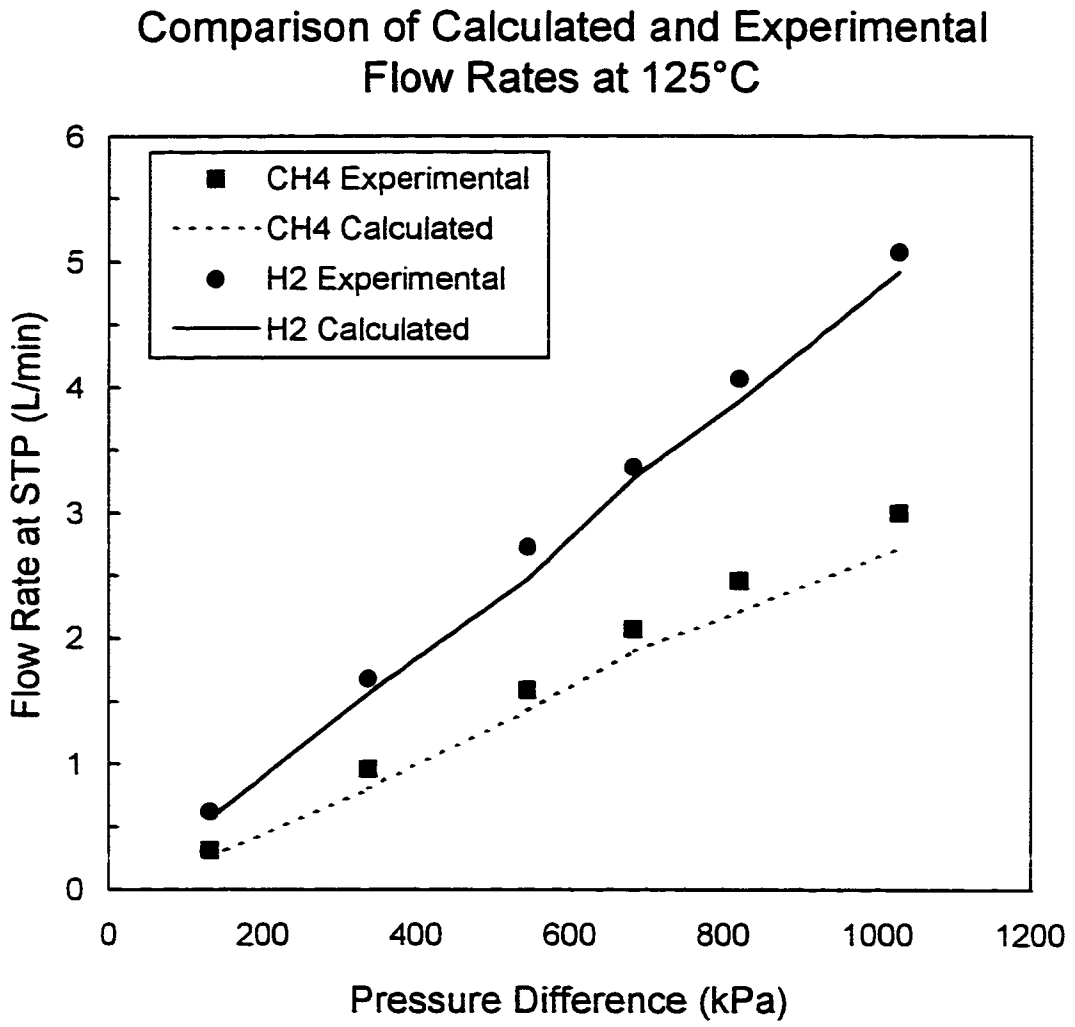

Figure 5.1: Results of equation 5.15 for predicting experimental methane and hydrogen flow rates at 125°C (M-2, feed pressures 20-150 psig).

Method 2

Equation 5.1 was also used to develop the following equation comparing the flux of two gases at the same temperatures and pressures.

$$J_{CH_4} = J_{H_2}\left(M_{H_2}/M_{CH_4}\right)^{1/2} \qquad (5.16)$$

Ash *et al* (1967) used this equation to predict the amount of gas phase flow occurring for gases that exhibited both gas phase and surface phase flow in porous media. For example, experimental values of hydrogen flux (J_{H2}) were substituted into equation 5.16 to predict the amount of methane gas phase flux (J_{CH4}) occurring at a specific temperature and pressure. Normally equation 5.16 is used to predict only the gas phase portion of flux for an adsorbing component, however, it was used to predict the *total* flux of methane. This was justified by using the equations at temperatures of 125°C and 155°C (temperatures at which methane was assumed to be non-adsorbing). The experimental values of hydrogen flux as well as the molecular weights of hydrogen and methane were substituted into equation 5.16. The results of using this equation to predict the flow rates of methane are shown in Figure 5.2. The results show that the calculated values for the flow rates of methane did not match the experimental rates. The percent differences were 40 and 35% for 125°C and 155°C respectively. A trend present in the data was the reduction in the difference between experimental and calculated values as the temperature increased. This suggested that if the temperature were raised high enough Knudsen flow would occur. The results of equation 5.16 at 65°C were also calculated to ensure the trend. The difference at 65°C was 60% and thus showed that the difference was decreasing as the temperature increased.

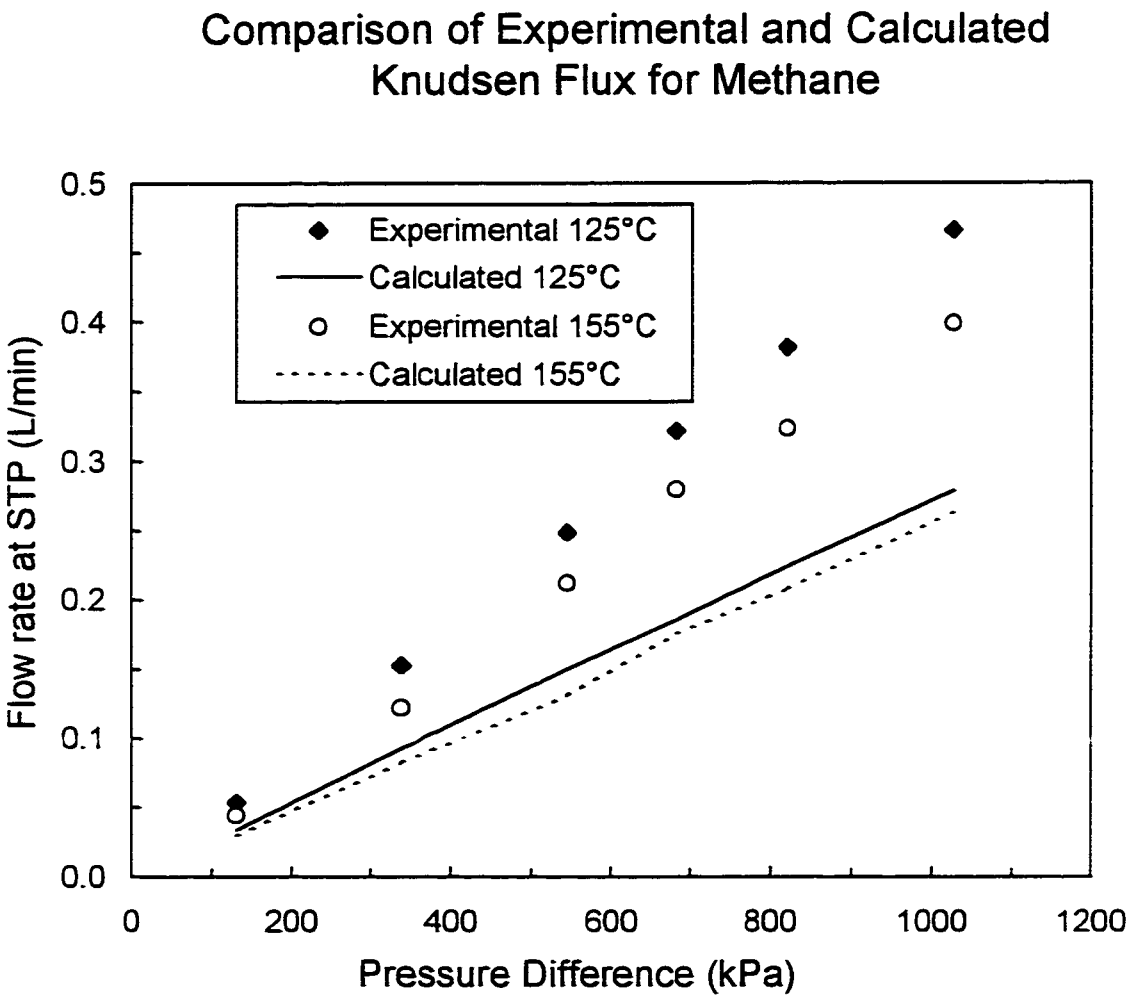

Figure 5.2: Results of equation 5.16 for predicting experimental methane flow rates at 125 and 155°C (M-2, feed pressures 20-150 psig)

The experimental values of flow rates of hydrogen and methane at these temperatures were higher than those predicted by the Knudsen equations (5.15 and 5.16). This suggested that the properties of the membrane layer produced steric effects that resulted in higher flow rates than would have occurred with Knudsen diffusion. The difference in the calculated values and the experimental values for the flow rates of methane demonstrated that Knudsen diffusion did not occur in the SSF membrane.

5.4 Permeation of Pure Hydrogen and Methane

In permeability tests, all feed gas diffused through the membrane layer to the permeate side of the membrane. The flow rate of gases in permeability tests is also referred to as permeation rate. Permeability tests were carried out at pressures of 20, 50, 80, 100, 120 and 150 psig. The permeation rates of hydrogen and methane as a function of pressure difference (or pressure driving force) for the temperature range of -25 to 155°C are shown in Figures 5.3 and 5.4. The permeation rates of hydrogen and methane both increased with decreasing temperature. This is in agreement with Smith's (1998) results. These results demonstrated the effect of the membrane layer with temperature. The separation mechanism of the SSF membrane involves the physical adsorption and surface diffusion of polar molecules through the pores of the membrane layer. With decreasing temperature, the flow rates of hydrogen and methane both increased due to the increased surface diffusion. Low temperatures increase adsorption effects due to the increased loading potential of the membrane layer at low temperatures.

For activated diffusion, it is often stated that flow rate increases with increasing temperature as more energy is supplied for diffusion to occur at high temperatures. This effect was not seen with the SSF membrane due to the strong adsorption effects. This is clarified by the equation for activated or surface diffusion (equation 5.17).

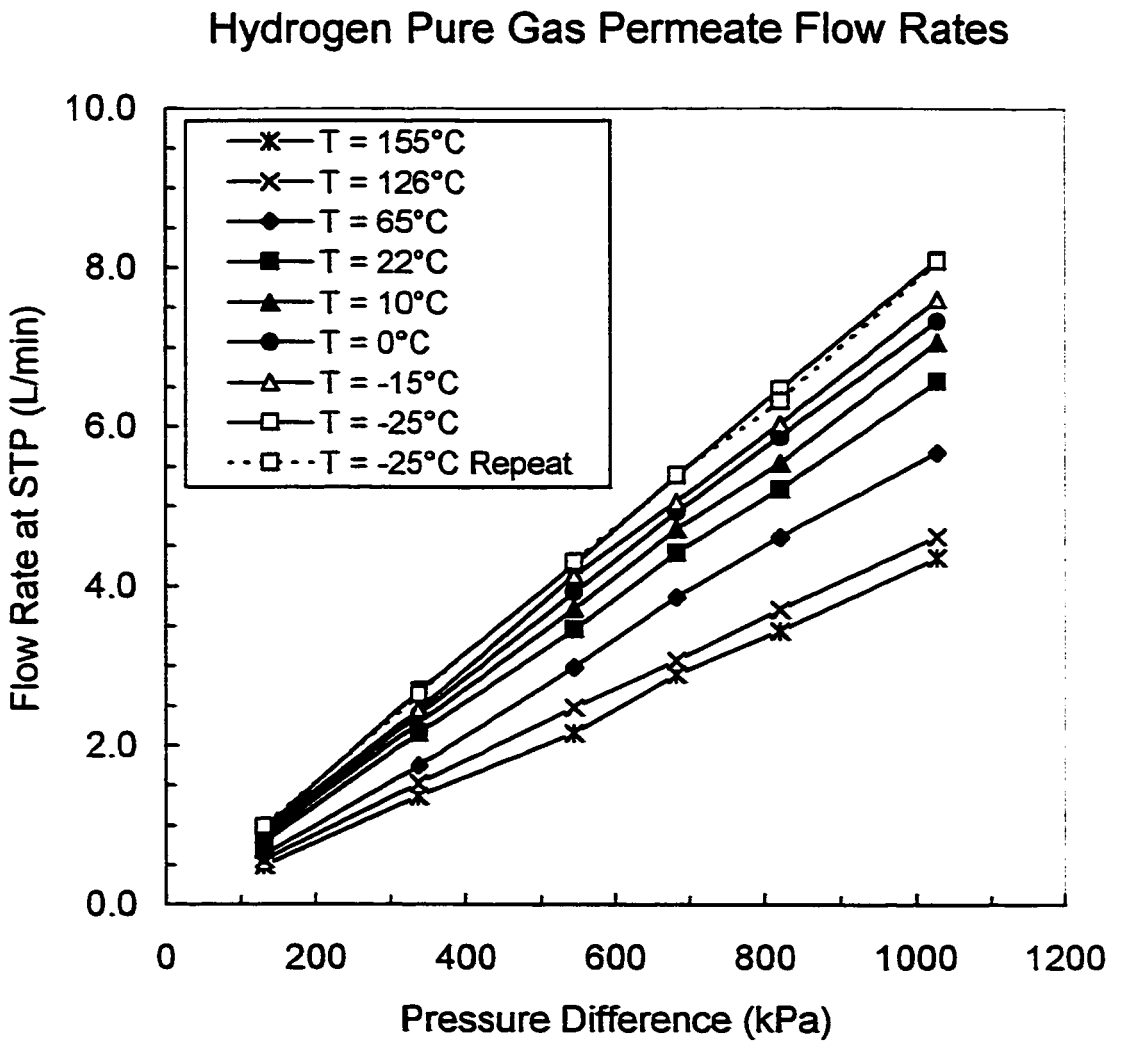

Figure 5.3: Pure hydrogen permeation rates as a function of pressure difference measured at temperatures ranging from -25 to 155°C (M-2, permeability tests, feed pressures of 20-150 psig)

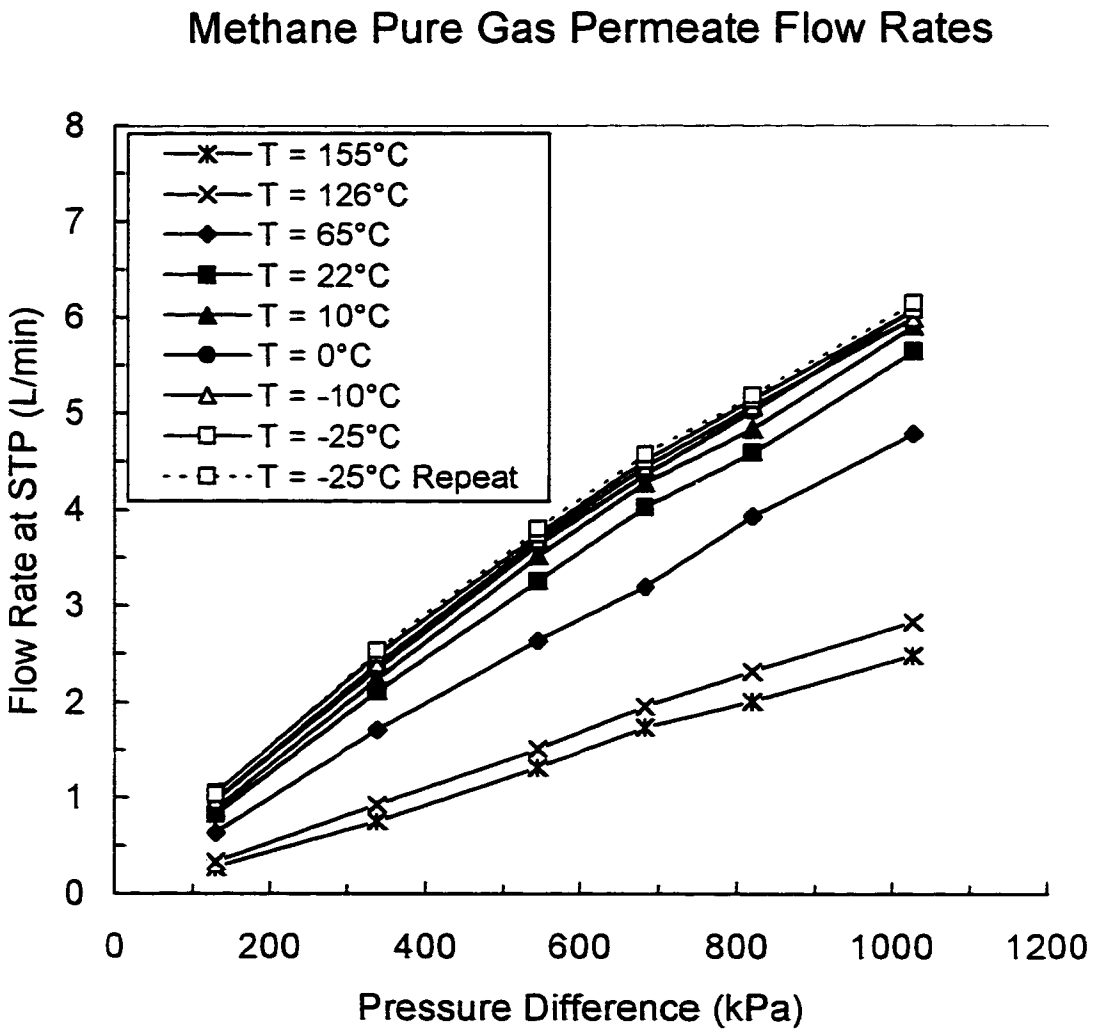

Figure 5.4 Pure methane permeation rates as a function of pressure difference measured at temperatures ranging from -25 to 155°C (M-2, permeability tests, feed pressures of 20-150 psig)

$$J = \rho D_s \frac{\Delta n_s}{\Delta x} \tag{5.17}$$

Diffusivity increases as the temperature increases according to equation 5.8. However, concentration loading (Δn_s) decreases as the temperature increases due to the decrease in adsorptivity of the adsorbent at high temperatures. Both the diffusivity and the surface loading terms are proportional to flux (J) as seen in equation 5.17. In the case of the SSF membrane, pure gas permeate flux (or flow rate) decreased as the temperature increased (Figures 5.3 and 5.4). This occurred because the effect of Δn_s was larger than the effect of diffusivity. For example the flow rate of methane at 155°C was lower than that at 125°C because the surface loading in equation 5.17 had an overall decreasing effect on flow rate.

From Figures 5.3 and 5.4 flow rates of hydrogen were higher than flow rates of methane. The flow rates are compared in Table 5.2 for a feed pressure of 100 psig.

Table 5.2: Permeation rates of hydrogen and methane corrected for STP. collected at 100 psig (M-2).

Temperature (°C)	H_2 Flow Rate (L/min)	CH_4 Flow Rate (L/min)
-25	5.38	4.57
-25 repeat	5.39	4.51
-10	4.89	4.44
0	4.92	4.36
10	4.71	4.28
22	4.41	4.02
65	3.86	3.20
125	3.07	1.96
155	2.90	1.74

Paranjape (1997) measured a permeation rate of 4.87 L/min for hydrogen at room temperature and 100 psig feed pressure. The difference between her

work and this data can be attributed to differences in the properties of the membrane surface layer which may occur during preparation. Rao and Sircar (1993) stated that very small changes in the pore size could have significant effects on permeation rates.

The effect of temperature on permeation rate was greater for hydrogen than for methane as can be seen by the proximity of the permeation rate isotherms for methane (Figure 5.4).

The permeation rate isotherms for hydrogen were linear with pressure as can be seen in Figure 5.3. Methane was slightly curved which suggests a non-linear variation of permeation rate with pressure driving force. The curvature is due to the non-linear relationship between methane adsorption and pressure. Methane is adsorbed on the surface layer of the membrane while the adsorption of hydrogen is minimal at all pressures. In fact, separation in the SSF membrane is only possible if the two components have different adsorption capacities. Stronger adsorption of one component results in an increase in surface diffusion and more blockage of non-adsorbing molecules. This occurs with methane as the temperature is decreased and is explained further in Chapter 6.

The permeation rates of methane at high temperatures (125 and 155°C) demonstrated less linearity than at low temperatures and suggests there are no adsorption effects for methane at these temperatures. This is explained further using calculated values of permeability.

5.5 Permeability of Hydrogen and Methane

Figures 5.5 and 5.6 show the permeabilities of hydrogen and methane calculated according to equation 4.3. Figure 5.5 shows data for feed pressures of 50-150 psig. Figure 5.6 shows data for feed pressures of 20-150 psig. The permeability of hydrogen was a relatively constant function of pressure difference for all temperatures. In Section 4.3 permeability was defined as the ratio of permeation rate to pressure difference across the membrane. The pressure

independence of hydrogen permeability was due to the linear relationship between permeation rate and pressure.

At low temperatures the permeability of methane was not constant, as permeation rate was not linearly dependent on pressure. Unlike for hydrogen, the curves representing permeation rate versus pressure difference in Figure 5.4 were non-linear. Consequently, dividing permeation rate by pressure difference to obtain permeability values resulted in non-constant values in Figure 5.6. Permeability clearly decreased at low temperatures, however, was relatively constant at high temperatures. The adsorption effects of the membrane layer can explain this. At low temperatures adsorption occurred and caused the decease in permeability. At high temperatures adsorption did not occur and the permeability was a linear function of pressure difference as with hydrogen. This showed that the assumption of non-adsorption of CH_4 at 125 and 155 °C (made when using Methods 1 and 2 to determine Knudsen diffusion) was reasonable.

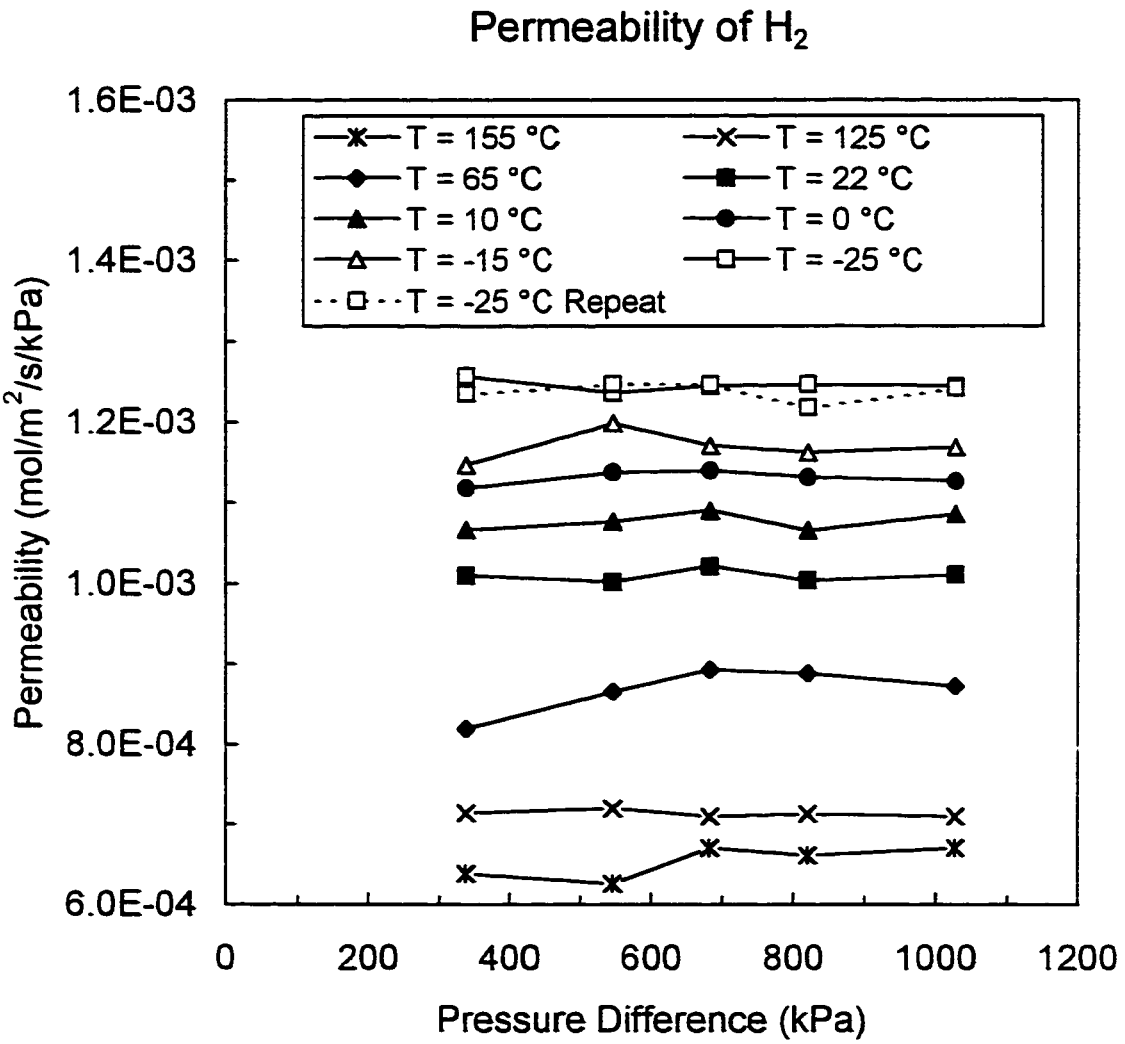

Figure 5.5: Permeabilities of pure hydrogen as a function of pressure difference measured at temperatures of -25 to 155°C (M-2, permeability tests, feed pressures 20-150 psig)

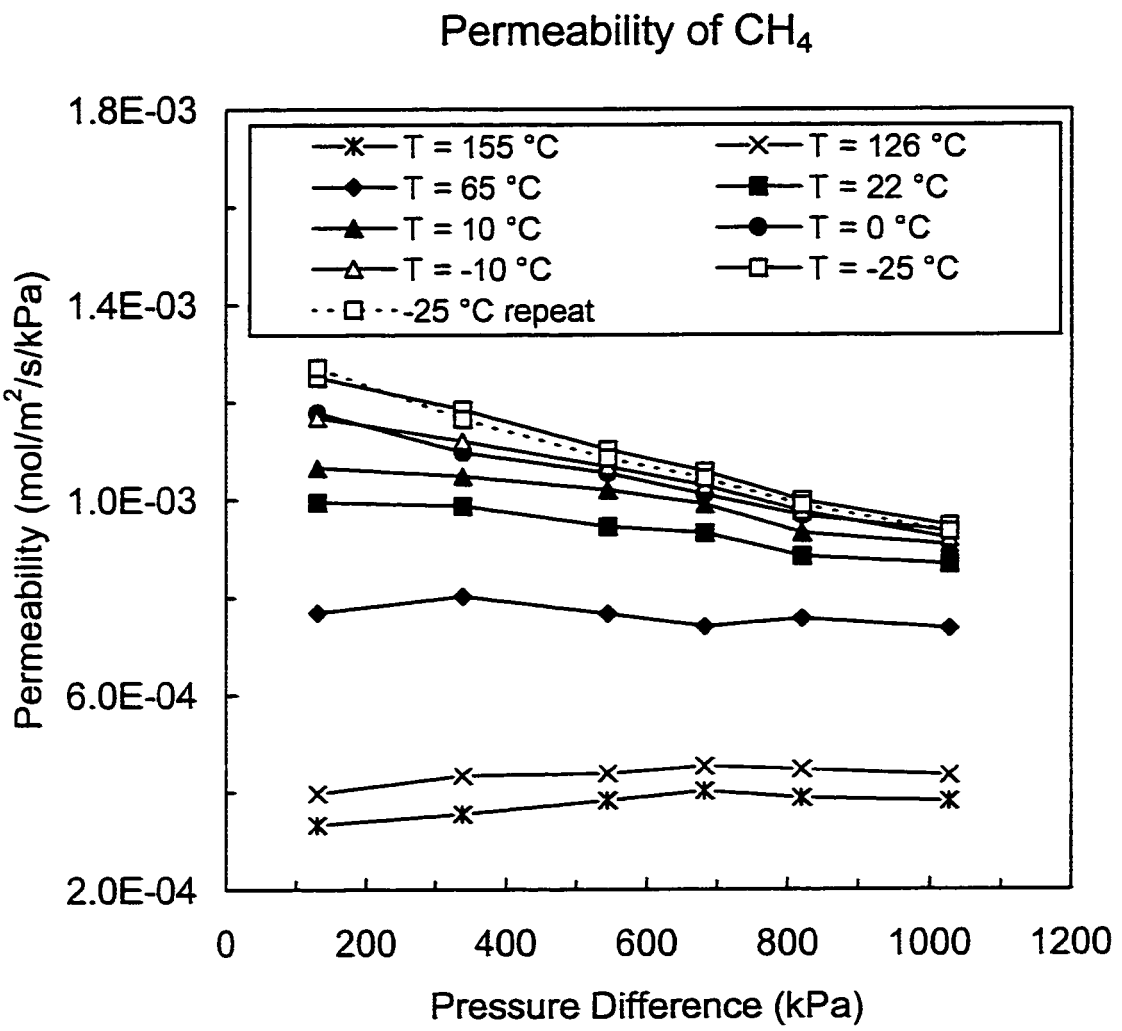

Figure 5.6: Pure gas permeability of methane as a function of pressure difference measured at temperatures of -25°C to 155°C (M-2, permeability tests, feed pressures 20-150 psig)

The decrease in methane permeability at low temperatures can be further explained using the adsorption theories developed by Brunauer. Activated carbon was classified as a Type I isotherm by Sircar *et al* (1996).

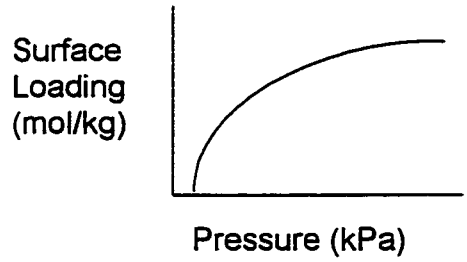

Figure 5.7: Example Type I (Brunauer classification) isotherm

With Type I Brunauer isotherms, surface loading increases non-linearly with pressure until a saturation point is reached. At saturation, the surface loading is independent of pressure. The decrease in permeability of methane occurred due to the non-linear relationship of surface loading with pressure. For a given pressure driving force, the surface loading did not increase proportionally and this caused the permeability (ratio of flux to pressure driving force) to decrease.

Decreasing permeability as a function of pressure difference was also found by Gilliland *et al* (1974) in their study of diffusion through porous Vycor glass (43 Å). The permeability of carbon dioxide at –50 °C was shown to reduce by approximately 4% for a pressure driving force increase of 540 torr (72 kPa) as seen in Figure 5.8. For temperatures of -78°C, the permeability of CO_2 first decreased and then increased at 27 kPa. This was the pressure at which monolayer coverage of the membrane had been reached. (Monolayer coverage is associated with the concentration at which the binding sites of the adsorbent are all occupied). At concentrations above monolayer coverage, it was postulated that diffusing molecules occupy a second layer temporarily. The bonds between the adsorbent and the molecules on the second layer are weaker than the bonds of the monolayer to the solid and diffusion occurs at a higher rate.

The increase in permeability at -78°C found by Gilliland *et al* could be explained by this mechanism. Above monolayer coverage, the weak physical bonds allow greater mobility of the gas molecules and this increases the overall diffusion rate. The increase in permeability of methane was not seen with the SSF membrane and therefore shows monolayer coverage was not reached.

Moreover, the mechanism for adsorption cannot be explained by capillary condensation as an increase in permeability would be seen with the onset of condensation, and this has not been the case in this work.

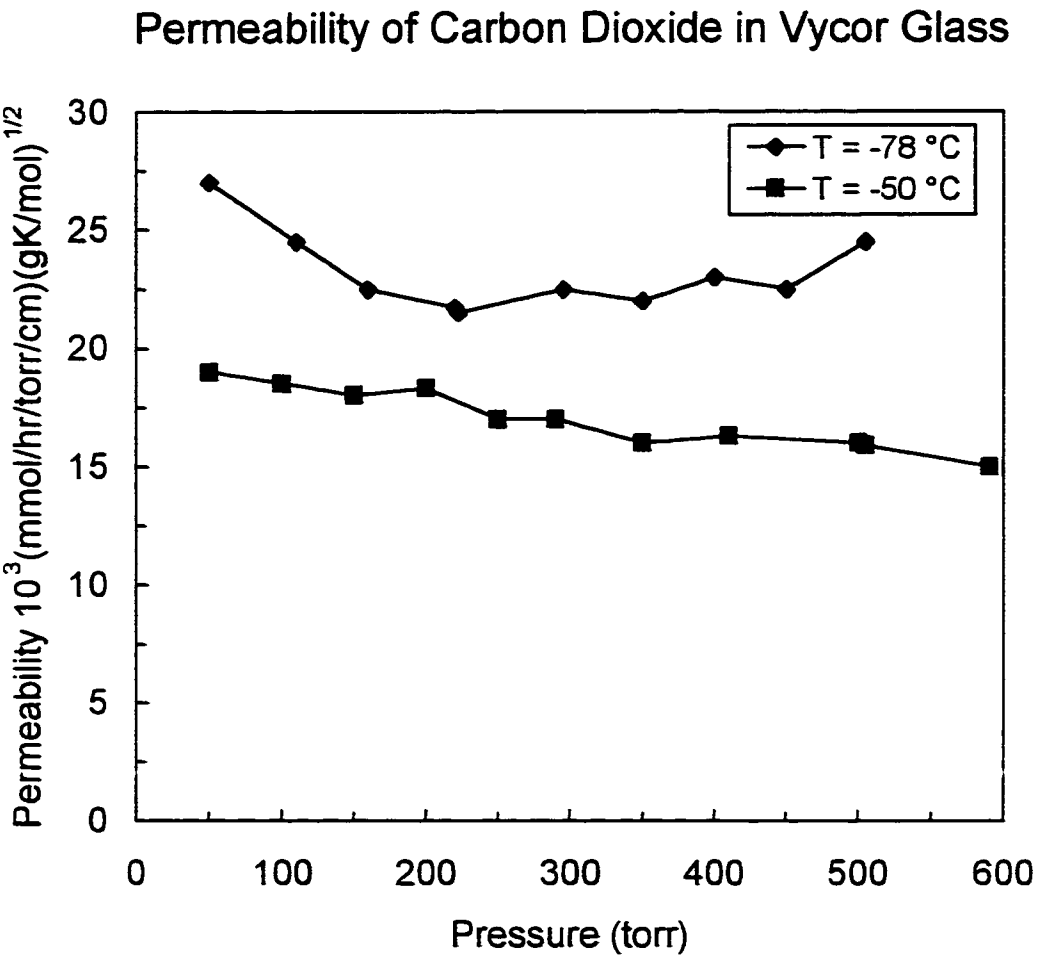

Figure 5.8: Permeability of carbon dioxide in Vycor Glass at -50° and -78°C as measured by Gilliland *et al*, (1974).

SUMMARY

This chapter outlines the experiments conducted to determine the type of diffusion occurring in the SSF membrane. High temperature was used to isolate gas phase flow from surface flow and two methods were used to determine whether gas phase flow occurred due to the Knudsen diffusion mechanism. The first method, which used an equation relating flow rate to temperature for a Knudsen diffusing gas, predicted the experimental data within 6 and 11%. The second method used a Knudsen equation relating the molecular weights of two gases to flow rate. This method predicted experimental values of methane within 35% and 40%. From these results it was concluded that Knudsen diffusion of hydrogen and methane is not a major contributor to overall flux in the SSF membrane.

Pure gas tests conducted for this study determined that permeation rates of hydrogen and methane decreased with increasing temperature. These results were explained by activated diffusion; the adsorption strength of the surface layer decreased the concentration of the surface phase and contributed significantly to the flow rate decrease. The diffusivity, however, increased due to the high temperature but its effect was not high enough to increase the overall flow rate as the temperature increased.

The overall decreases in flow rate and permeability for hydrogen and methane were shown in Figures 5.3-5.6. The increasingly negative slopes of the methane permeability curves as the temperature decreased were explained by the non-linear relationship of surface loading with pressure. The behaviour of methane with temperature and pressure showed that the assumption that the SSF membrane layer is a Type I isotherm (monolayer coverage) was reasonable. Methane was proven to be non-adsorbing at high temperatures as the permeability was constant with pressure. Hydrogen was shown to be non-adsorbing for all temperatures.

CHAPTER 6.0

LOW TEMPERATURE SEPARATION EXPERIMENTS

Experiments were conducted with hydrogen and methane to determine the effect of mixture concentration, mixture composition, temperature, pressure and flow rate on separation performance of the SSF membrane. Table 6.1 lists these experiments. The findings concerning flow rate, pressure and temperature for all mixtures are in Sections 6.1 to 6.3. Mixture permeabilities are compared to pure gas permeabilities in Section 6.4. Section 6.5 compares the two kinds of separation factors which can be computed, real and log-mean. Section 6.6 discusses the results of experiments in which 2% ethane was added to an equimolar mixture of hydrogen and methane.

Table 6.1: Experimental conditions for each hydrogen-methane mixture.

Mixtures (mol%)	Temperatures (°C)	Feed Pressures (psig)	Flow Rates
50% methane 50% hydrogen	-25, -10, 0, 10, 22, 65, 125, 155	20, 50, 80, 100, 120, 150	high and low at
25% methane 75% hydrogen	-25, -10, 0, 10, 22	50, 80, 100, 120, 150	high and low at –25°C
75% methane 25% hydrogen	-25, -10, 0, 10, 22	50, 80, 100, 120, 150	high and low at –25°C
49% methane 49% hydrogen 2% ethane	-25, -10, 0, 10, 22	50, 80, 100, 120, 150	high and low at –25°C

For each mixture a repeat experiment was conducted to ensure that the properties of the membrane had not changed over time. The repeat experiment was conducted at –25°C after all other temperature data had been collected. This ensured that the membrane properties were not affected by time usage or temperature fluctuations of –25°C to room temperature (22°C). Experiments were also conducted with high feed flow rates at –25°C.

6.1 Flow Rate

Feed flow rates ranging from 4 to 7 L/min were investigated. Paranjape (1997) determined that permeate flow rate at a given feed pressure was independent of feed flow rate for mixtures. This effect was also seen in this study. This meant that an increase in feed flow rate, for example from 5 to 6 L/min, resulted in a retentate increase of 1 L/min with the permeate flow rate remaining constant. Table 6.2 shows data for runs of 50/50 mixtures at different feed flow rates. The total permeate flow rate was found to vary by less than 8.5% for each temperature listed. The same trend was found when comparing the permeate flow rates of 25% and 75% methane. The average variations in permeate flow rates with changing feed flow rates for these mixtures (at 100 psig

and –25 °C) were 1% and 3%. The flow rates are shown in Table 6.3. A high flow rate experiment was not conducted at 22°C.

Table 6.2: Variation in permeate flow rates with changing feed flow rates for the 50/50 mixture at a feed pressure of 100 psig.

Temperature (°C)	Permeate Flow Rate (L/min at STP)	Feed Flow Rate (L/min at STP)	Temperature (°C)	Permeate Flow Rate (L/min at STP)	Feed Flow Rate (L/min at STP)
22	**3.78**	6.26	-10	**3.00**	5.71
10	**3.07**	4.68	-10	**2.77**	4.76
10	**3.24**	7.18	-25	**2.86**	4.61
0	**3.14**	4.32	-25	**2.75**	4.81
0	**3.14**	5.42	-25	**2.63**	5.27

Table 6.3: Variation in permeate flow rates with changing feed flow rate for 75% and 25% methane at -25°C and 100 psig.

Mixture	Permeate Flow Rate (L/min at STP)	Feed Flow Rate (L/min at STP)
75% Methane	**3.00**	4.48
75% Methane	**3.03**	5.11
25% Methane	**2.68**	4.36
25% Methane	**2.75**	5.66

The data in Table 6.2 also shows that permeate flow rate increased as the temperature increased for the 50/50 mixture. This was the opposite of pure hydrogen and methane results that showed an increase in pure gas permeation rates with decreasing temperature. The decreasing flows in Table 6.2 with decreasing temperature are explained by blockage in the membrane. Selectively adsorbed compounds on the SSF membrane are capable of blocking the permeation of hydrogen. When the temperature decreased this blockage increased and caused the overall flow rate to decrease. This result was also found with the 25% methane mixture. The permeate flow rates at 100 psig are shown in Table 6.4. This trend was not seen for the 75% methane mixture. This is most likely due to the counter-acting effects of methane concentration as a

function of temperature. At low temperatures the flow rate is low due to the blockage effects. At higher temperatures (22°C) adsorption is not as strong and the flow rate was low due to the decrease in surface flow.

Table 6.4: Permeate flow rates as a function of temperature and mixture concentration at 100 psig.

Temperature (°C)	Permeate Flow Rates (L/min at STP) 25% methane	Permeate Flow Rates (L/min at STP) 75% methane
22	3.21	2.91
10	3.19	2.32
0	3.09	3.14
-10	3.05	3.25
-25 (low flow rate)	2.67	3.00

Looking at the permeate flow rates at -25°C for different mixtures it was also shown that permeate flow rates increased with increasing methane concentration (for example the average permeate flow rates calculated using repeat data and the data above; 25%-2.72 L/min, 50%-2.75 L/min, 75%-3.02 L/min). When the methane concentration increased the amount and mobility of the adsorbed molecules on the surface of the membrane contributed a slight increase in permeate flow rate. This effect was, however, not always seen with other temperatures and pressures. The increase in flow with increasing methane concentration is inconclusive due to the range of experimental error. Uncertainty in the data is ±3.0%.

6.1.1 Feed Flow Rate and Separation

Two feed flow rates were used at -25°C for each mixture to determine the effects of flow rate on separation. Figures 6.1-6.3 show the results of varying flow rate on the rejection of CH_4 and recovery of H_2. The high flow rate rejection-recovery curves followed the same trend as the curves for low feed flow rates, however, they were shifted towards higher recovery rates and lower rejection

rates. For example low flow rate data at a pressure of 80 psig (25% CH_4, 5.64L/min) produced rejection-recovery results (64.2%, 56.3%) that matched closely with the high flow rate rejection recovery data of 100 psig (66.8%, 56.1%). This effect was due to the relatively constant permeate flow rate. For varying feed flow rates, a constant volume of gas passed through the membrane. The retentate flow increased as the feed flow rate increased and resulted in a higher concentration of hydrogen retained and lower rejection of methane.

This result allows easy prediction of the performance of the membrane for different flow rates. Given the rejection-recovery results for one flow rate, it was possible to predict the results of the rejection-recovery data for higher feed flow rates (it is simply shifted down on the rejection-recovery plot). It also shows that to attain the same separation, high flow rates require larger pressure driving forces than low feed flow rates and there is a limit to feed flow rate in the membrane. The membrane would require a larger surface area to produce a separation for high flow rate feed streams.

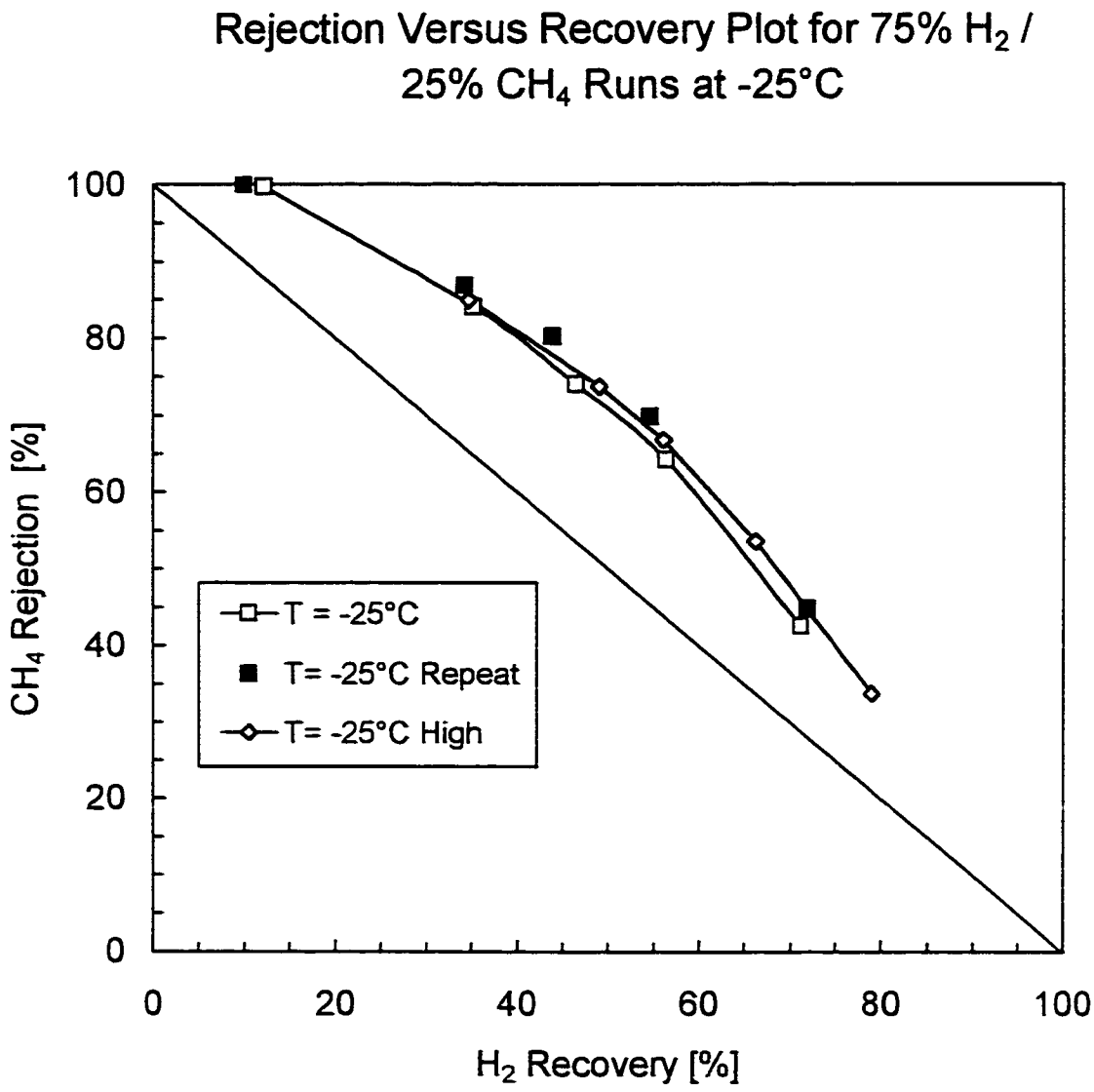

Figure 6.1: Methane rejection versus hydrogen recovery for a feed of 75% hydrogen and 25% methane at -25°C (M-2, feed pressures of 50-150 psig)

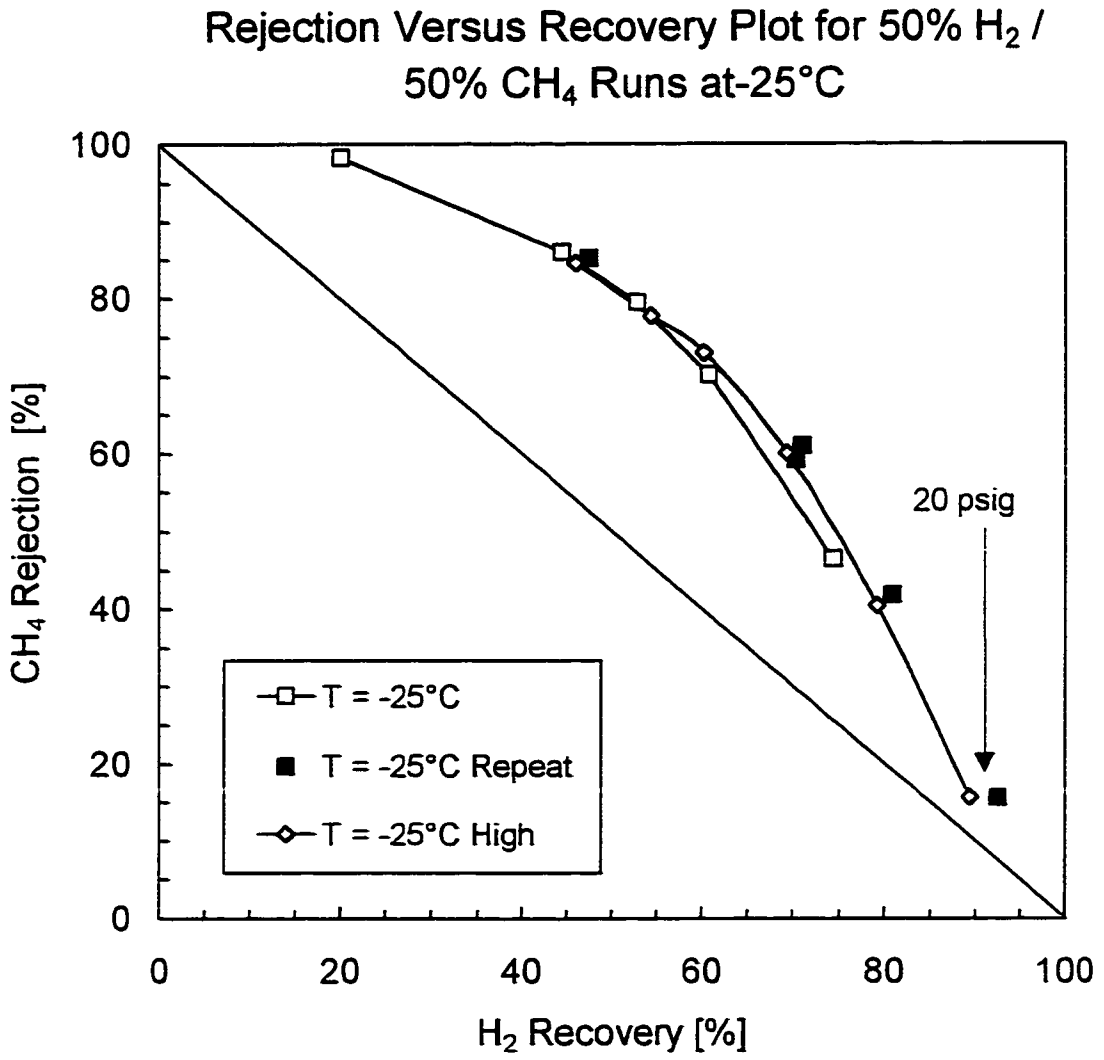

Figure 6.2: Methane rejection versus hydrogen recovery for a feed of 50% hydrogen and 50% methane at -25°C (M-2, feed pressures of 50-150 psig, low feed flow rates)

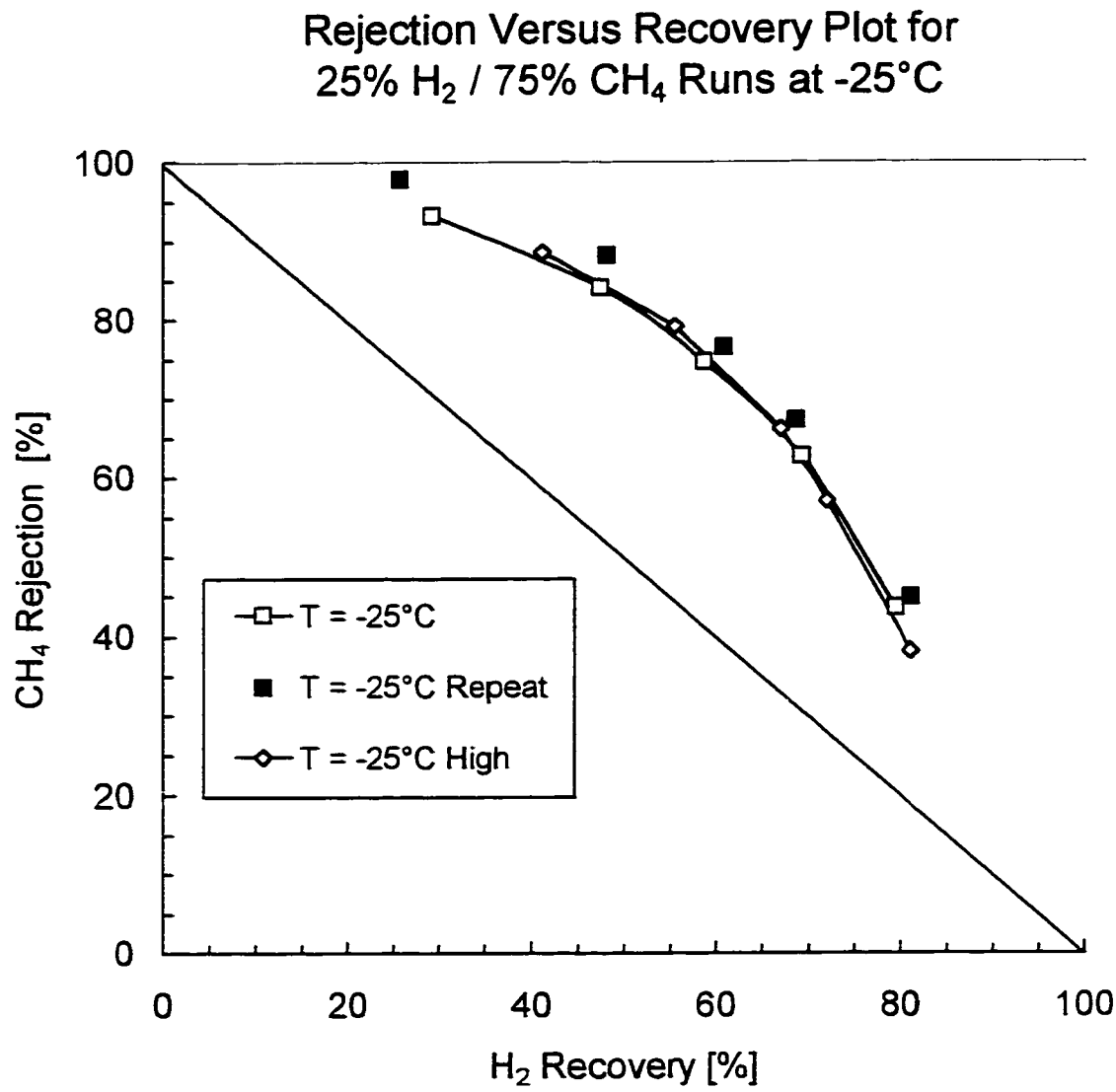

Figure 6.3: Methane rejection versus hydrogen recovery for a feed of 25% hydrogen and 75% methane at -25°C (M-2, feed pressures of 50-150 psig).

6.2 Pressure

As with the pure gas tests, increasing feed pressure increased the permeation rate for the mixtures. This was due to the increase in driving force for permeation as the feed pressure increased. Driving force increased due to the increase in partial pressure differences for all mixtures. (The permeate side pressure was maintained at 1 psig for all experiments.) A feed pressure range of 20-150 psig was investigated for the equimolar mixture of hydrogen and methane. Rejection-recovery results of the -25°C runs with this mixture are shown in Figure 6.2. The rejection of methane at feed pressures of 20 psig was less than 27% and therefore it was decided that this pressure would not be investigated for subsequent mixtures. For the flow rates investigated, pressures in the range of 80-120 psig were shown to give the best rejection-recovery results. At low feed pressures, the retentate flow rate was too high and this resulted in high recovery rates but low rejection rates as most feed gas was retained at feed pressure. For high feed pressures, rejection rates were high and recovery rates were low.

6.3 Temperature

For all mixtures, a decrease in temperature resulted in a separation improvement. Figures 6.4-6.7 show the rejection-recovery results for the 25% methane mixture, the 50/50 mixture at high and low flow rates and the 75% methane mixture. The curves moved closer to the upper right side of the rejection-recovery plot as the temperature decreased, demonstrating an improvement in separation.

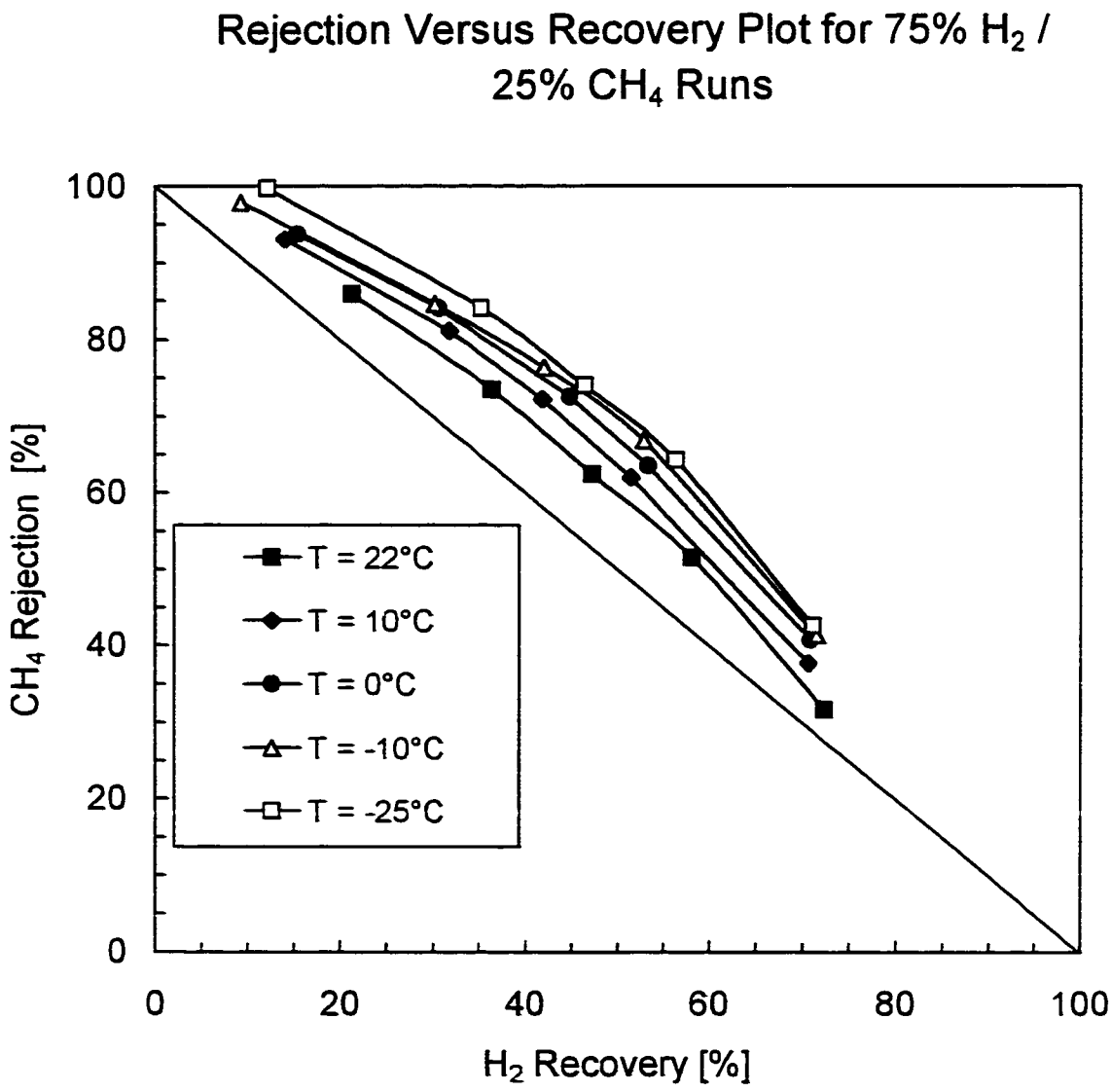

Figure 6.4: Methane rejection versus hydrogen recovery for a feed of 75% hydrogen and 25% methane at different temperatures (M-2, feed pressures of 50-150 psig)

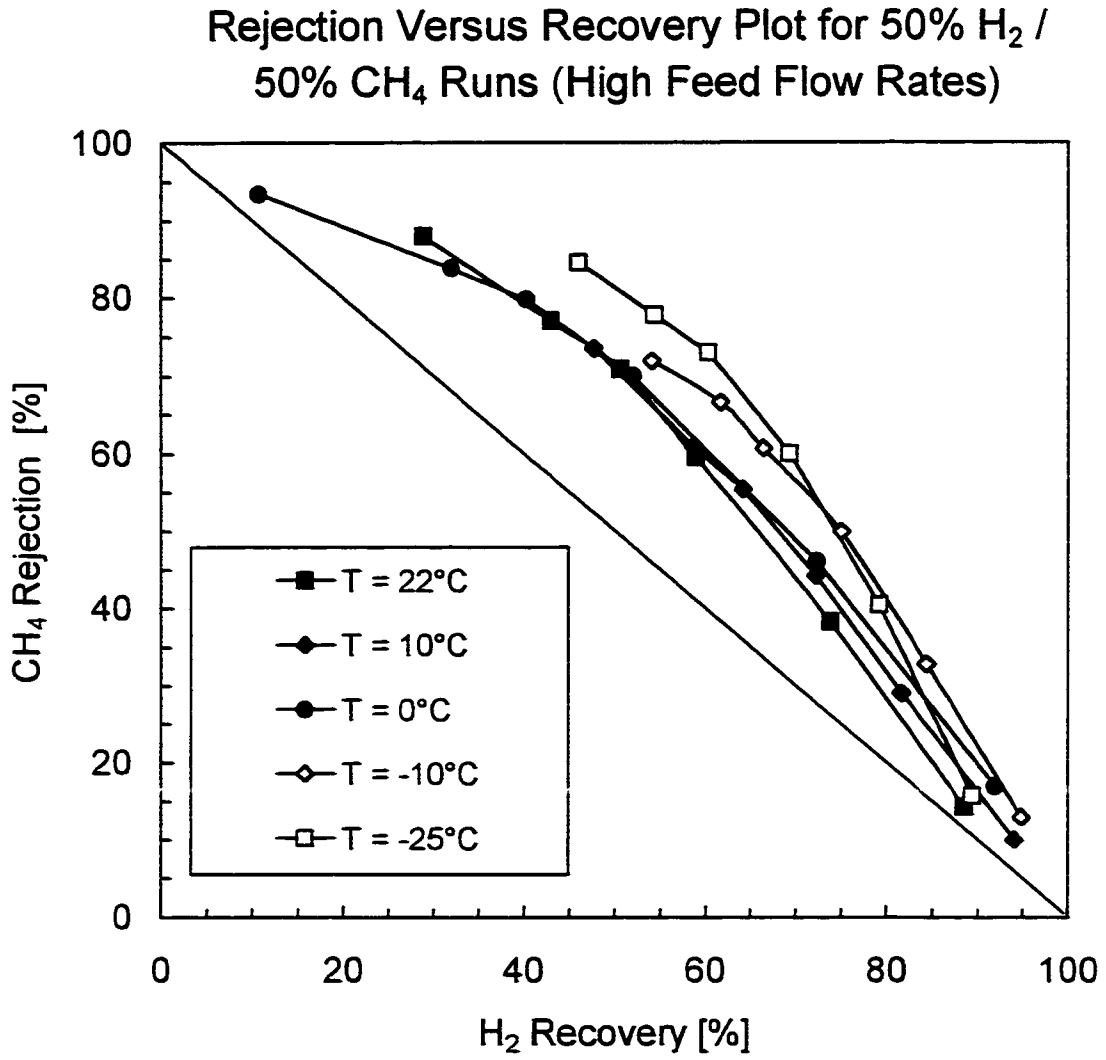

Figure 6.5: Methane rejection versus hydrogen recovery for a feed of 50% hydrogen and 50% methane at different temperatures and high feed flow rates (M-2, feed pressures of 50-150 psig)

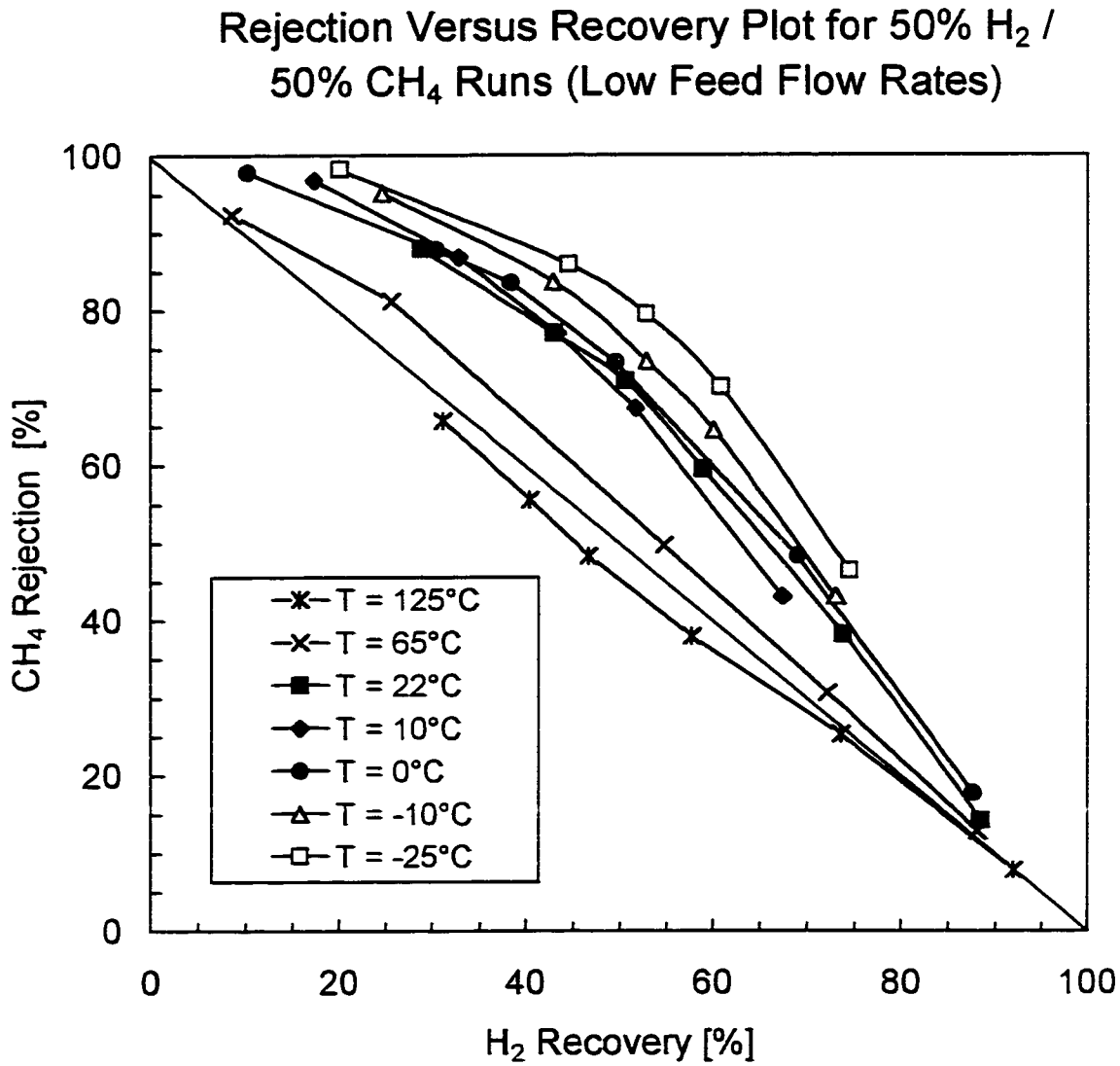

Figure 6.6: Methane rejection versus hydrogen recovery for a feed of 50% hydrogen and 50% methane at different temperatures and low feed flow rates (M-2, feed pressures of 20-150 psig).

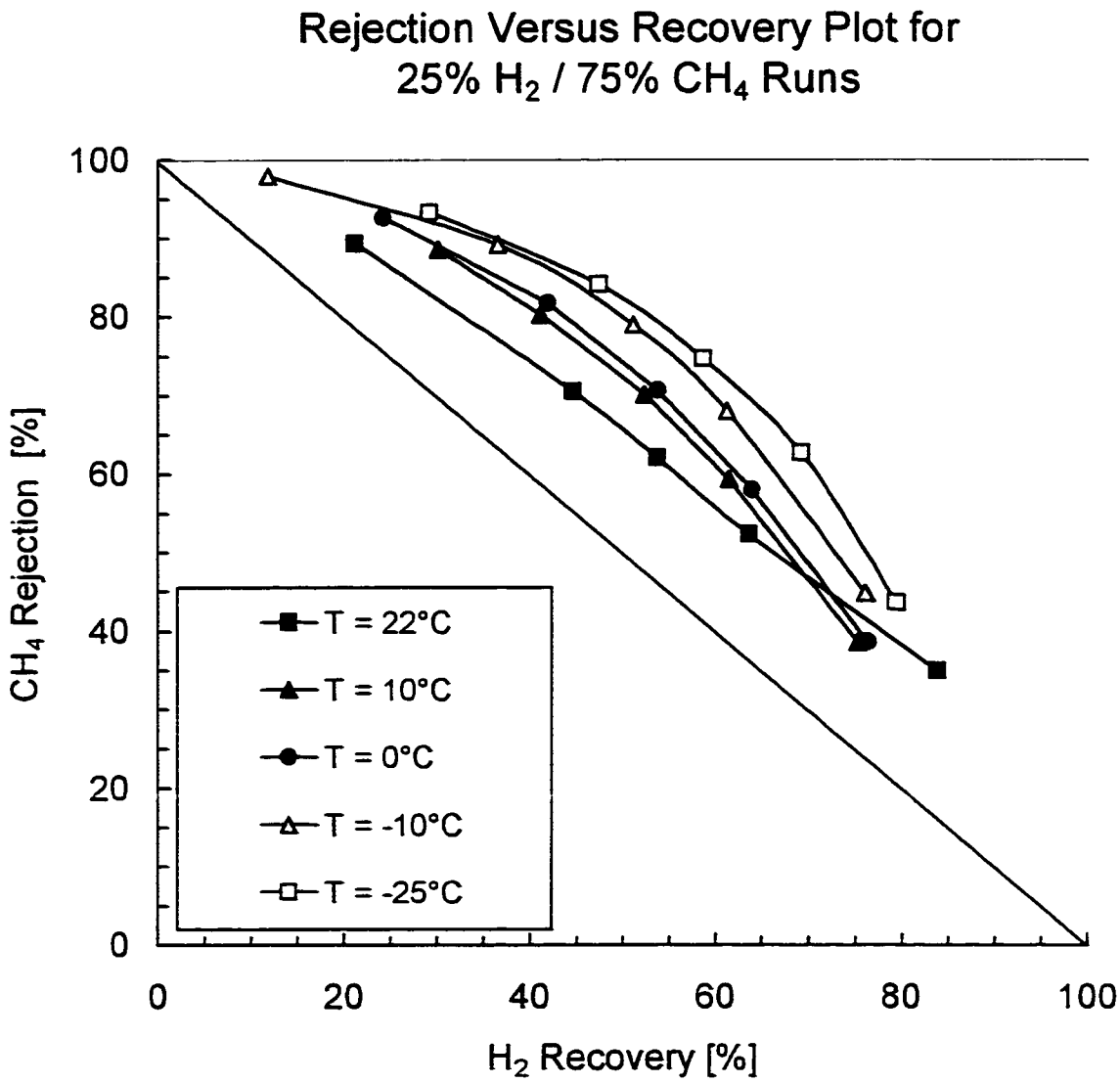

Figure 6.7: Methane rejection versus hydrogen recovery for a feed of 25% hydrogen and 75% methane at different temperatures (M-2, feed pressures of 50-150 psig)

The rejection and recovery rates for decreases in temperature from 22°C to -25°C are shown in Table 6.5. The results from the repeat -25°C runs were averaged.

Table 6.5: Comparison of rejection-recovery rates for temperatures of –25 and 22°C at feed pressures of 80 and 100 psig.

Mixture	T (°C)	80 psig		100 psig	
		Rejection %	Recovery %	Rejection %	Recovery %
25% CH_4	22	51.5	58.1	62.4	47.2
	-25	67.2	56.0	78.3	45.7
50% CH_4 (high)	22	59.6	58.9	70.9	50.6
	-25	59.6	69.9	72.1	60.7
50% CH_4 (low)	22	59.6	58.9	70.9	50.6
	-25	79.5	52.8	70.1	60.8
75% CH_4	22	52.3	63.6	62.1	53.7
	-25	64.5	68.9	75.5	59.7

Table 6.5 shows that the greatest improvement with temperature occurred in the mixture with the highest concentration of methane. The rejection and recovery rates both improved at pressures of 80 and 100 psig. Rejections improved by at least 12% and recoveries improved by at least 5.3%. The positive results were attributed to higher amounts of methane in the feed. hindering the permeation of hydrogen.

For the 50/50 mixture at -25°C, there were large improvements (>10%) in recoveries over 22°C for high flow rates. However, there was no improvement in the rejection rates. Recoveries improved due to the stronger adsorption of methane at lower temperatures. This blocked the permeation of hydrogen and a higher concentration remained in the retentate. For low flow rates, the rejection increased by approximately 20% at 80 psig however the recovery rate decreased by approximately 6%. At 100 psig the recovery improved by approximately 10% but the rejection declined by approximately 1%. For each experiment there was

a trade off between rejection and recovery at some point along the curve. For the low flow rate experiment the trade off occurred between 80 and 100 psig and therefore showed a decrease in recovery at one pressure and a decrease in rejection at the other pressure.

The 25% methane mixture showed rejection improvements of approximately 15% for both pressures. However the recovery rates were the lowest of all mixtures. Insufficient blockage of the pores of the membrane perhaps caused high permeation rates of hydrogen with this mixture and produced low recovery rates. This showed that the SSF membrane was best suited for feeds with low concentrations of hydrogen.

As the temperature decreased, the non-linearity of the rejection-recovery curves increased. This was noticeable in looking at Figures 6.6. This was due to the non-linear relationship of surface loading and pressure for methane discussed in Section 5.4. Each point represents a different feed pressure and therefore a non-linear curve was created as the temperature decreased. Non-linearity was also related to feed concentration. As the amount of methane in the feed increased the non-linearity increased.

6.3.1 High Temperature

The non-linearity of the rejection recovery lines was most apparent in the comparison of the high and low temperature experiments. Figure 6.6 includes the results of separation experiments with a 50/50 mixture at 65 and 125°C. The results show that the data was represented by nearly straight lines at these temperatures. This is in agreement with the results found with pure methane at these temperatures. The straight lines were indicative of little or no adsorption occurring.

The 45° lines on the rejection-recovery curves indicate no separation. The longest perpendicular extension from this 45° line represented the best separation. The longest *possible* perpendicular line was the line drawn from the

45° line to the upper right side of the rejection-recovery plot. At 125°C separation did not occur as the rejection-recovery curve was below the 45° line. A perpendicular extension was in the opposite direction to improving separation and therefore no separation occurred. From the definitions of rejection and recovery, this meant that more hydrogen was permeating than methane. This was due to the absence of any adsorption effects for the methane molecule at high temperatures and the smaller size of the hydrogen molecule.

The length of an extended perpendicular line from the 45° line increased as the non-linearity in the rejection-recovery line increased. This finding was interesting as it further supported the result that a higher concentration of methane improved separation.

Figure 6.8 shows the flow rates for pure hydrogen and methane and compares them to the mixture (50/50) flow rates. The mixture flow rate at -25°C is lower than at 22°C and shows the significant effect of low temperatures on the separation of the membrane. Permeate flow rates are constant for a given feed pressure and temperature. With a decrease in temperature, it would be necessary to decrease the feed flow rate of a mixture to the SSF membrane to achieve optimal separation. The effect of high temperature on mixture flow rate was similar to the effect of low temperature (both lower than 22°C). This is in contrast to the pure gas results that showed that there was only a small flow rate effect at low temperatures while high temperatures significantly decreased flow rates.

Air Products have determined that the pore dimensions and structure of the membrane layer are not affected by temperatures up to approximately 350°C.

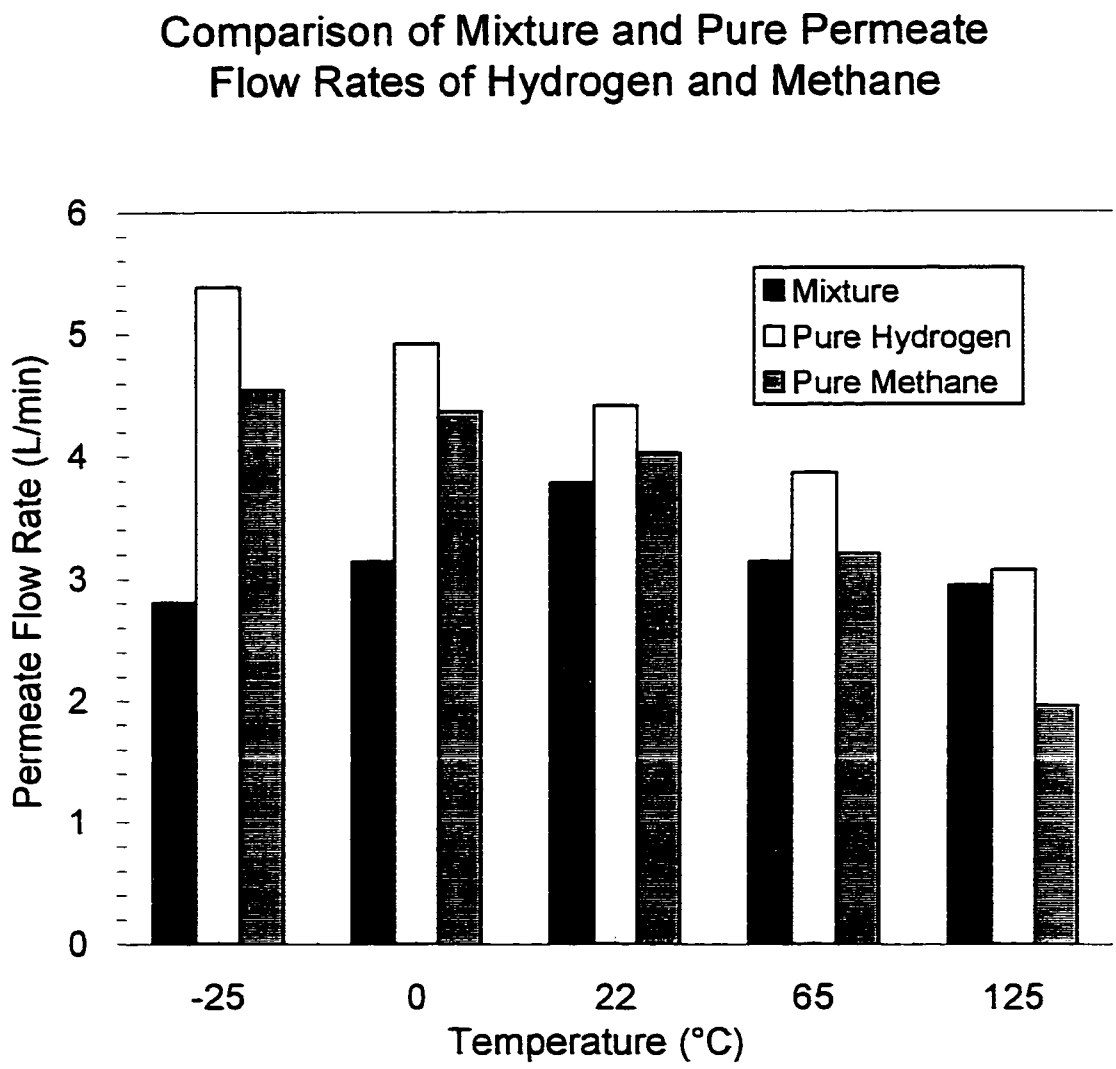

Figure 6.8: Permeate flow rates of mixture (50/50) and pure hydrogen and methane determined experimentally at temperatures ranging from -25 to 125°C (M-2, 100 psig feed pressure, low flow rates)

6.4 Permeability

Equation 4.4 was used to calculate the permeabilities of hydrogen and methane mixtures. The logarithmic mean partial pressure difference (equation 4.5) was calculated to determine the driving force for permeation. This was the method used by Rao and Sircar (1993, 1996) to calculate mixture permeabilities.

Figure 6.9 shows that the permeability of hydrogen in an equimolar mixture was lower than pure gas permeability at -25 °C and 22°C for all feed pressures. This was due to the increase in permeation hinderance of hydrogen at lower temperatures.

The 50% methane permeabilities shown in Figure 6.10 at 22°C and -25°C were both higher than the pure gas permeabilities at feed pressures of 80-150 psig. Figure 6.10 also shows that the mixture permeabilities of methane increased with increasing temperature. This was perhaps due to the increase in total mixture permeate flow rate with temperature discussed in Section 6.1.

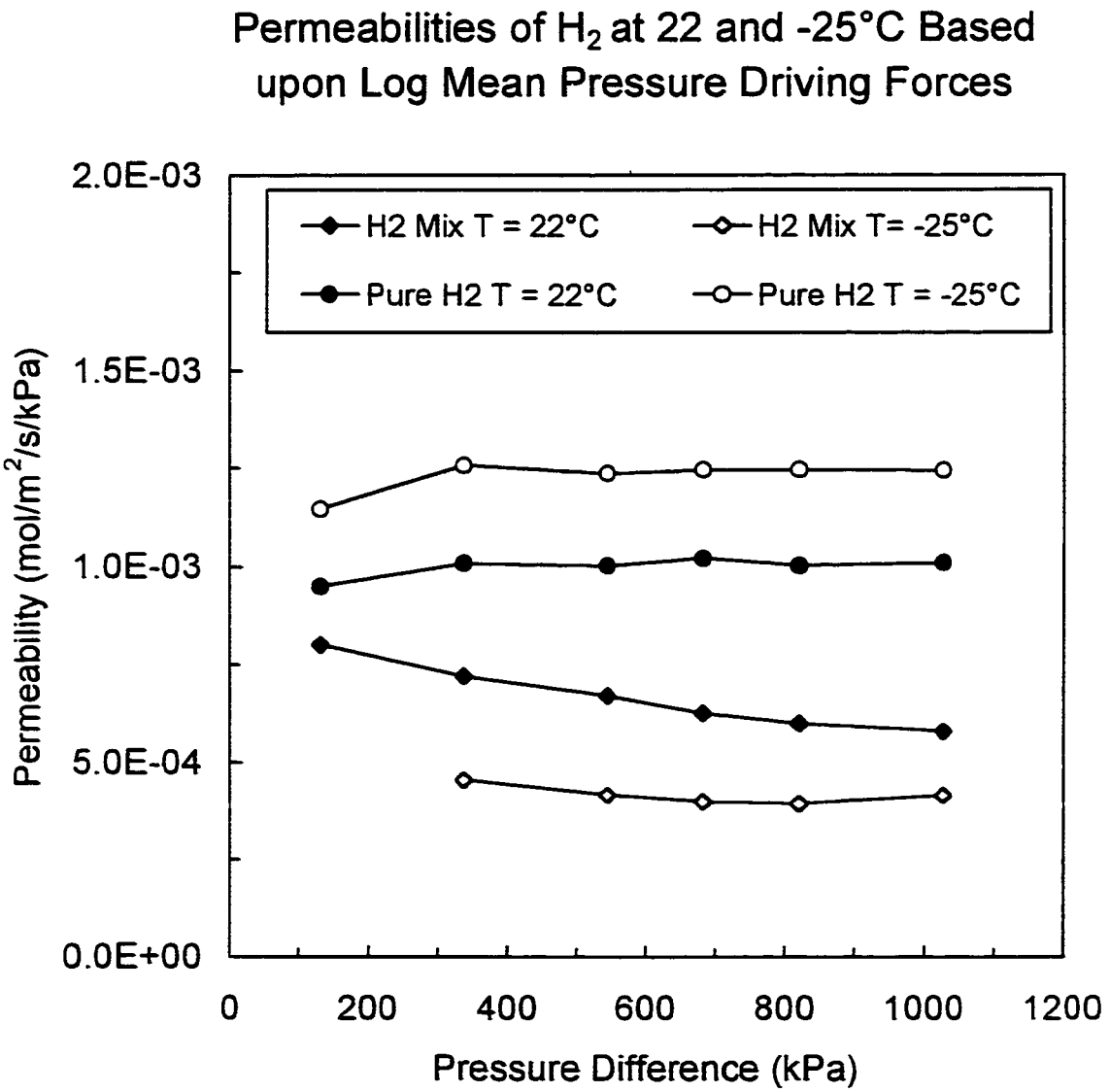

Figure 6.9: Comparison of pure hydrogen permeabilities with 50/50 mixture permeabilities calculated using log mean pressure driving forces, equation 4.5 (M-2, feed pressures 20-150 and 50-150 psig, T=-25°C and T=22°C)

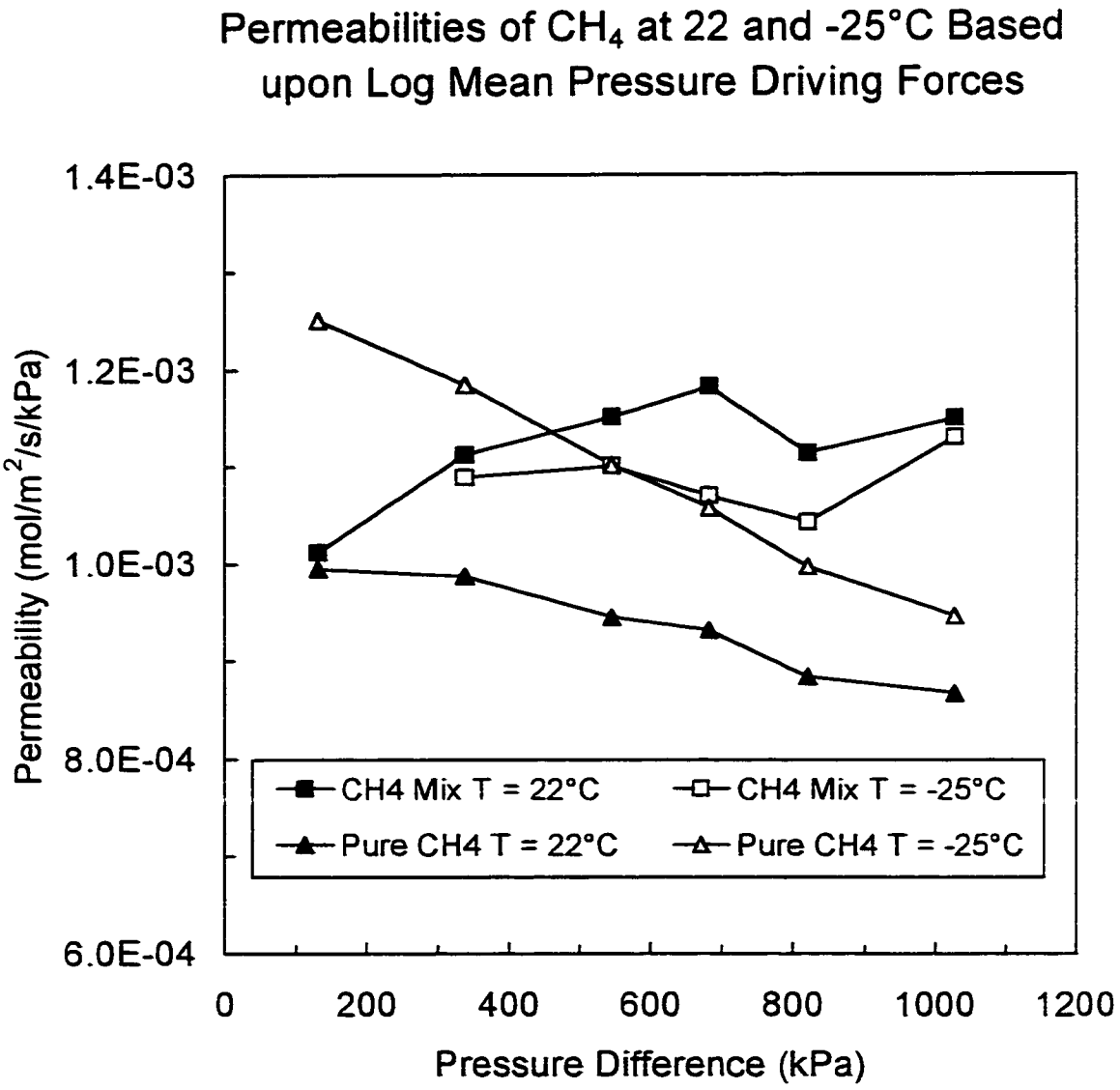

Figure 6.10: Comparison of pure methane permeabilities with 50/50 mixture permeabilities calculated using log mean pressure driving forces, equation 4.5 (M-2, feed pressures 20-150 and 50-150 psig, T=-25°C and T=22°C)

6.5 Separation Factors

Real separation factors (equation 4.8) were calculated for the hydrogen-methane mixtures. The calculated ideal separation factors are discussed in Appendix A. The separation factor is a measure of the difference of the permeate and feed concentrations. High separation factors occur if there is a high concentration of methane in the permeate and a low concentration of methane in the feed. Figures 6.11 to 6.13 show the real separation factors for the 25%, 50% and 75% methane mixtures.

Separation factors decreased as temperature and pressure increased. The highest separation factors occurred with mixtures of 75% methane. The highest separation factor corresponded to a hydrogen recovery rate of approximately 25% and a methane rejection rate of approximately 97%.

For the 50% methane mixture at the lowest pressure (20 psig) the permeation rate of methane was most likely too low to allow significant blockage and this resulted in low separation factors. At 125°C, the separation factors were below 1, which was in agreement with the results of the rejection recovery curve (Figure 6.5 showed that there was no separation at this temperature as the curve was below the 45° line). For all the mixtures there was a significant increase in separation factors between the temperatures of -25°C and -10°C compared to other temperatures

Separation factors did not give a proper indication of the performance of the SSF membrane as the highest separation factor corresponded to the lowest recovery rates of hydrogen. The rejection-recovery curves gave a better measure of the separation.

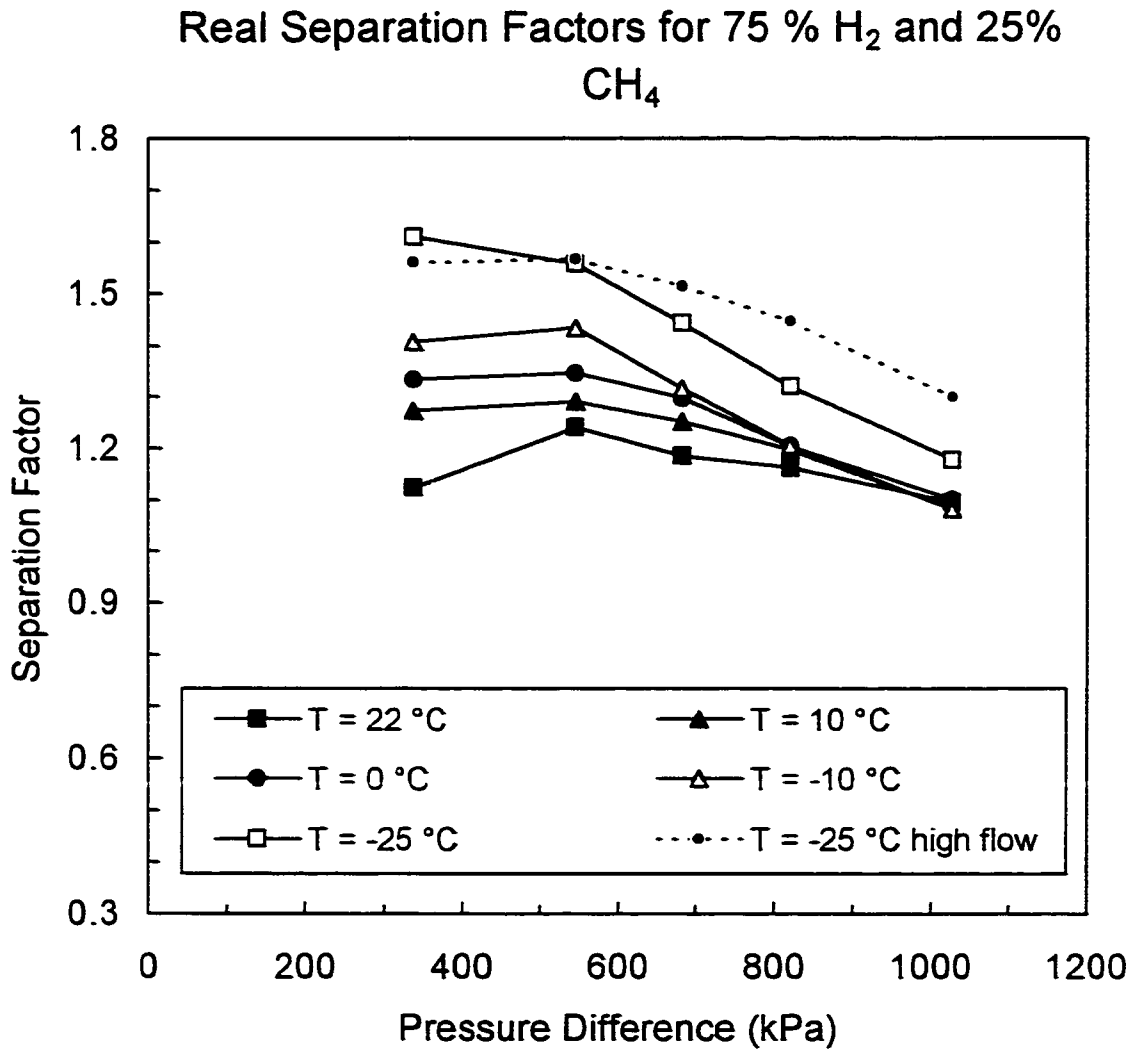

Figure 6.11: Real separation factors for 25% methane mixtures as a function of temperature (M-2, feed pressures of 50-150 psig)

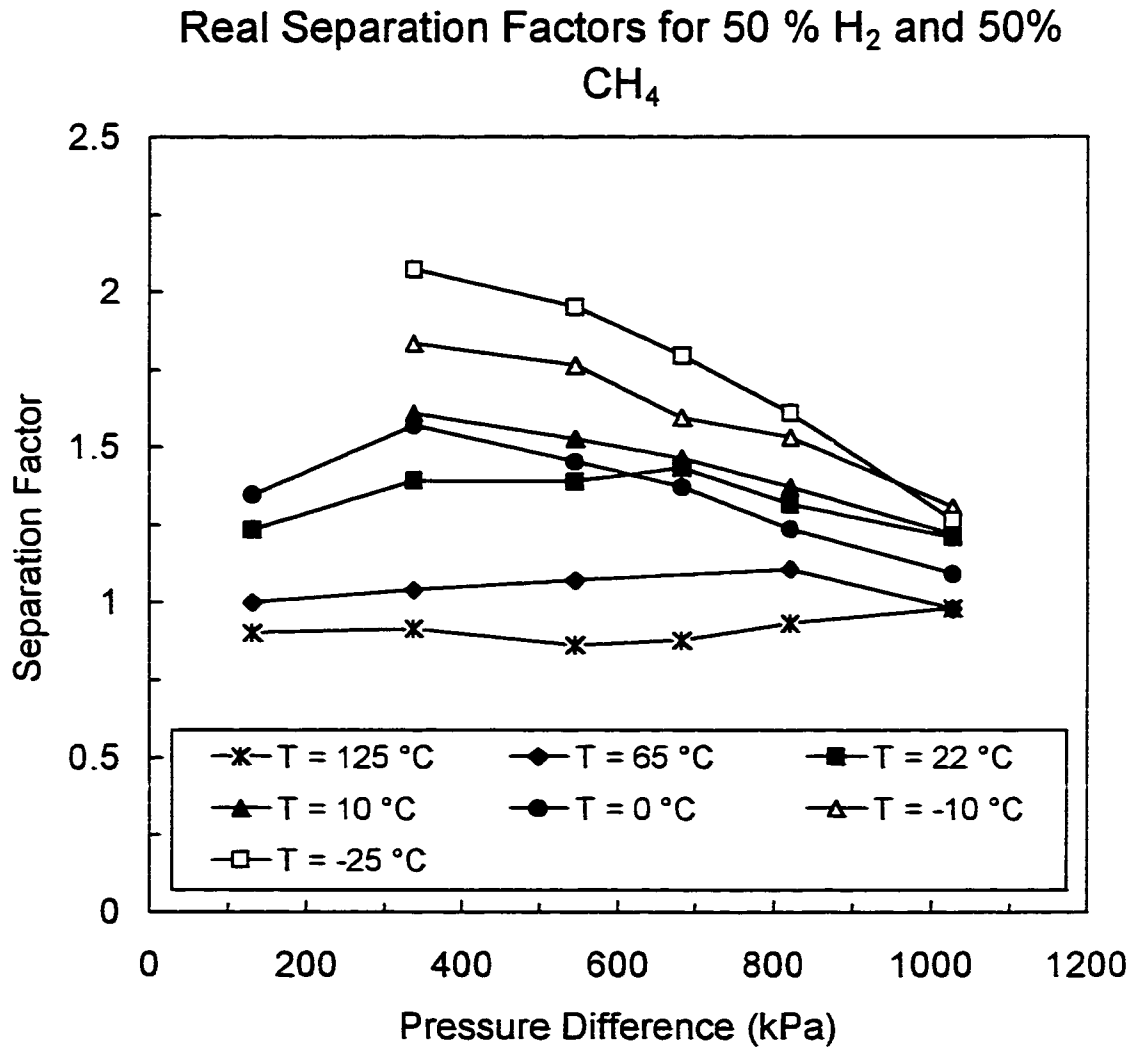

Figure 6.12: Real separation factors for 50% methane mixtures as a function of temperature (M-2, feed pressures of 50-150 psig)

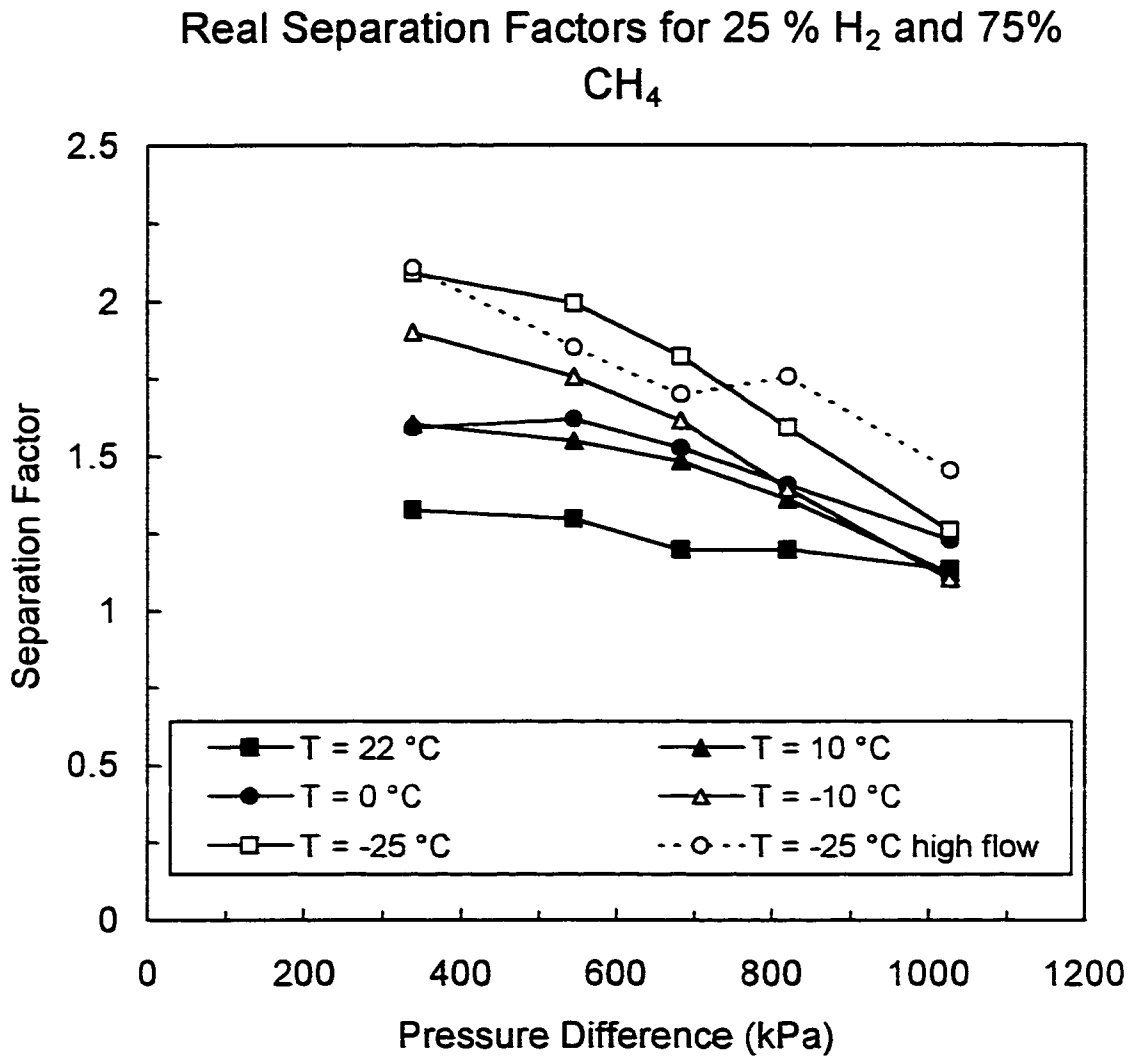

Figure 6.13: Real separation factors for 75% methane mixtures as a function of temperature (M-2, feed pressures of 50-150 psig)

6.6 Effect of 2% Ethane in Equimolar Mixture

A mixture of 2% ethane, 49% methane and 49% hydrogen was used in separation experiments to determine if the increased amount of more polar molecules in the feed would improve H_2/CH_4 separation. It was presumed the stronger adsorption effects of the ethane would create more blockage in the pores of the membrane and improve hydrogen recovery. Experiments were conducted at temperatures of –25 (high flow rate), -10, 0 and 22°C.

Figure 6.14 compares the rejection recovery curves for the 2% ethane mixture with the 50/50 methane-hydrogen mixture. The first experiment to be conducted was the high flow rate test at –25°C and was shown to give a slight improvement in separation over the 50/50 mixture. The second test was at -10°C and was also shown to improve the separation.

An experiment at a lower flow rate was conducted at -25°C, however, the results were significantly different than the results of the high flow rate experiment, as seen in Figure 6.15. The permeate flow rates were much lower and the rejection recovery results showed a poorer separation than predicted from the high flow rate results. The reduction in permeate flow rate was assumed to be the result of contamination of the membrane layer with a component present in the mixture cylinder. For the hydrogen and methane mixtures, the activated carbon trap was changed approximately every 20 hours. Only four experiments were conducted with the 2% ethane mixture (12 hours) and the effects of irreversible adsorption were found. It was presumed the activated carbon was unable to adsorb the required amount of impurities due to the higher affinity of ethane (compared to CH_4) on the adsorbent pore sites. Regeneration of the membrane was attempted but it was unsuccessful.

The comparison of the ambient temperature runs in Figure 6.14 shows that the mixture with no ethane produced significantly better results. The room temperature run with 2% ethane was, however, conducted the day before the membrane was found to have decreased in permeability.

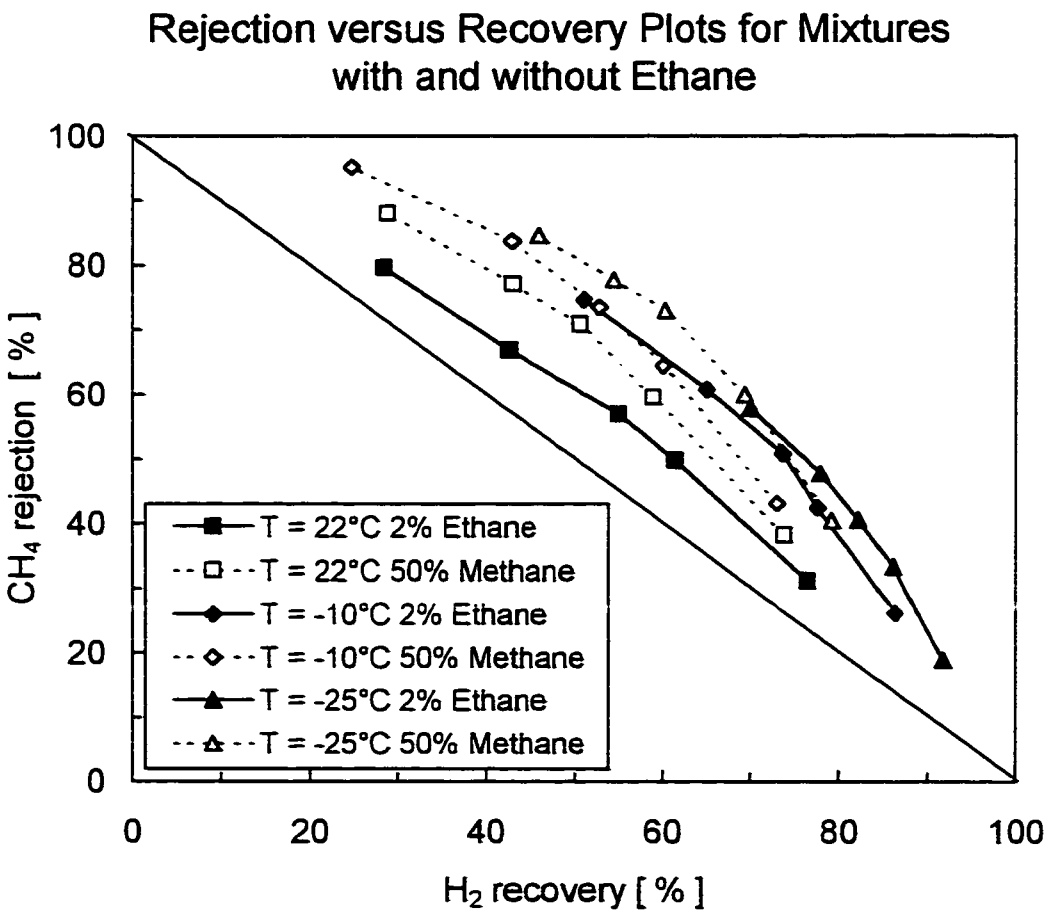

Figure 6.14: Comparision of methane rejection versus hydrogen recovery curves for a 50/50 mixture and a 49/49/2% ethane mixture (M-2, feed pressures of 50-150 psig high and low feed flow rates)

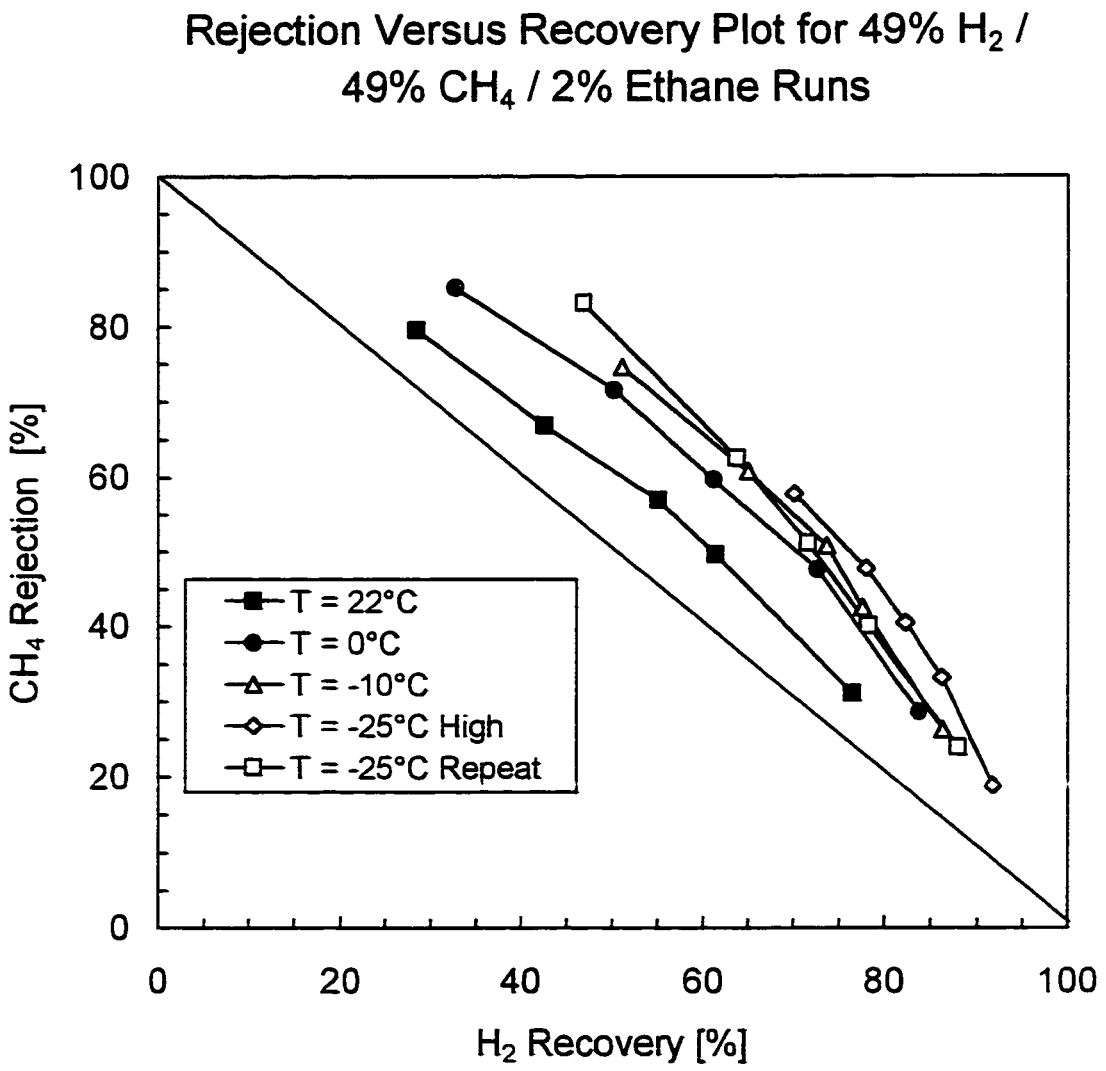

Figure 6.15: Methane rejection versus hydrogen recovery for a feed of 49% hydrogen and 49% methane and 2% ethane at different temperatures (M-2, feed pressures of 50-150 psig, high and low feed flow rates)

The permeate flow rates of the mixture with ethane were lower in comparison with 50/50 mixture. This was most likely due to a combination of the reduced mobility of the ethane molecule and blockage of the membrane pores. Table 6.6 shows the permeate flow rates for the two mixtures at –25 and –10°C. For feeds with high concentrations of polar components it would be necessary to investigate the feed pressures and feed flow rates required to give optimal separation conditions at low temperatures. Low permeate flow rates could effect the rejection rate and it would be necessary to decrease the feed flow rate or increase the pressure driving force to reach optimal separation.

Table 6.6: Comparison of mixture permeate flow rates with and without ethane at –10 and -25°C.

Pressure Driving Force (kPa)	Permeate Flow Rates at -10°C (L/min at STP)		Permeate Flow Rates at -25°C (L/min at STP)	
	50/50 H_2 /CH_4	2% Ethane	50/50 H_2 /CH_4	2% Ethane
338	1.62	0.79	1.65	0.62
545	2.4	1.28	2.35	1.07
682	2.78	1.55	2.63	1.34
820	3.37	1.86	3.27	1.60
1027	4.06	2.37	3.82	2.01

Table 6.6 also shows that the reduction in permeate flow rate as the temperature decreased was greater for the mixture containing ethane. For example the reduction in permeate flow rate at 1027 kPa was 6% for the 50% methane mixture, however, the reduction was 15% for the mixture containing ethane. This suggests that the permeation rates of components with higher polarity are affected strongly by temperature.

Figure 6.16 compares the separation factors for the 2% and 50% methane mixtures at -25°C. The real separation factors for the mixture containing ethane are greater than the separation factors for the 50% methane mixture.

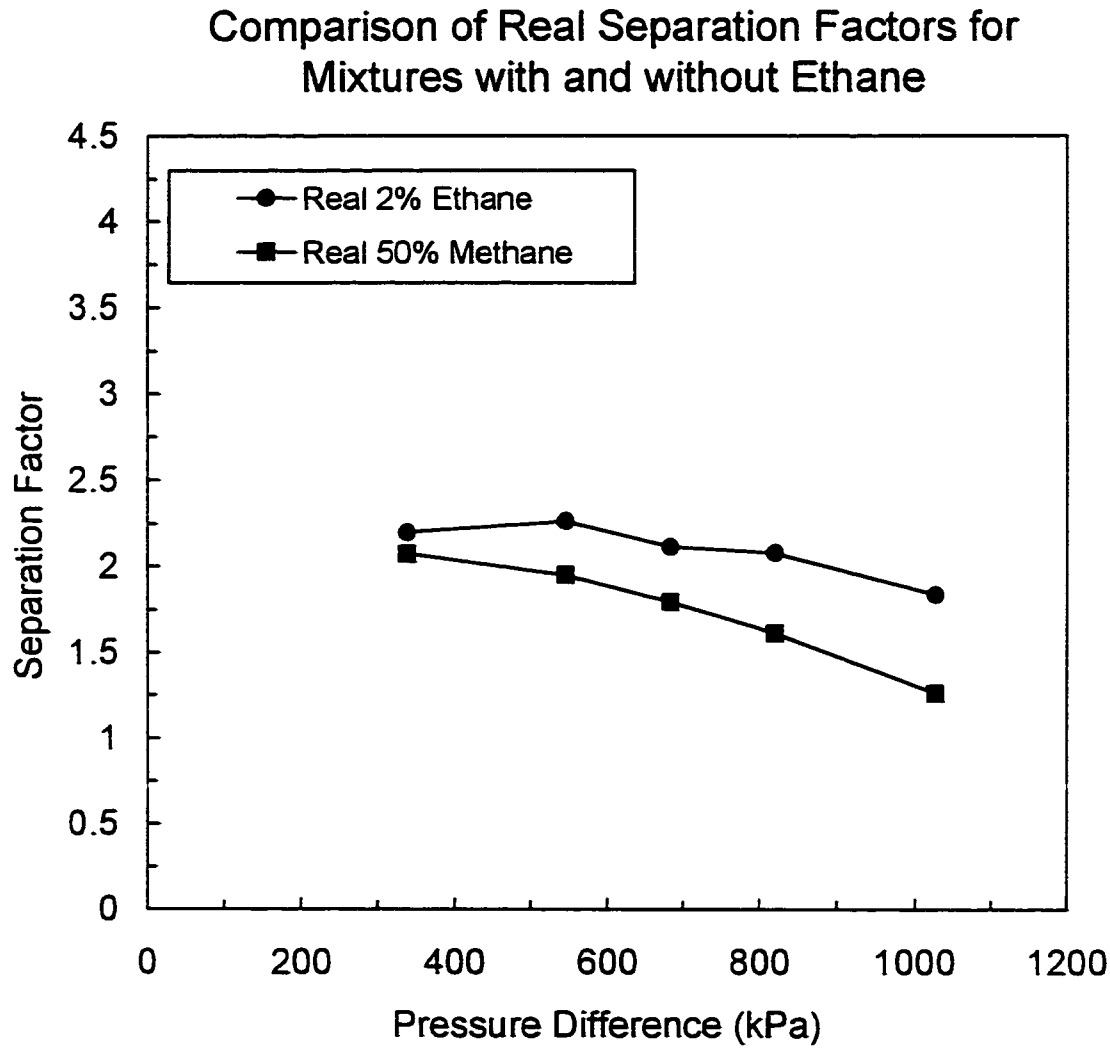

Figure 6.16: Real separation factors for the 50/50 CH_4/H_2 mixture and the 49/49/2% ethane mixture calculated at -25°C (M-2, feed pressures 50-150 psig).

SUMMARY

Total mixture permeate flow rates were found to be independent of feed flow rate. The equimolar mixture and the 75% methane mixture permeation rates were found to decrease as the temperature decreased (opposite of pure gas results).

High feed flow rates required larger pressure driving forces than low feed flow rates to attain optimal separation. The high flow rate methane rejection-hydrogen recovery curves were found to follow the same trend as the low flow rate curves, however, they were shifted towards higher recovery rates.

There is a limit to feed flow rate in the SSF membrane as the permeate flow rate is limited for a given pressure.

Lower temperatures improved separation for all mixtures in the SSF membrane. The stronger adsorption of methane on the membrane layer probably increased the hindrance of hydrogen permeation and improved the rejection-recovery results. The best improvements were with the 75% methane mixture as there was sufficient methane to block the hydrogen along the whole length of the membrane. For the 25% and 50% methane mixtures, there was generally a large improvement in rejection or recovery (depending upon feed flow rate and pressure) but a small trade off in either rejection or recovery. The 75% methane mixture produced higher rejection and recovery rates with decreasing temperature.

As the temperature decreased, the non-linearity of the rejection-recovery curves increased, demonstrating the non-linear relationship between pressure and methane adsorption. The rejection-recovery curves at high temperatures were relatively straight due to the absence of any adsorption effects at high temperatures (65 and 125 °C). There was no separation occurring at 125°C as the rejection-recovery curve was below the 45° line at this temperature.

The mixture permeability of methane increased with decreasing temperature (more adsorption) while the permeability of hydrogen decreased

with decreasing temperature. This was due to the significant blockage of the hydrogen at low temperatures.

The separation factors increased as temperature decreased. The highest separation factors occurred with the 75% methane mixture and ranged from an average of approximately 1.3 at 22°C to 2.1 at -25°C. The separation factors ranged from approximately 1.2 to 2.1 for the 50% methane mixture and 1.1 to 1.6 for the 25% methane mixture. Separation factors did not give a good indication of the performance of the membrane, as it did not take into account recovery rates. For this reason rejection-recovery data is preferred.

The addition of 2% ethane produced a slight improvement in separation at -10 and -25°C. However, permeation rates decreased significantly with temperature. This was presumed to be caused by the stronger adsorption of ethane on the surface of the membrane layer and suggests that investigation of the effect of temperature on more polar molecules is required.

CHAPTER 7.0

SURFACE DIFFUSION MODELLING

Mathematical modelling is the simulation of a process based upon fundamental laws governing the system. Models are useful in predicting system behaviour and help avoid time and monetary expenditure required for experimentation. For this work, a model was developed to predict the flux of pure and mixtures of hydrogen and methane for the SSF membrane as a function of temperature and pressure. The model required the calculation of surface diffusivity in order to predict flux. This was conducted by modelling the surface of the membrane layer as a Type 1 adsorbent and using Langmuir equations to mathematically define the properties of the activated carbon layer. The resultant pure gas surface diffusivities were then compared with mixture surface diffusivities. The model was useful as it identified and predicted the true driving force for permeation: surface loading. The details of the model for pure gases are explained in Section 7.1. The calculations and results of the model developed for the mixtures are explained in Section 7.2.

OVERVIEW

The basic function of the model was to obtain the surface diffusivities of pure hydrogen and methane and compare these values with mixture surface diffusivities. The motivation for developing the model was to prove that the true driving force for permeation could be represented by the difference in surface loading on the high and low pressure sides of the membrane. The agreement of the mixture and pure surface diffusivities would then prove that the membrane layer could be adequately defined as a simple Type 1 adsorbent and the Langmuir assumptions would be valid for the SSF membrane. The model was used to determine the relationship between diffusivity, temperature and pressure for both hydrogen and methane. Pure surface diffusivities and the Langmuir constants were determined for temperatures ranging from -25°C to 155°C. These surface diffusivities were then compared to mixture surface diffusivities for 25%, 50% and 75% methane at temperatures of 22°C and -25°C.

7.1 Model Development for Pure Gas Data

7.1.1 Determination of Langmuir Constants b *and* n_s^*

It was determined in Chapter 5 that the adsorption of methane on the membrane layer matched the behaviour of gas adsorption on a Type 1 isotherm (monolayer adsorption). The simplest theoretical model developed to describe monolayer adsorption was developed by Langmuir and has the following assumptions [Ruthven, 1984].

1. Molecules are adsorbed on a fixed number of adsorption sites.
2. Each site can hold one adsorbate molecule.
3. All sites are energetically equivalent.
4. There is no interaction between molecules adsorbed on neighbouring sites.

The total number of moles adsorbed per unit weight of adsorbent for a particular gas is defined as n_s. The number of moles at saturation (where all

adsorption sites are taken) is defined as n_s^*. The ratio of these is Θ. The rates of adsorption and desorption are defined as;

$$r_a = k_a P(1-\Theta) \tag{7.1}$$

$$r_d = k_d \Theta \tag{7.2}$$

Defining the adsorption constant $k_a/k_d = b$, the equations can be rearranged to give the following for a pure gas:

$$\frac{n_s}{n_s^*} = \frac{bP}{1+bP} \tag{7.3}$$

This equation was used for hydrogen and methane to determine the constants b and n_s^*. The novel technique used in the literature for determining the constants is fitting the parameters to experimental isotherm data. Isotherm data is collected by measuring the surface loading of a component on a sample of the adsorbent at a constant temperature and varying pressure. The SSF membrane layer was permanently bound to the porous support and prevented the collection of a sample of the adsorbent. For this reason, literature data for the surface loading of hydrogen and methane on activated carbon was collected. Isotherm data was collected by Sircar *et al* (1996) for the adsorption of hydrogen and methane on a commercial sample of activated carbon (BPL carbon, British Petroleum Ltd.). The experimental isotherm and the fitted Langmuir isotherm are shown for hydrogen and methane in Figure 7.1. Equation 7.3 was used to fit the data. The values of n_s and P were taken from the experimental data and the parameters b and n_s^* were found by plotting $1/n_s$ versus $1/P$. This gave a slope of $1/(bn_s)$ and an intercept of $1/n_s^*$. Table 7.1 shows the values of the Langmuir constants used to fit the data in Figure 7.1 for hydrogen and methane on BPL carbon.

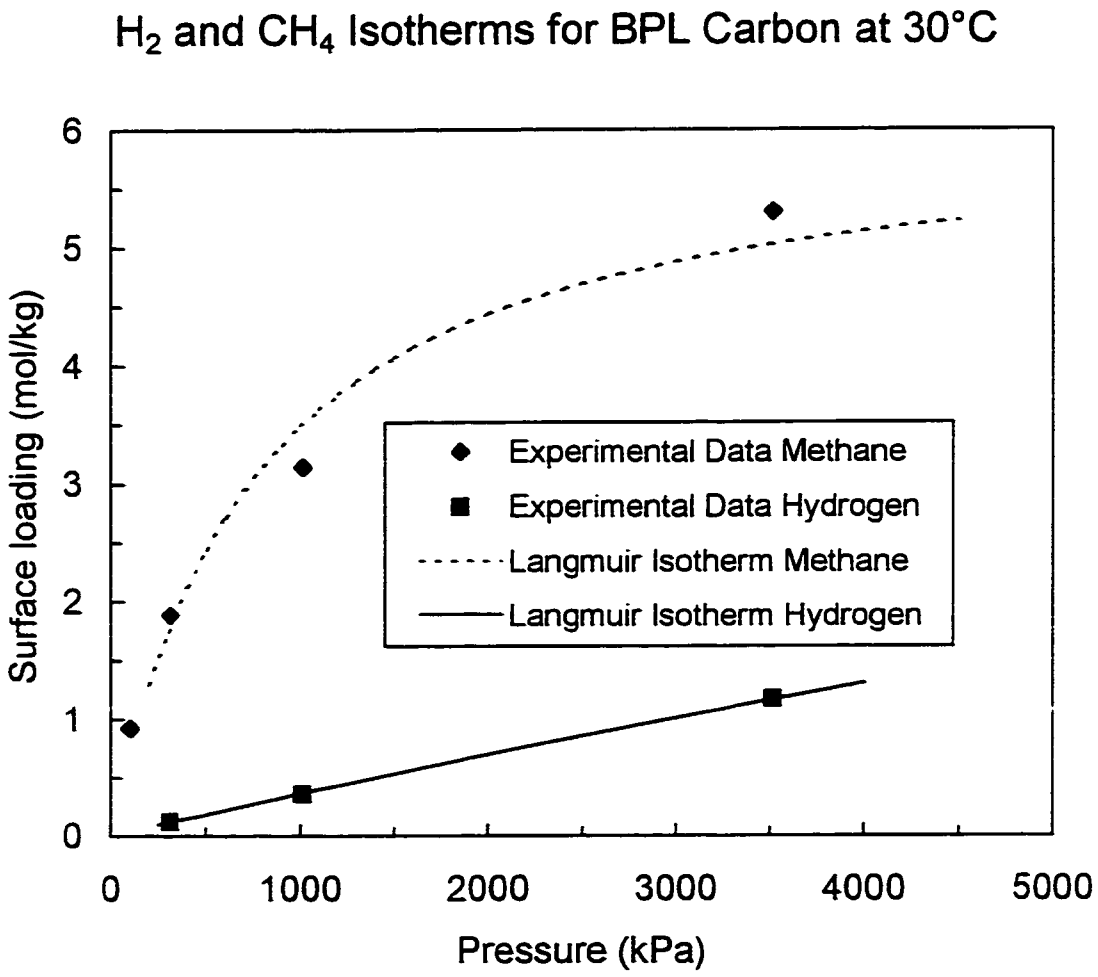

Figure 7.1: Experimental isotherm data [Sircar *et al*, 1996] and fitte Langmuir isotherms for hydrogen and methane on activated carbon at 30°C.

Table 7.1: Langmuir Adsorption Constants for H_2 and CH_4 on BPL Carbon.

Constant	Hydrogen	Methane
n_s^* (mol/kg)	9.68	6.1
b (kPa^{-1})	3.89×10^{-5}	1.34×10^{-3}

The next step was to determine if the experimental data for BPL carbon would adequately define the adsorption of hydrogen and methane on the membrane layer. Equations were developed to relate the Langmuir equations to the driving force for diffusion in the SSF membrane. Equation 5.17 defines surface diffusion using a diffusivity term (D_s) and surface loading driving force term (Δn_s). The Langmuir isotherm data was related to the driving force through the following equations, where *i* represents the components (hydrogen or methane).

$$J_i = \rho D_{is} \frac{\Delta n_{si}}{\Delta x} \tag{7.5}$$

$$\Delta n_{si} = n_{si}^H - n_{si}^L \tag{7.6}$$

$$n_{si}^H = \frac{n_{si}^* b_i y_i P^H}{1 + \sum_i b_i y_i P^H} \tag{7.7}$$

$$n_{si}^L = \frac{n_{si}^* b_i y_i P^L}{1 + \sum_i b_i y_i P^L} \tag{7.8}$$

The results of using these equations for the calculation of surface diffusion for mixtures are explained in Section 7.2.

7.1.2 Determination of Surface Diffusivities using Pure Gas Data

It was determined in Chapter 5 that diffusion in the SSF membrane was an activated process and that activated and surface diffusion were defined by the same mathematical equations. Activated diffusion (or surface diffusion, equation 5.17) includes a diffusivity term (D_s) that increases with increasing temperature according to an Arrehenius expression (equation 5.8). In order to develop a model that adequately predicted experimental values of flux, it was necessary to

investigate the effect of temperature. The Langmuir parameter *b*, which is the equilibrium constant for adsorption/desorption is also a function of temperature (maximum loading n_{si}^* is independent of temperature). The parameter *b* follows a vant Hoff equation [Ruthven, 1984] which decreases as the temperature increases (adsorption is exothermic, ΔH is negative).

$$b = b_o \exp\left(\frac{-\Delta H_o}{RT}\right) \tag{7.9}$$

For a pure gas, the equations for surface diffusion were defined as:

$$J = \rho D_s \frac{n_s^H - n_s^L}{\Delta x} \tag{7.10}$$

$$n_s^H = \frac{n_s^* b P^H}{1 + b P^H} \tag{7.11}$$

$$n_s^L = \frac{n_s^* b P^L}{1 + b P^L} \tag{7.12}$$

In order to determine the values for diffusivity for hydrogen and methane at different temperatures and pressures, it was necessary to find values of D_o and E in equation 5.8 and values of b_o and ΔH_o in equation 7.9. The bulk density, ρ, of the activated carbon layer was assumed to be 600 kg/m^3. The thickness of the membrane layer was assumed to be 2μm. The constants were determined in different methods for hydrogen and methane and therefore are explained separately.

Determination of Hydrogen Model Parameters

The surface diffusivity of hydrogen was found to be independent of feed pressure. This meant that for all feed pressures investigated at a given temperature, only one diffusivity value needed to be found. This independence can be explained by equation 7.10. Hydrogen flux *J*, increased linearly with pressures as seen in Figure 5.3. The surface loading also increased linearly with pressure as seen in Figure 7.1. The flux increase with pressure was directly

accounted for by the linear increase in surface loading in equation 7.9 and therefore diffusivity was independent of pressure. Methane surface loading was not linearly dependent on pressure as seen in Figure 7.1 and diffusivity was a strong function of pressure and thus needed to be determined using a different method than for hydrogen.

To determine the constants D_o, E, b_o and ΔH_o, pure hydrogen data at temperatures of 0°C and 22°C were used. It was assumed the Langmuir constants at 30°C were suitable to use in the determination of D_s at 22°C. The experimental flux data was used to solve for the surface diffusivity at this temperature. The flux at 100 psig was chosen as the experimental flux value from which diffusivity would be calculated. Using the resultant value for diffusivity, equation 7.10 was used to calculate the flux values at other pressures. Figure 7.2 compares the observed and calculated values of flux for this temperature. There was only a small difference between the values and therefore it was concluded that hydrogen diffusivity was independent of pressure. The experimental data collected at 0°C was used to determine new D_s and b values, as they are functions of temperature. Different experimental values of flux with temperatures at 100 and 120 psig were used to solve for the two unknowns (D_s and b). With the knowledge of two different D_s values and two different b values, calculated at two different temperatures (22°C and 0°C), it was possible to solve for the constants defining the relationship between D_s, b and temperature. Table 7.2 shows the values of the constants found by this method. These constants were used to calculate D_s and b values at different temperatures using equations 5.9 and 7.9.

Table 7.2: Diffusivity and Langmuir Constants for Hydrogen

	D_o (m^2/s)	E (J/mol)	b_o (kPa^{-1})	ΔH_o (J/mol)
H_2	9.61×10^{-8}	5723	1.16×10^{-6}	-8601

A physical adsorption process typically has heats of adsorption of less than -10 Kcal/mol [Ruthven, 1984]. The term, ΔH_o, represents the heat of adsorption of hydrogen on the membrane layer and is equal to -8.6 KJ/mol (-2.1 Kcal/mol). To ensure this data was correct, a second literature source was used to determine the heat of adsorption of hydrogen on activated carbon. Zhou and Zhou (1996) measured the surface loading of hydrogen on activated carbon at pressures ranging from 1 to 6 MPa and at temperatures of 77 to 298K. At room temperature, the surface loading of hydrogen as a function of pressure measured by Zhou and Zhou (1996) was represented by a straight line and this is in agreement with the data of Sircar *et al* (1995) in Figure 7.1. The heat of adsorption (ΔH_o) of hydrogen calculated from the Zhou and Zhou (1996) data, at 298 and 213K was found to be -9.6 KJ/mol which is within 10% of the ΔH_o calculated from the Sircar *et al* (1996) data (ΔH_o in Table 7.2). From this it is concluded that the heat of adsorption calculated for the membrane layer is an acceptable value.

From the known temperature relationship, it was possible to determine hydrogen diffusivities at other temperatures and back calculate values of flux. The flux values were then compared to experimental values. Figure 7.3 compares the calculated (using equation 7.10) and experimental values of flux at temperatures of 0, -25 and 125°C. The results show that the constants found in Table 7.2 are capable of predicting experimental values of pure hydrogen flux for a wide range of temperatures. The temperatures investigated ranged from -25°C to 155°C and the pure gas flux data for hydrogen was predicted by the model within 4% at all temperatures. Figure 7.4 shows the values of pure gas diffusivities for hydrogen. The diffusivity increases as a function of temperature as required. The comparison of these values to mixture surface diffusivities is explained in Section 7.2.

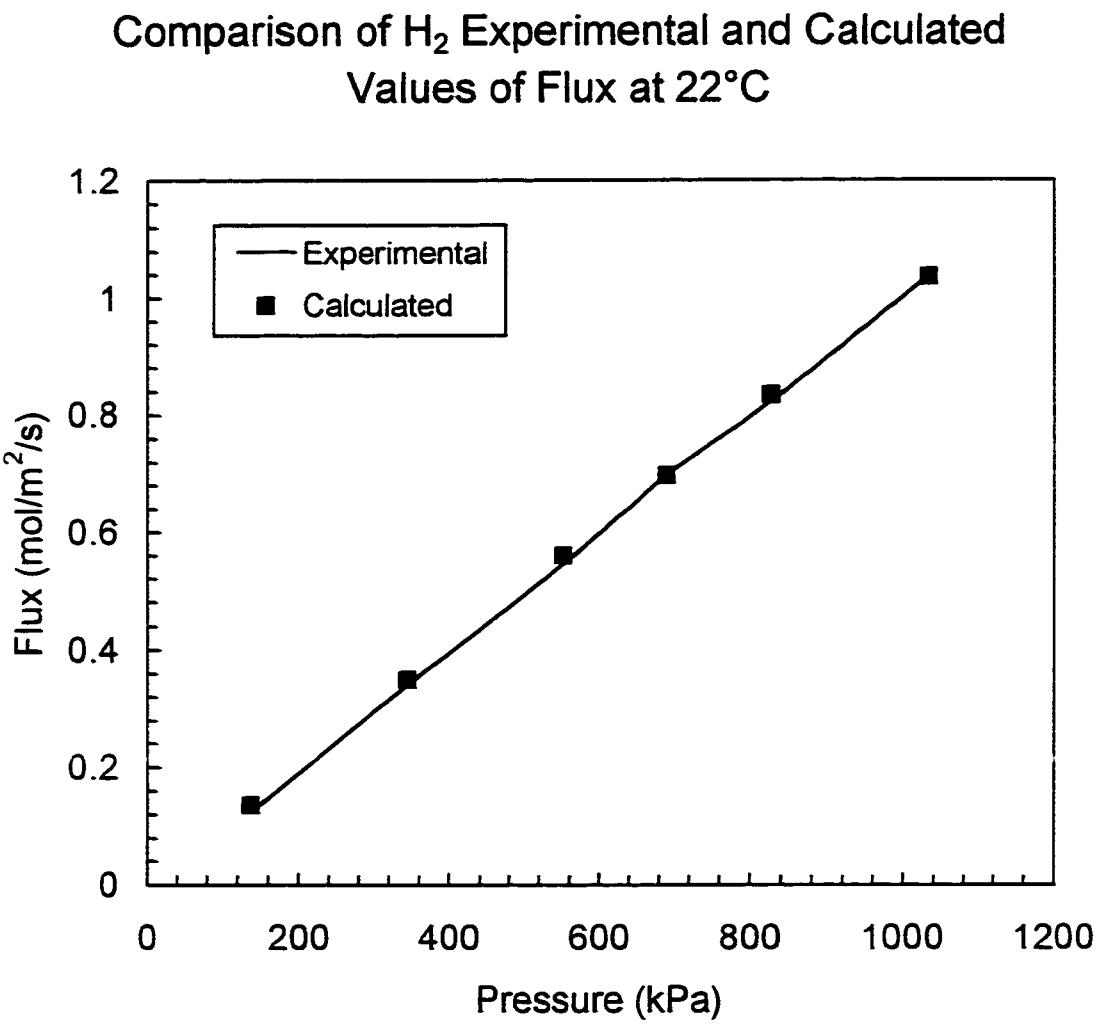

Figure 7.2: Comparison of calculated (equation 7.10) and experimental flux of pure hydrogen at 22°C (M-2, pressures 20-150 psig)

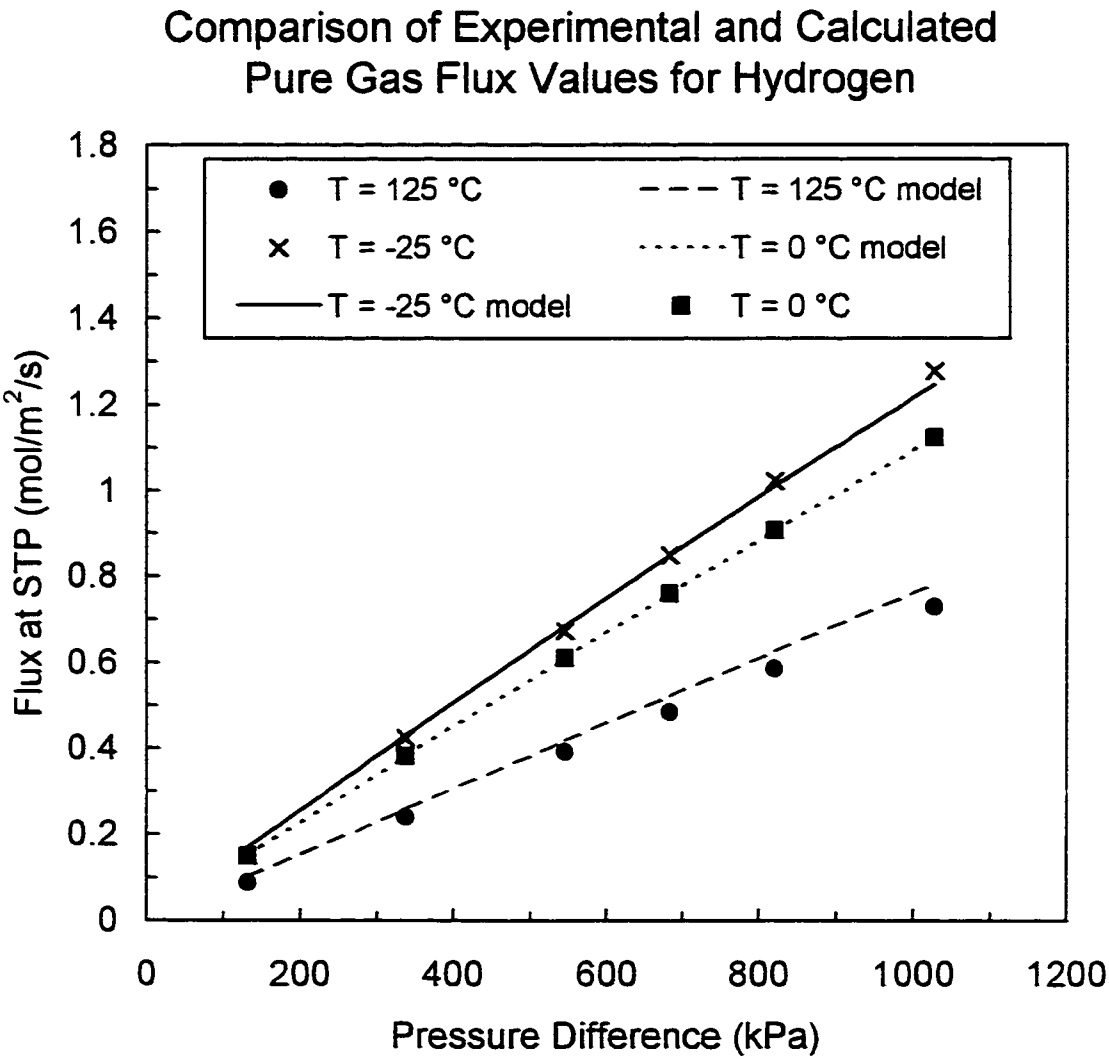

Figure 7.3: Comparision of experimental and calculated values for hydrogen flux (equation 7.10) using the Langmuir adsorption model at -25, 0 and 125°C (M-2, feed pressures of 20-150 psig)

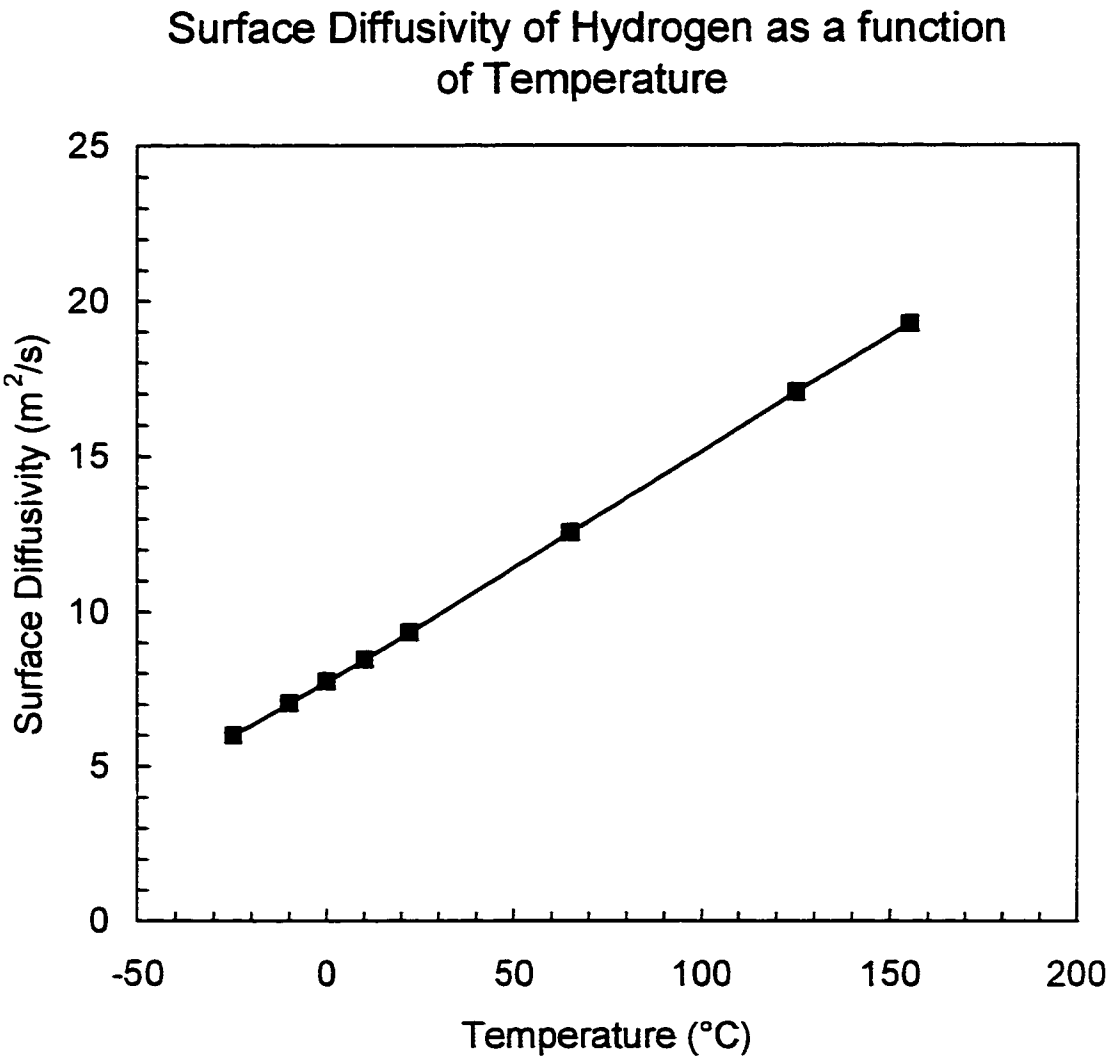

Figure 7.4: Calculated surface diffusivities (equation 7.10) of pure hydrogen as a function of temperature (M-2, temperatures -25 to 155°C)

Determination of Methane Model Parameters

Methane diffusivity was a function of pressure and therefore required that individual diffusivities be found at each pressure and temperature at which methane flux was measured. The temperature relationship could not be found in the same manner as for hydrogen as the effect of pressure had to be considered. For hydrogen, flux values at 80 and 100 psig were enough to solve for the diffusivity at a given temperature. There were essentially two equations (J_{80} = f(D_s, b), J_{100} = f(D_s, b)) and two unknowns (D_s, b). However for methane D_s, was not equal for two different pressures and thus more information was required.

Additional data from the literature was collected to solve for *b*. Costa *et al* (1989) measured the surface loading of methane on activated carbon at temperatures of 25°C and 50°C and pressures up to 100 kPa. Their data is shown in Figure 7.5. The relationship of the Langmuir parameter *b*, to temperature was determined from this experimental data. The saturation loading, n_s^*, was found from the data of Sircar *et al* (1996) shown in Table 7.1. The Langmuir isotherm model (equation 7.10) was used to fit the experimental data and the two resultant curves are shown in Figure 7.5. The *b* values used to match equation 7.10 to the experimental data are shown in Table 7.3a. The constants for the vant Hoff are included in Table 7.3b. With the *b* values known as a function of temperature, the diffusivity as a function of temperature and pressure could then be found. The value of *b* at 25°C was assumed to be valid at 22°C and the diffusivity was found at each feed pressure (*b* was not a function of pressure) by matching the experimental values to the values calculated using equation 7.10. This gave values of diffusivity at 22°C for each feed pressure. This procedure was repeated for the data at 0°C. The *b* value for 0°C was determined from equation 7.9 using the constants in Table 7.3. The diffusivities were calculated for each pressure by matching experimental to values calculated using equation 7.10

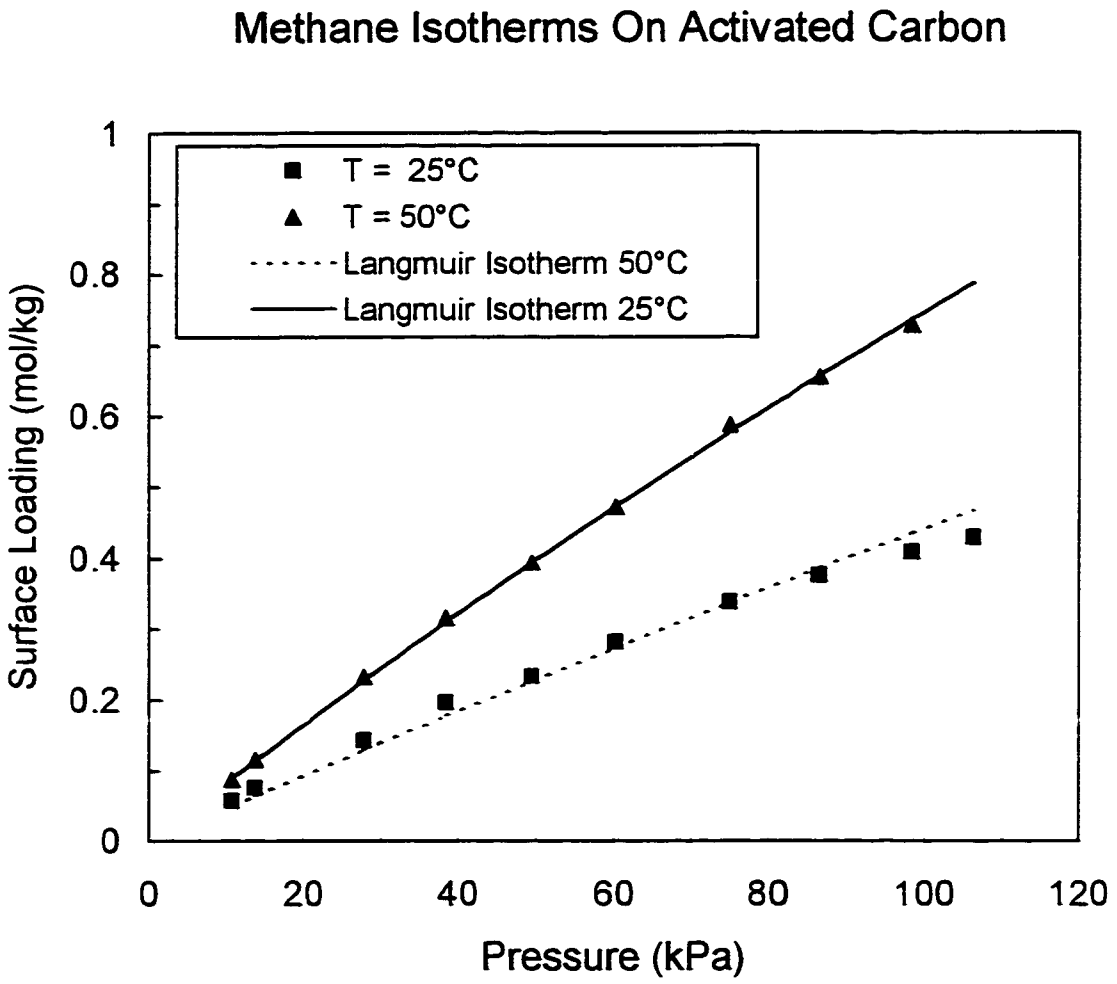

Figure 7.5: Fitted Langmuir isotherms to experimental data obtained from Costa *et al* (1989) for methane adsorption on activated carbon at 25°C and 50°C.

Table 7.3: Langmuir constants found for experimental data of Costa *et al* (1989) **a)** *b* values found from fitting a Langmuir isotherm to experimental data at 25°C and 50°C, **b)** vant Hoff constants found using values in Table 7.3a and equation 7.9.

a)

T (°C)	b (kPa^{-1})
25	0.001396
50	0.00782

b)

vant Hoff constants	
b_o (kPa^{-1})	4.38×10^{-7}
ΔH_o (J/mol)	-19984 (-4.78 Kcal/mol)

The heat of adsorption (ΔH_o), (listed in Table 7.3b)) found for methane on the membrane layer was compared to the heat of adsorption of methane on 5A zeolite (-4.54Kcal/mol, Ruthven, 1984) and was found to be quite similar.

The relationship between diffusivity, temperature, and pressure was evaluated by finding an Arrhenius expression for diffusivity at each feed pressure. The data at 22°C and 0°C was used as the basis for the determination of the pressure relationships. Table 7.4 shows the constants found for each pressure. Diffusivities were calculated at different temperatures using equation 5.9 and the values in Table 7.4. The diffusivities were then used in equation 7.10 to predict the experimental values of pure methane flux in the SSF membrane. The comparison of the model and experimental results are shown in Figure 7.6 for temperatures of 125 °C, 22°C and -25°C. Figure 7.7 shows the comparison for temperatures of 10°C and -10°C. The model predicts the pure gas flux of methane within 10% at -25°C. The model begins to fail however at high temperatures as was seen with hydrogen. The experimental flux of methane at 125°C was predicted by the model to within 25%. The poor predictions at high temperatures were perhaps due to the Langmuir constant, *b*, no longer being valid at high temperatures.

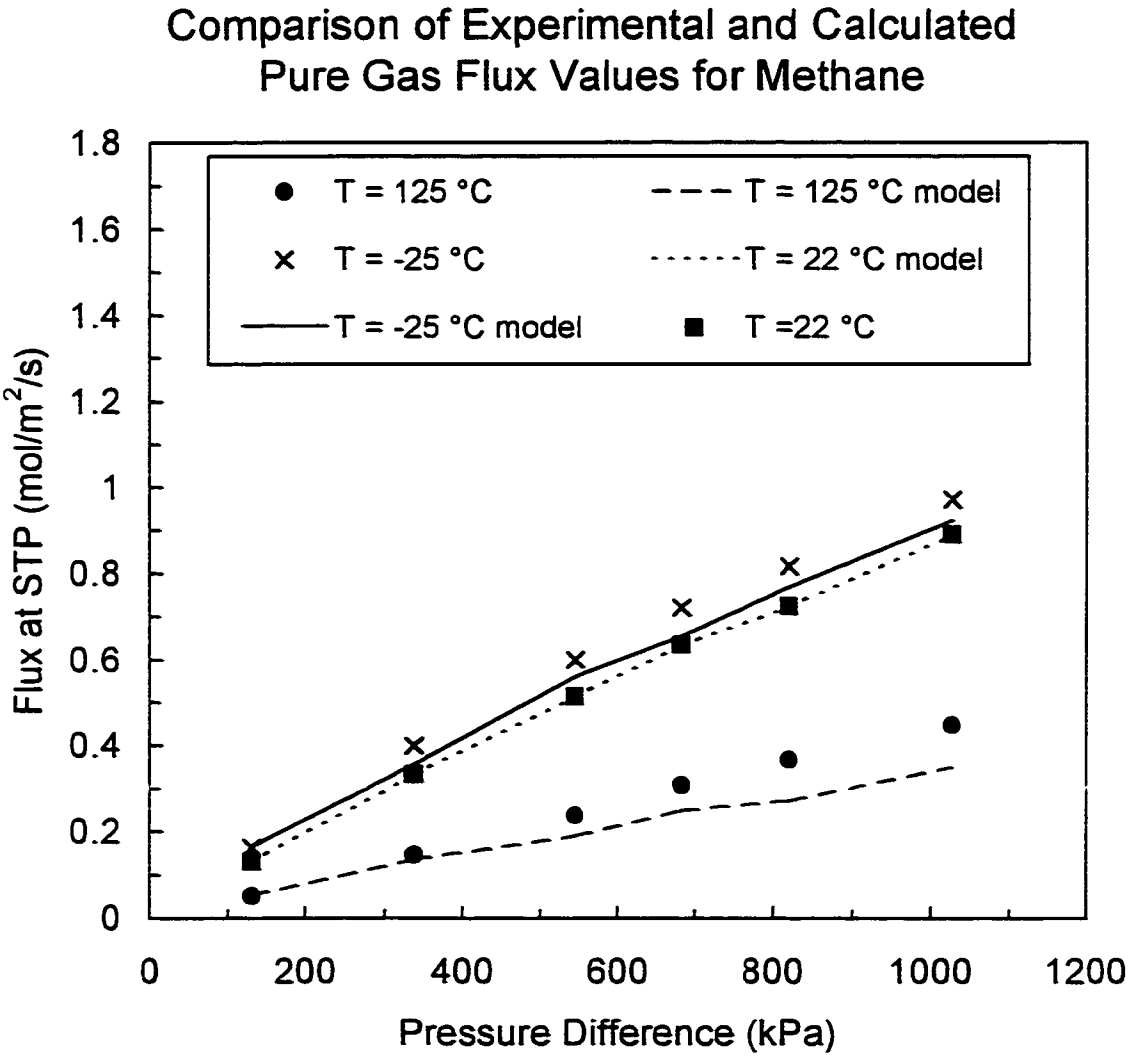

Figure 7.6: Comparision of experimental and calculated (equation 7.10 values for pure methane flux using the Langmuir adsorption model at -25, 22 and 125°C (M-2, feed pressures 20-150 psig).

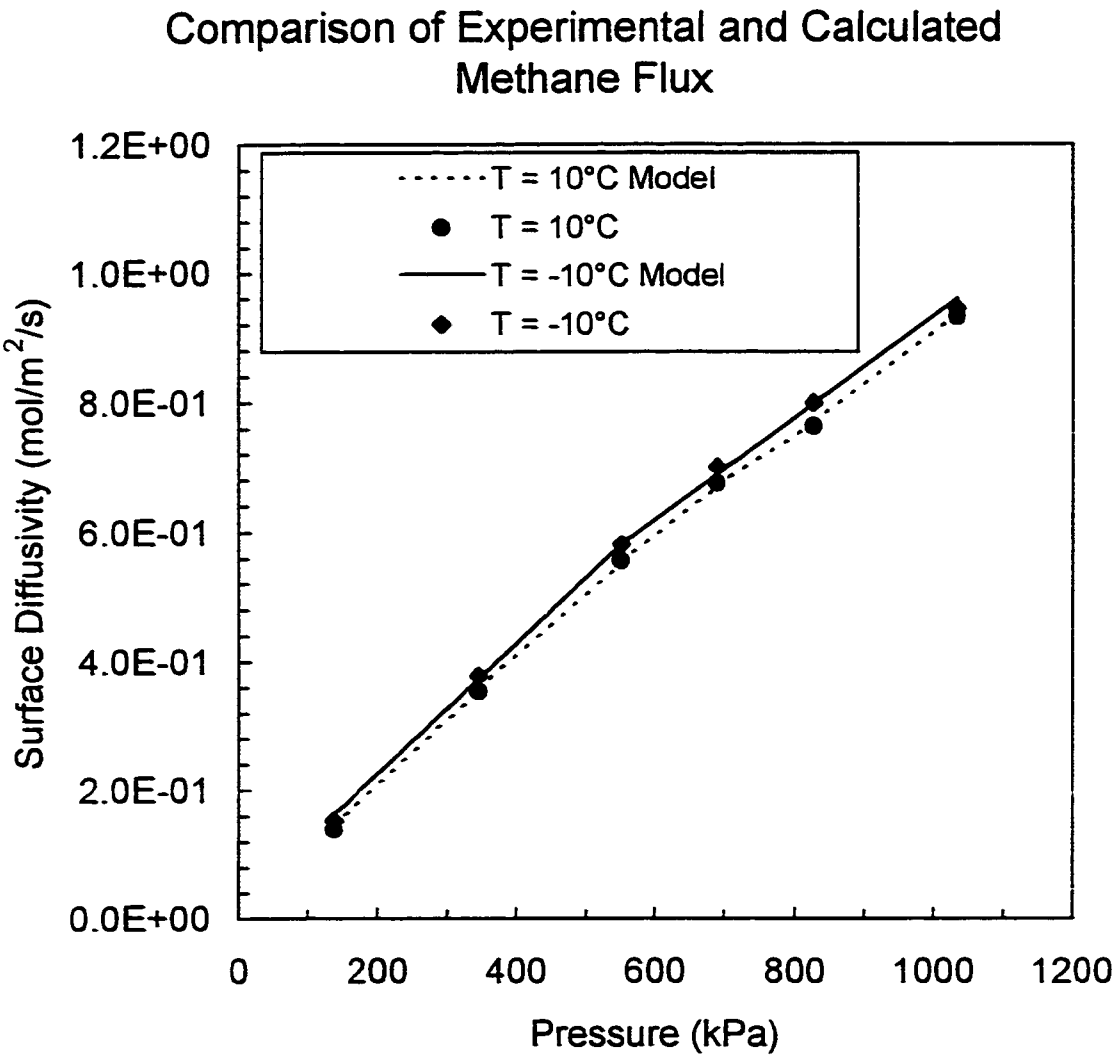

Figure 7.7: Comparision of experimental and calculated (equation 7.10) values for pure methane flux using the Langmuir adsorption model at -10 and 10°C (membrane 3, feed pressures 20-150 psig)

Table 7.4: Values of constants used in equation 5.9 for methane

Pressure (psig)	$D_o \times 10^8$ (m^2/s)	E (J/mol)
20	2.62	10035
50	1.48	8083
80	0.630	5642
100	0.630	5410
120	0.417	4290
150	0.377	3772

Figure 7.8 shows the values of methane diffusivity as a function of temperature and pressure. Diffusivity increased as the temperature and pressure increased.

The model did not predict methane flux data at low temperatures as well as it had for hydrogen. The values of D_s and b were found from references of 22°C and 0°C. The experimental isotherm data taken from the literature was measured at 25°C and 50°C. The temperature relationships found for b and D_s were perhaps not ideal at low temperatures. The data would be improved if the exact relationship between surface loading and temperature were known. as no extrapolation would be necessary. The ideal situation would be to collect isotherm data for hydrogen and methane on the activated carbon layer of the membrane .

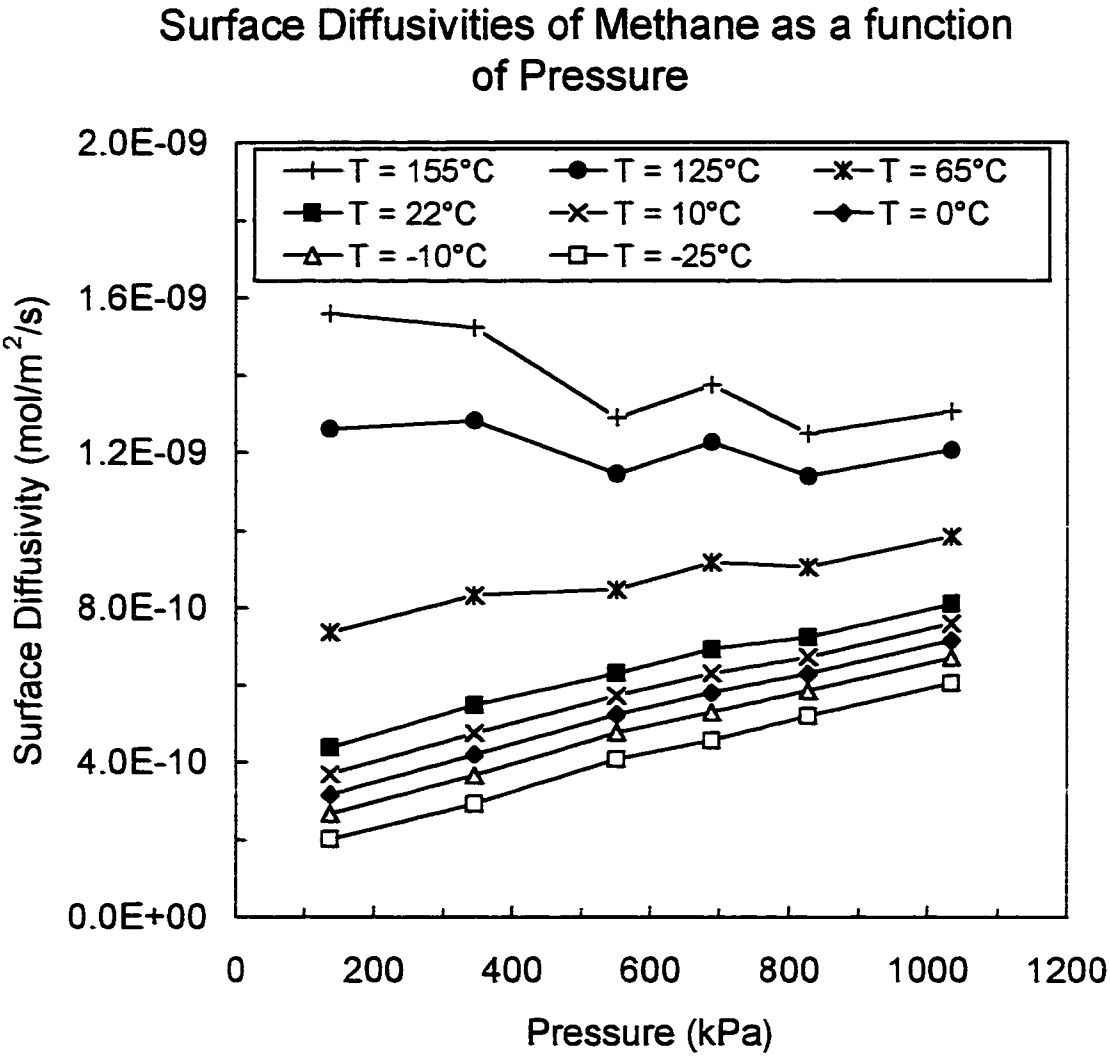

Figure 7.8: Pure gas surface diffusivities of methane as a function of temperature and pressure calculated by the Langmiur adsorption model (M-2, temperatures -25 to 155°C, feed pressures 20-150 psig)

For both hydrogen and methane at any given temperature the agreement between the model and experimental values was best at low feed pressures. This was perhaps due to the low surface loading, for example, at 20 psig. The Langmuir model is based on the assumption that there are no interactions between adsorbed molecules on neighbouring sites. When surface loading increases, molecular interactions are known to become more pronounced and the conformation to the Langmuir model deteriorates [Ruthven, 1984]. This may also explain the difference between the model and experimental data for methane at low temperatures. Surface loading increases and thus interactions increase at lower temperatures.

The isotherm data for methane on activated carbon was taken from two different sources (Costa *et al*, 1989 and Sircar *et al*, 1996) however the Langmuir parameters collected from the data were in agreement. In Table 7.1 the *b* value from Sircar *et al* (1996) is shown for 30°C. In Table 7.3 the *b* value from Costa *et al* (1989) is shown for 25°C. The difference between the two parameters is minimal and can be attributed to the difference in temperature.

7.2 Model Development for Mixture Data

The data collected from the pure gas model were used in developing the model for the mixtures. The Langmuir constant, n_{si}^*, shown for hydrogen and methane in Table 7.1 was used in equations 7.5 to 7.8 to calculate the mixture surface diffusivities. The *b* values used in equations 7.5 to 7.8 were calculated as a function of temperature using equation 7.9 and the constants in Tables 7.2 and 7.3. The surface mixture diffusivities were calculated by substituting the experimental values for methane or hydrogen flux into equation 7.10 and rearranging. They were calculated at -25°C and 22°C for mixtures of 25%, 50% and 75% methane.

Figure 7.9 shows the comparison of pure gas diffusivities with equimolar mixture diffusivities for hydrogen and methane at 22°C. The model predicted the

mixture and surface diffusivities of methane within less than 4% (the values are shown in Table 7.5). Surface loading of methane was independent of hydrogen concentration as the mixture and pure methane surface diffusivities matched. It also showed that the driving force for permeation could be effectively modelled as surface loading and not partial pressure difference. The Langmuir model adequately predicted the diffusivities of methane and showed that the membrane was successfully modelled as a Type 1 isotherm. It also provided equations that can be used to predict the flux and therefore separation performance of the membrane for other methane mixtures.

Table 7.5: Pure and mixture methane (50%) surface diffusivities predicted by the Langmuir model at 22°C.

Feed Pressure (psig)	Pure Gas Diffusivities $D_s \times 10^{10}$ (m^2/s)	Mixture Diffusivities $D_s \times 10^{10}$ (m^2/s)
20	4.38	4.23
50	5.47	5.39
80	6.32	6.43
100	6.93	7.18
120	7.25	7.30
150	8.11	8.53

The mixture hydrogen diffusivities were not very well predicted by the pure gas diffusivities, as seen in Figure 7.9. Pure hydrogen diffusivity was found to be independent of pressure. However, the mixture diffusivity clearly decreased as a function of pressure. This was due to the increased surface loading of methane. This effect was also seen by Barrer (1978) when measuring the diffusivity of hydrogen as a function of the amount of ammonia adsorbed on the surface of a sample of one-dimensional zeolite (mordenite).

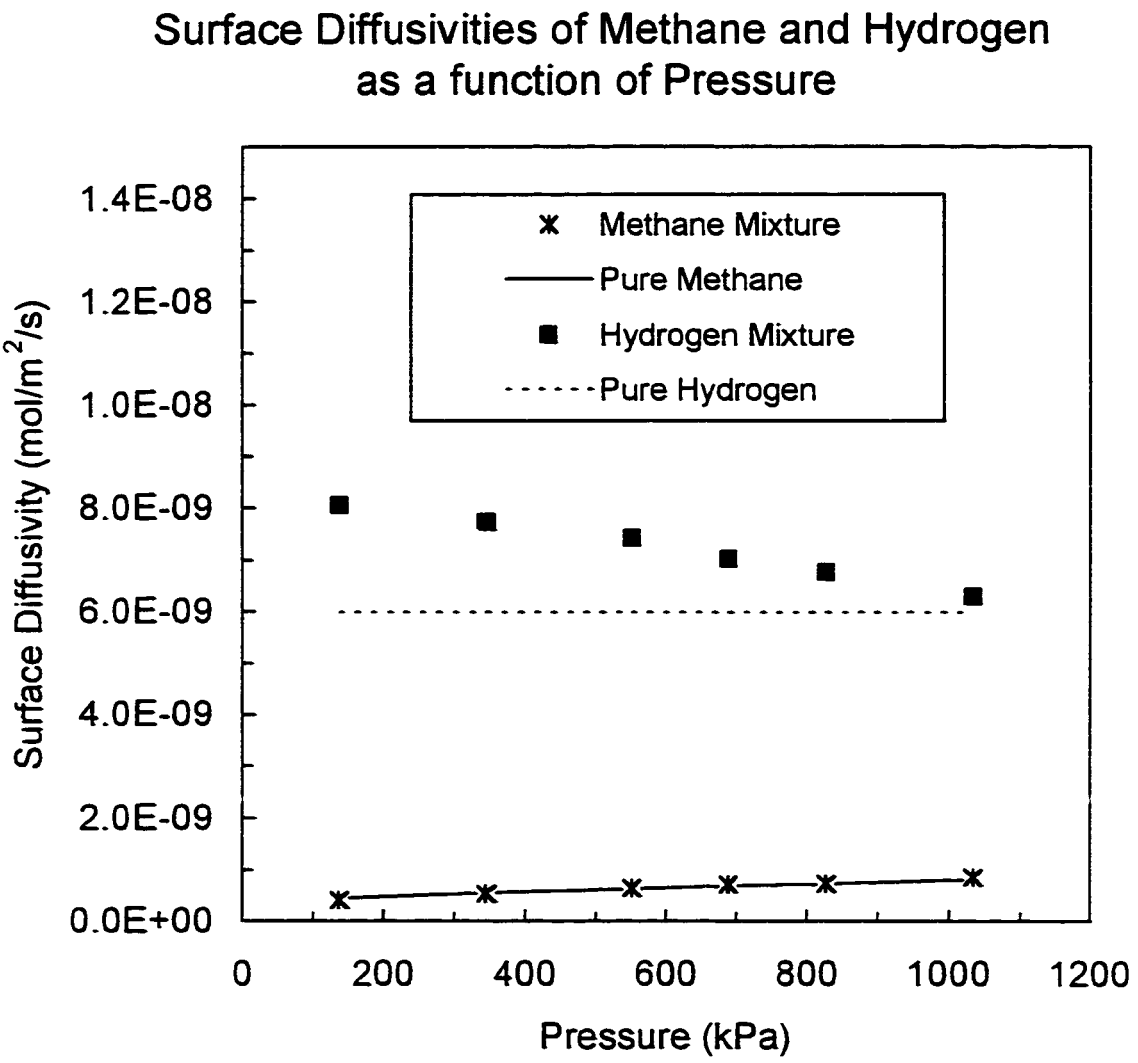

Figure 7.9: Comparison of mixture (equation 7.5) and pure gas diffusivities (equation 7.10) of hydrogen and methane at 22°C for mixtures of 50% methane (M-2, feed pressures 20-150 psig)

The mixture diffusivities (in Figure 7.9) were also higher than the pure diffusivities. This result was unexpected (and considered anomolous) as it seems that the highest diffusivities would occur in the absence of any hindering components. However, the result can be explained by equation 7.5. Diffusivity is only one component contributing to flux (J_i). The driving force for permeation, surface loading (Δn_{si}), also contributed to flux. The surface loading (calculated using equations 7.6 to 7.8) could not numerically account for the majority of flux. The diffusivity then increased so that the total experimental flux could be accounted for mathematically. In other words, diffusivity was compensating for the low surface loading calculated by the model. The Langmuir model clearly did not predict correct surface diffusivities for hydrogen, as it would be impossible to have higher mixture surface diffusivities than pure surface diffusivities. To find accurate results of hydrogen diffusivities in mixtures it would be necessary to take into account the decrease in adsorption of hydrogen in the presence of polar molecules. Ideally a measure of the surface loading of hydrogen in the presence of methane is required. Unfortunately, as with pure gas isotherm data, this is not possible for the SSF membrane due to the difficulty in obtaining an adsorbent sample.

In an attempt to improve the model for predicting diffusivities of hydrogen, the adsorption of hydrogen was assumed to be zero in the presence of methane. The diffusivity of hydrogen was then found from an equation for gas phase diffusivity. Rao and Sircar (1996) used the following equations to calculate the gas phase diffusivities of helium and hydrogen (initially introduced in Chapter 5.0 but re-introduced here for clarification in this Chapter).

$$D = \left(\frac{\tau}{\varepsilon}\right)\left[\frac{Jl}{A\Delta C_g}\right] \tag{7.13}$$

$$\Delta C_g = \left(\frac{P_H - P_L}{RT}\right) \tag{7.14}$$

The term, τ, was the tortuosity of the membrane and was assumed to be 1.0. The term ε was the porosity of the membrane layer and was assumed to be 0.4. The experimental flux J was measured and l was the thickness of the membrane layer. These equations were used to predict the gas phase diffusivities of hydrogen in the presence of methane. Table 7.6 shows the results at 22°C. The diffusivities were lower than pure gas diffusivities of hydrogen and they decreased slightly with pressure. It was concluded that these values were more suitable for quantifying hydrogen diffusivity in mixtures. Mixture diffusivities calculated by equation 7.13 were lower than pure gas diffusivities, which was the expected behaviour. Equation 7.13 was also used to calculate the pure gas diffusivities of hydrogen. Comparison of the hydrogen diffusivities calculated by this equation and the Langmuir equation resulted in a difference of approximately 15% (5.1×10^{-9} versus 6.0×10^{-9}).

Table 7.6: Gas phase diffusivities calculated for hydrogen in a 50/50 mixture at 22°C.

Feed Pressure (kPa)	Diffusivity $\times10^{9}$(m^2/s)
138	1.96
345	1.81
551	1.76
689	1.69
827	1.66
1034	1.69

Figure 7.10 shows the pure and mixture methane diffusivities at 22°C for the 25% and 75% methane mixtures. The mixture diffusivities were both lower than pure gas. The differences were an average of 34% and 28% below the pure gas results. The agreement between the 50% mixture and pure diffusivities for methane and the disagreement between the data for the other mixtures may be attributed to the reasons:

- The model may not work as well for asymmetric mixtures due to changes in surface loading of hydrogen or methane with concentration.

- The permeability of the membrane may have dropped over time, decreasing the pure gas diffusivity. Only one set of pure gas data was collected. The order in which the experiments was conducted is included in Appendix B.
- The 50/50 mixture was the first to be tested in the SSF membrane after the pure gas data for methane was collected. The properties of the membrane may have not changed between the time the pure gas and mixture data was collected.

The 50% methane mixture experiment was conducted the day after the pure gas test at this temperature. The second mixture used was the 75% methane, which had the second lowest difference from pure gas. The 25% and 75% mixtures were both tested more than a month after the pure gas test. It was described in Chapter 4 that the membrane was very sensitive to impurities and the permeability of the membrane decreased if it came in contact with them. Perhaps if additional pure gas tests were conducted immediately prior to the mixture tests, the results would have improved. They may have been able to account for any drop in permeability and the pure and mixture results would have been more agreeable.

Figure 7.11 shows the pure and mixture methane diffusivities at -25°C for the 25%, 50% and 75% methane mixtures. The results showed that the pure gas surface diffusivities at this temperature were higher than the mixture diffusivities. The difference may be attributed in part to the timing of the experiments and perhaps due to the assumed relationship between temperature and surface loading as explained in Section 7.1.

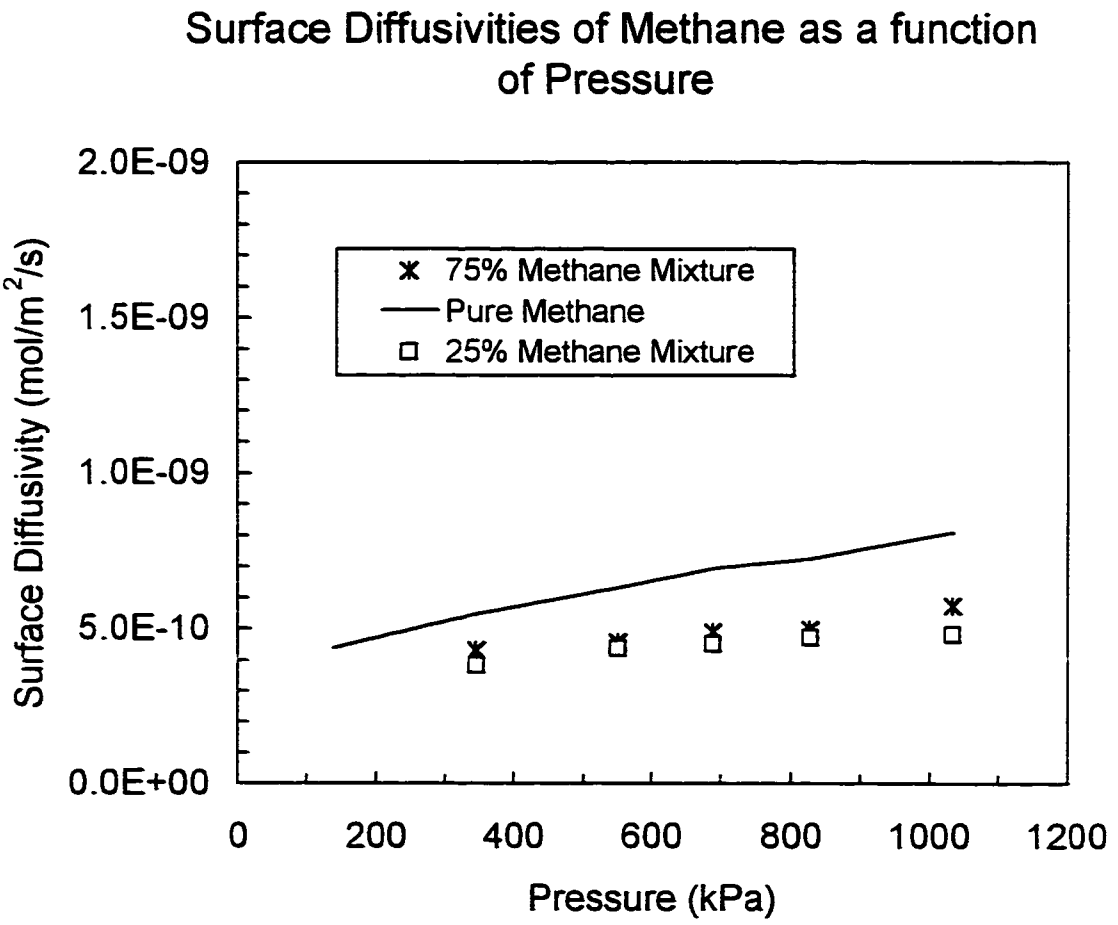

Figure 7.10: Comparision of pure and mixture surface diffusivities of methane using the Langmuir adsorption model for mixtures of 25% and 75% at 22°C (M-2, feed pressures 50 to 150 psig).

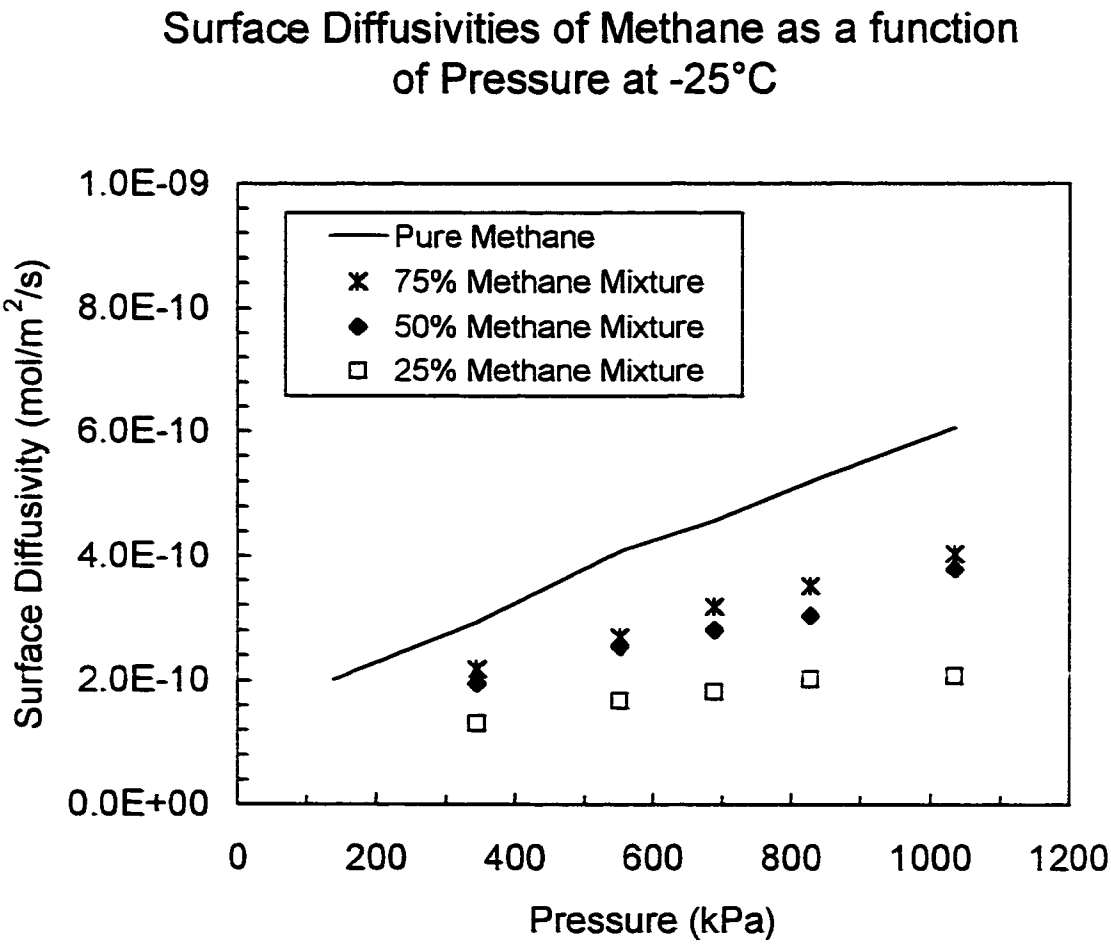

Figure 7.11: Comparision of pure and mixture surface diffusivities of methane using the Langmuir adsorption model for mixtures of 25%, 50% and 75% at -25°C (M-2, feed pressures 50 to 150 psig).

SUMMARY

A model was developed to predict the pure gas diffusivities of hydrogen and methane as a function of temperature. The membrane layer was successfully modelled as a Type 1 isotherm and the Langmuir assumptions were found to be valid for certain temperature ranges. The Langmuir parameters predicted experimental fluxes of hydrogen successfully at temperatures of -25°C to 65°C. The Langmuir model was able to predict flux values of methane at temperatures of -10°C to 65°C. At high temperatures, the calculated and experimental flux values deviated for both hydrogen and methane. This was assumed to be due to the questionable validity of the Langmuir parameters at high temperatures. The parameters were used to predict adsorption effects and as was seen in Chapter 5 there were no adsorption effects at high temperatures. The Langmuir parameters found from the pure gas data were then used to determine mixture diffusivities from equations 7.5-7.8. With a mixture of 50% methane and hydrogen at 22°C, the mixture diffusivities were found to equal pure gas diffusivities within 3%. A match in diffusivities meant that the surface loading of methane was unaffected by the concentration of hydrogen. It also showed the model was an effective way to predict the flux of methane within the membrane.

The model did not correctly predict the surface diffusivities of hydrogen as they were higher than those predicted for pure gas. The flux of hydrogen molecules is hindered in the SSF membrane and therefore surface diffusivities should have been much lower than pure gas. This showed that the flux of hydrogen in the presence of methane could not be effectively predicted by a model that calculates diffusivity based upon surface loading. The diffusivity of hydrogen was instead calculated from an equation that assumed no adsorption effects and the results were more meaningful as the mixture surface diffusivity was lower than for pure gas.

The model was also used to predict diffusivities of methane for different mixtures and at temperatures of -25°C. The results showed that the predicted

mixture diffusivities were lower than the pure gas diffusivities. The results with 25% and 75% methane at 22°C were thought to be poorly predicted by the model due to there being a drop in permeability of the membrane that was not taken into account with the pure gas data. It is recommended in the future that pure gas data be collected for methane prior to mixture experiments to obtain a measure of the drop in permeability, if any. The poor results at -25°C for all mixtures was perhaps due to a change in the membrane surface layer over time or the invalid extrapolation of the relationship between surface loading and temperature. Ideally, isotherm data needs to be collected from the membrane layer to allow for the proper prediction of the Langmuir constants at different temperatures and to predict the behaviour of hydrogen in the presence of methane. The volume of activated carbon on the membrane is quite small (0.0095 cm^3) and even if it could be removed, it would be insufficient for analysis.

CHAPTER 8.0

CONCLUSIONS AND RECOMMENDATIONS

The main objective of this study was to determine the effect of temperature on the separation of hydrogen and methane within the SSF membrane. Experiments were conducted to determine the effect of temperature on pure gases and on mixtures of hydrogen and methane. The following conclusions were drawn from these tests:

Pure Gas Permeability Tests

- No significant amount of Knudsen diffusion occurred in the membrane pores. It was concluded that diffusion in the SSF membrane occurred due to activated or surface diffusion (for both hydrogen and methane at temperatures ranging from -25°C to 155°C)
- Both hydrogen and methane pure gas permeate flow rates decreased with increasing temperature. Hydrogen flows were greater than methane flows.
- Hydrogen permeability was independent of pressure for temperatures of

-25°C to 155°C whereas methane permeability decreased with pressure due to the non-linear relationship of surface loading and pressure in the temperature range of
-25°C to 22°C. This was in agreement with results from the literature.

- Methane permeability was independent of pressure at 65°C to 155°C. This was due to the absence of any adsorption effects at high temperatures.

Hydrogen-Methane Separation Experiments

Results of the separation experiments were presented in terms of methane-rejection, hydrogen-recovery plots and in terms of separation factors for the four mixtures:

1. 25% CH_4 - 75% H_2
2. 50% CH_4 - 50% H_2
3. 75% CH_4 - 25% H_2
4. 49% CH_4, 49% H_2, 2% ethane.

The following conclusions were drawn from the hydrogen-methane separation experiments;

- Low temperature improved hydrogen-methane separation for all mixtures. Methane rejection increased by 13%, 15% and 17% for the first three mixtures (at 60% hydrogen recovery, when comparing -25°C to 22°C)
- There was a limit to permeate flow rate for a given feed pressure. As the feed flow rate was increased the permeate flow rate remained constant and all excess feed remained on the feed (retentate) side of the membrane.
- The results of separation experiments conducted with the first three mixtures showed that the high flow rate experiments followed the same trend as the low flow rate experiments but were shifted towards higher recovery rates. This was due to the higher amount of retentate flow (and thus hydrogen flow) with high flow rate experiments.

- The largest improvements in separation occurred with the 75% methane mixture due to an increased amount of hydrogen blockage at low temperatures.
- The mixture permeability of hydrogen was lower than pure gas permeability due the hindered permeation of hydrogen in the presence of methane. The lowest permeability occurred at -25°C.
- Separation factors did not give a good measure of the performance of the membrane. The highest separation factors corresponded to the lowest hydrogen recovery rates.
- The addition of 2% ethane produced a slight improvement in separation at -10 and -25°C however permeation rates decreased with temperature.

Surface Diffusion Modelling

The membrane layer was modelled as a Type 1 adsorbent using Langmuir equations to mathematically define the properties of the activated carbon layer. Langmuir parameters were obtained from the literature for a similar type of carbon and surface diffusivities were found from experimental pure gas data at 22°C and 0°C. These values were used to predict experimental flux of pure hydrogen and methane at other temperatures and within hydrogen-methane mixtures.

- Flux for hydrogen alone was predicted within 5% for -25°C to 65°C.
- Flux for hydrogen alone was predicted within 5% for –10°C to 22°C and within 10% for -25°C.
- The model failed (>20% differences) at high temperatures (125°C, 155°C) possibly due to the absence of adsorption effects at high temperatures.
- The model was used to predict the surface diffusivities of methane within an equimolar mixture at 22°C. The mixture diffusivities matched the pure gas diffusivities at pressures of 50-150 psig within 4%, showing that the model

was an effective way of predicting the flux of methane for this mixture and temperature.

- Predicted diffusivities for other mixtures were 10 to 15% lower than pure gas.

Recommendations:

- A study into increasing the robustness of the membrane layer should be initiated
- It was beyond the scope of this work to investigate surface properties of the membrane such as tortuosity, pore shape and functional groups, however, these properties may have profound effects on the diffusion mechanisms and modelling of the SSF membrane and should be investigated.
- An investigation into the flow patterns of the SSF membrane is recommended. This would allow the development of a model to predict the partial pressure driving forces and the permeabilities in the SSF membrane. The log-mean partial pressure driving force assumptions may not be valid for the SSF membrane. With the ability to compute partial pressure driving forces it would then be possible to calculate true values of permeability for mixtures.
- It is recommended that real or ideal separation factors not be used, as they do not give a good indication of the performance of the membrane. Rejection-recovery curves should be used to obtain an idea of the extent of separation in the SSF membrane.
- Further investigation of the effects of temperature on permeate flow rates of mixtures containing polar components is required. Polar components may reduce the permeate flow rate and therefore limit the separation at low temperatures
- Isotherm data should be collected for the membrane layer. Surface loading measurements should be made for pure hydrogen and methane at -25°C to 155°C. This would allow the calculation of actual Langmuir parameters and

may improve the model predictions at high and low temperatures for pure gases and mixtures

- Isotherm data should be collected for hydrogen in the presence of methane and vice versa. This would give insight into the poor predictions of the model for asymmetric mixtures and determine if the gas phase diffusivity equations are valid for hydrogen in mixtures.
- In situations where SSF membranes are proposed to be used, the cost of cooling the gas should be included in the economics as this could be a major factor.

REFERENCES

Ash, R., R.M. Barrer and C.G. Pope, "Flow of Adsorbable Gases and Vapours in a Microporous Medium", *Proc. R. Soc. London Ser. A*, 1963, 271,1

Ash, R., R.M. Barrer and P. Sharma, "Sorption and Flow of Carbon Dioxide and Some Hydrocarbons in a Microporous Carbon Membrane" *J. Mem. Sci.*, 1976, 17, 32.

Ash, R., R.W. Baker and R.M. Barrer, "Sorption and Surface Flow in Graphitized Carbon Membranes I. The Steady State", *Proc. R. Soc. London Ser. A*, 1966, 299,434

Aylmore, L.A.G. and R.M. Barrer, "Surface and Volume Flow of Single Gases and of Binary Gas Mixtures in a Microporous Carbon Membrane", *Proc. R. Soc. London Ser. A*, 1966, 290,477

Barrer, R.M., "Surface and Volume Flow in Porous Media", E.A. Flood (Editor), Chapter 19, "The Gas Solid Interface", Volume 2, Marcel Dekker, Inc., New York, ©1967.

Barrer, R.M., "Zeolites and Clay Minerals as Sorbents and Molecular Sieves", Academic Press Inc., New York, ©1978.

Costa, E., G. Calleja, C. Marron, A. Jimenez and J. Pau, "Equilibrium Adsorption of Methane, Ethane, Ethylene and Propylene and Their Mixtures on Activated Carbon", *J. Chem. Eng. Data*, 1989, 34, 156.

de Lange. K. Keizer and A.J. Burggraaf, "Analysis and Theory of Gas Transport in Microporous Sol-Gel Derived Ceramic Membranes", *J. Mem. Sci.*, 1995, 104, 81.

Gilliland, E.R., R.F. Baddour, G.P. Perkinson and K.J. Sladek, "Diffusion on Surfaces: Effect of Concentration on the Diffusivity of Physically Adsorbed Gases", *Ind. Eng. Chem. Fundam.*, 1974, 13 (2), 95.

Golden, T.C, R.G. Jenkins, Y. Otake, and A. Sarconi, "Oxygen Complexes on Carbon Surfaces", *Proceedings of the Workshop on the Electrochemistry of Carbon*, Aug. 17-19, 1983, 84, 61.

Heyd, J., "Hydrogen Recovery Using Membranes in Refining Applications". NPRA Annual Meeting, Los Angeles, March 1986.

Koros, W.J., "Gas Separation" Volume II, Chapter 3, "Membrane Separation Systems: Recent Developments and Future Directions", Noyes Data Corporation. New Jersey, ©1991.

Miller, G.Q and J. Stoecker, "Selection of a Hydrogen Separation Process", NPRA Annual Meeting, San Francisco, March 1989.

Miller, J.R. and W.J. Koros, "The Formation of Chemically Modified γ-Alumina Microporous Membranes", *Separation Science and Technology*, 1991, 25 (13-15), 1257.

Mulder, M., "Basic Principles of Membrane Technology", Kluwer Academic Publishers, Netherlands, ©1996.

Naheiri, T., K.A. Ludwig, M. Anand, M.B. Rao and S. Sircar, "Scale up of Selective Surface Flow Membrane for Gas Separation", *Separation Science and Technology*, 1997, 32 (9), 1589

Noble, R.D. and S.A. Stern, "Membrane Separations Technology Principles and Applications", Elesevier Science, B.V., Netherlands, ©1995.

Paranjape, M., "Hydrogen Enrichment by SSF Membranes", M.Sc. Thesis, University of Calgary, Calgary, Canada, February 1997.

Parillo, D.J., C. Thaeron and S. Sircar, "Separation of Bulk Hydrogen Sulfide-Hydrogen Mixtures by Selective Surface Flow Membrane", *AIChE J.*, 1997, 43 (9), 2239.

Peramanu, S. B.G Cox and B.B. Pruden, "Economics of Hydrogen Recovery Processes for the Purification of Hydroprocessor Purge and Off-Gases", *Int. J. Hydrogen Energy*, 1998, 24 (4).

Rao, M.B. and S. Sircar, "Performance and Pore Characterization of Nanoporous Carbon Membranes for Gas Separation", *J. Membrane Sci.*, 1996, 110, 109.

Rao, M.B. and S. Sircar, "Nanoporous Carbon Membranes for Gas Separation". *Gas Separation and Purification* 1993, 7 (4), 279.

Rao, M.B. and S. Sircar, "Nanoporous Carbon Membranes for Separation of Gas Mixtures by Selective Surface Flow", *J. Membrane Sci.* 1993, 85, 253.

Roy, S., "FBMR with High Flux Membranes and Oxygen Output", Ph.D. Thesis, University of Calgary, Calgary, Canada, December 1998.

Ruthven D.M., "Principles of Adsorption and Adsorption Processes", John Wiley and Sons, Toronto, ©1984.
Satterfield, C.N. and T.K. Sherwood, "The Role of Diffusion in Catalysis", Addison-Wesley Publishing Company Inc., Massachusetts, ©1963.

Scott D.S. and A.L. Dullien, "Diffusion of Ideal Gases in Capillaries and Porous Solids", *AIChE J.*, 1962, 8 (1), 113.

Sircar, S. and M.B. Rao, "Estimation of Surface Diffusion Through Porous Media", *AIChE J.*, 1990, 36 (8), 1249.

Sircar, S., T.C. Golden and M.B. Rao, "Activated Carbon for Gas Separation and Storage", *Carbon*, 1996, 34 (1), 1.

Ulhorn R.J.R, K. Keizer and A.J. Burgraaf, "Gas Transport and Separation with Ceramic Membranes Part I. Multilayer Diffusion and Capillary Condensation. *J. Mem. Sci.*, 1992, 66, 259.

Ulhorn R.J.R, K. Keizer and A.J. Burgraaf, "Gas Transport and Separation with Ceramic Membranes Part II. Synthesis and Separaton Properties of Microporous Membranes", *J. Mem. Sci.*, 1992, 66, 271.
Zhou, Li and Yaping Zhou, "A Comprehensive Model for the Adsorption of Supercritical Hydrogen on Activated Carbon", *Ind. Eng. Chem. Res.*, 1996, 35, 4166.

APPENDIX A

Ideal separation factors (equation 4.9) were found for the hydrogen-methane separation experiments using values of log-mean permeabilities. Equation 4.5 was used to calculate the partial pressure driving forces and equation 4.4 was used to calculate the permeabilities.

Figure A1 compares the real and log-mean separation factors for the 25%, 50% and 75% methane mixtures at -25°C. The results showed that the real separation factors were lower than the log-mean separation factors for all mixtures. Ideal separation factors are calculated based upon the assumption that the permeate pressure is much lower than feed pressure. It was therefore expected that the difference between the ideal (or log-mean) separation factors and the real separation factors would be a minimum at the highest feed pressures. In fact, the opposite was true; the separation factors were less different at low pressures. From this it was concluded that the log-mean partial pressure driving forces were invalid for the SSF membrane. The log-mean partial pressures are found based upon an assumption that the differences between inlet and outlet concentrations on the permeate and retentate sides of the membrane are small. This assumption may be acceptable for the permeate side of the SSF membrane (it may be well-mixed) however it is most likely invalid for the retentate side.

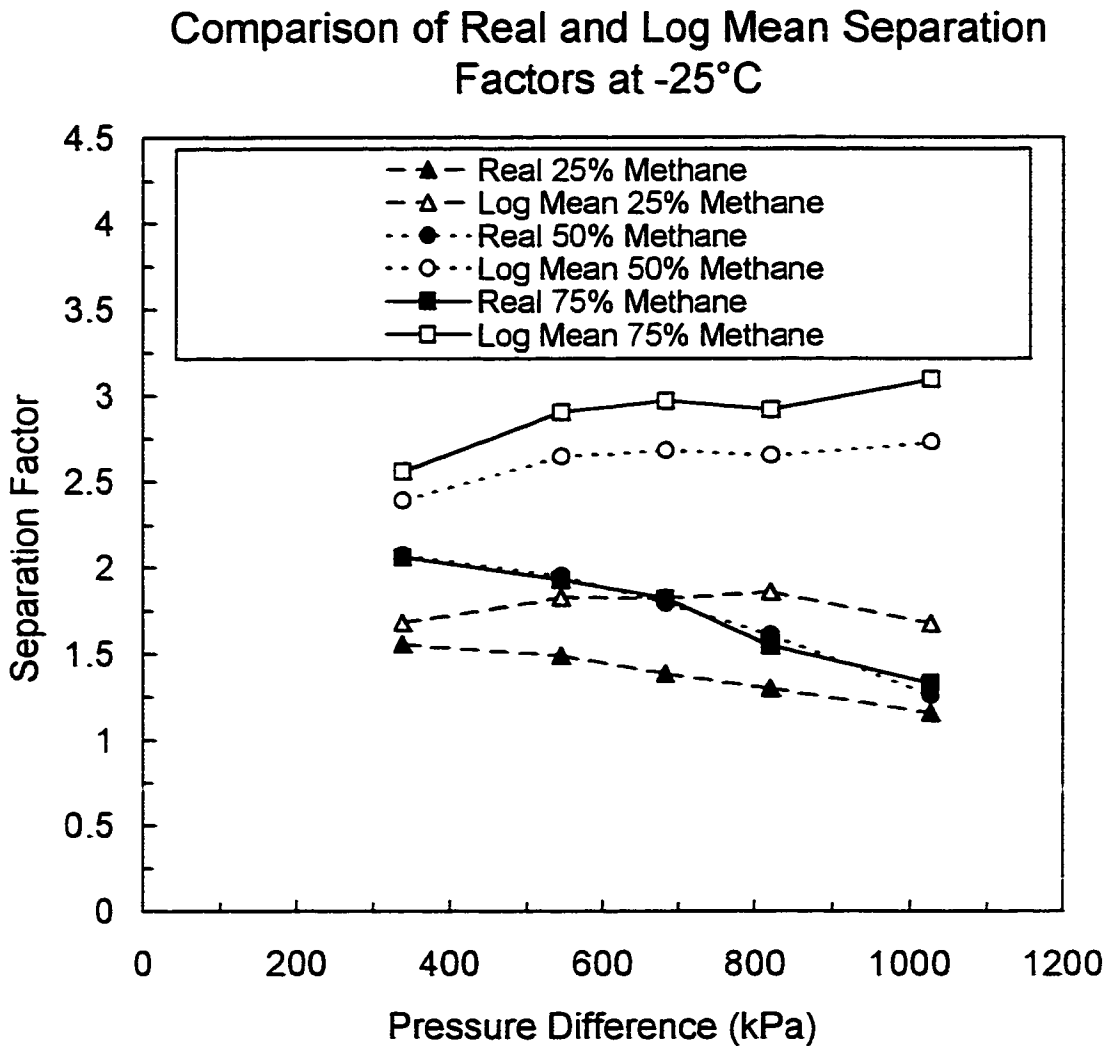

Figure A1: Real separation factors (equation 4.8) and separation factors calculated with log mean pressure differences (equation 4.9) for 25%, 50% and 75% methane mixtures at -25°C (M-2).

APPENDIX B

Table B1: Schedule of pure gas and hydrogen-methane separation experiments.

Exp.	Gas Cylinder	Date
1	Pure Gas Hydrogen 22°C	Sept. 9, 1998
2	Pure Gas Hydrogen 65°C	Sept. 10, 1998
3	Pure Gas Hydrogen 155°C	Sept. 10, 1998
4	Pure Gas Hydrogen 125°C	Sept. 10, 1998
5	Pure Gas Hydrogen 22°C Repeat	Sept. 11, 1998
6	Pure gas Methane 22°C	Sept.12, 1998
7	Pure gas Methane 126°C	Sept. 13, 1998
8	Pure gas Methane 155°C	Sept. 13, 1998
9	Pure gas Methane 65°C	Sept. 14, 1998
10	**Pure gas Methane 22°C Repeat**	**Sept. 14, 1998**
11	**Mixture 50/50 22°C**	**Sept. 15, 1998**
12	Mixture 50/50 125°C	Sept. 16, 1998
13	Mixture 50/50 155°C	Sept. 17, 1998
	CSChE, data analysis, cold T set up	Sept and Oct
14	**Pure gas Methane 22°C Repeat**	**Oct. 9, 1998**
15	Pure gas Methane -25°C	Oct. 11, 1998
16	Pure gas Methane -15°C	Oct. 12, 1998
17	Pure gas Methane -10°C	Oct. 13, 1998
18	Pure gas Methane 10°C	Oct. 13, 1998
19	Pure gas Methane 0°C	Oct. 13, 1998
20-24	50/50 Cold T experiments high flow rates (10, -25, -10, 0, -25°C repeat)	Oct. 14-Oct.18, 1998
25-29	50/50 Cold T experiments low flow rates (-25, -10, 10, 0, -25°C repeat)	Oct. 19-Oct.22, 1998
30-36	Pure gas hydrogen (0, 10, 22, -25, -15, -10, -25°C repeat)	Oct. 22-Oct.24, 1998
37	75/25% methane -25°C High Flow	Oct. 25, 1998
38	75/25% methane -25°C Low Flow	Oct. 29, 1998
39	75/25% methane -10°C	Oct. 30, 1998
40	75/25% methane 0°C	Oct. 31, 1998
41	75/25% methane 10°C	Nov. 1, 1998
42	**75/25% methane 22°C**	**Nov. 2, 1998**
43	75/25% methane -25°C Repeat	Nov. 2, 1998
44	25/75% methane -25°C	Nov.3, 1998
45	25/75% methane -25°C High Flow	Nov.4, 1998
46	25/75% methane 0°C	Nov. 5, 1998
47	25/75% methane -10°C	Nov. 10, 1998
48	25/75% methane 10°C	Nov. 10, 1998

49	**25/75% methane 22°C**	**Nov. 11, 1998**
50	25/75% methane -25°C Repeat	Nov. 11, 1998
51	49/49/2% ethane -25°C	Nov. 20, 1998
52	49/49/2% ethane -10°C	Nov. 21, 1998
53	49/49/2% ethane 0°C	Nov. 21, 1998
54	49/49/2% ethane 22°C	Nov. 22, 1998
55	49/49/2% ethane -25°C Repeat	Nov. 23, 1998